

Interplay of Kondo effect and RKKY interaction in magnetic clusters

D i s s e r t a t i o n

zur Erlangung des Doktorgrades
des Department Physik
der Universität Hamburg

vorgelegt von

Philipp Knake

aus Oldenburg

Hamburg
2010

Gutachter der Dissertation:	PD Dr. Alexander Chudnovskiy Prof. Dr. Alexander Lichtenstein
Gutachter der Disputation:	PD Dr. Alexander Chudnovskiy Prof. Dr. Michael Potthoff
Datum der Disputation:	27.01.2010
Vorsitzender des Prüfungsausschusses:	Prof. Dr. Hans Peter Oepen
Vorsitzender des Promotionsausschusses:	Prof. Dr. Joachim Bartels
Leiterin des Departments Physik:	Prof. Dr. Daniela Pfannkuche
Dekan der Fakultät für Mathematik, Informatik und Naturwissenschaften:	Prof. Dr. Heinrich Graener

Abstract

We consider an arbitrary number of singly occupied one-level magnetic impurities supported by a metallic host, and describe this system using an Anderson model in the small tunnelling regime. The physics of such a system is not only determined by the Kondo effect, but also by effective inter-impurity interactions like the RKKY effect. For an arbitrary number of impurities the local density of states of the problem is being formally computed, using a mean field approach in the low temperature limit. As a concrete example of such a magnetic cluster we consider an isosceles trimer and determine the behaviour of the Kondo temperature at certain impurity sites with varying inter-impurity coupling. The overall outcome is that the Kondo effect is enhanced for completely ferromagnetically coupled trimers, while it is suppressed for antiferromagnetically coupled ones. The magnitude of this enhancement or suppression in the above cases depends on the geometric configuration of the trimer. Antiferromagnetically coupled chain like systems show a very strong decrease of the Kondo temperature, while systems in which one atom is more and more separated from the remaining two experience a decomposition into dimer systems which we call "dimerisation". In trimer systems in which two atoms are coupled antiferromagnetically among each other while interacting ferromagnetically with the remaining atom the Kondo temperature is influenced by frustration effects at all impurity sites.

Inhaltsangabe

In dieser Arbeit wird ein System untersucht, das aus einer zunächst beliebigen Anzahl einfach besetzter, magnetischer Störatome mit nur einem relevanten Energieniveau besteht, welche auf ein metallisches Substrat aufgebracht werden. Zur Beschreibung des Systems wird ein Andersonmodell im Grenzwert kleiner Tunnelamplituden herangezogen. Das physikalische Verhalten eines Systems mehrerer magnetischer Verunreinigungen in einem Substrat wird sowohl vom Kondoeffekt bestimmt als auch von Spin-Spin Wechselwirkungen zwischen den verschiedenen Störatomen, z.B. dem RKKY-Effekt. Für eine zunächst beliebige Zahl von Störstellen im System wird der Tieftemperaturlimites der lokalen Zustandsdichte mit Hilfe einer Mean-Field-Theorie bestimmt. Als konkretes Beispiel eines magnetischen Clusters wird ein gleichschenkliger Trimer betrachtet, anhand dessen jeweils am Ort der Verunreinigungen die Abhängigkeit der Kondotemperatur von den interatomaren Kopplungen untersucht wird. Das wesentliche Ergebnis ist, dass ausschließlich ferromagnetisch gekoppelte Trimere eine Verstärkung des Kondoeffekts erfahren, während dieser in ausschließlich antiferromagnetisch gekoppelten Trimeren abgeschwächt wird. Diese Verstärkung bzw. Abschwächung hängt von der geometrischen Konfiguration des Trimers ab. In antiferromagnetisch gekoppelten, kettenartigen Trimeren wird der Kondoeffekt stark vermindert. Systeme, in denen ein Atom von den restlichen beiden immer weiter entfernt wird, zerfallen in verbundene Dimersysteme, ein Vorgang der als Dimerisation bezeichnet werden kann. In Trimersystemen, in denen ein Atom ferromagnetisch an die restlichen beiden Atome gekoppelt wird, welche wiederum untereinander antiferromagnetisch verbunden sind, wird die Kondotemperatur für alle Störstellen von Frustrationseffekten beeinflusst.

Contents

1	Introduction	1
2	Literature survey	5
3	The model	17
3.1	N atomic cluster	17
3.2	Magnetic isosceles trimer	20
4	Cluster of N atoms	23
4.1	Hubbard-Stratonovich transformation and mean field approximation of the interaction	23
4.2	Partition function in mean field theory	25
4.2.1	RKKY interaction	28
4.3	Mean field equations	29
4.4	Green's function and local density of states	30
4.4.1	The "touching ground" theorem for the local density of states	33
4.5	Single impurity limit	36
4.6	Summary	37
5	Isosceles Trimer	39
5.1	General case	39
5.1.1	Useful formulas for the isosceles trimer	42
5.2	Dimer	45
5.2.1	Ferromagnetic dimer coupling	48
5.2.2	Antiferromagnetic dimer coupling	50
5.3	Equilateral trimer	52
5.3.1	Ferromagnetic trimer coupling	53
5.3.2	Antiferromagnetic trimer coupling	54
5.4	Linear chain	56
5.4.1	Ferromagnetic chain interactions	57
5.4.2	Antiferromagnetic chain interactions	58
5.5	Asymmetric isosceles trimer	59
5.5.1	Ferromagnetic interactions	59
5.5.2	Antiferromagnetic interactions	61
5.5.3	Mixed type interactions	62
5.6	Summary	65
6	Conclusion	69
7	Outlook	75

Appendices

A Preliminary Considerations	79
A.1 Mathematical definitions and useful relations	79
A.2 $SU(N)$ -generators	81
A.3 Conductance at low temperatures	83
A.4 Schrieffer-Wolff transformation	84
A.5 Spin Hamiltonians and the Popov-Fedotov method	90
B General calculations for a cluster of N atoms	95
B.1 Hubbard-Stratonovich transformation	95
B.2 Partition function in mean field theory	98
B.3 Mean field equations	104
B.4 Green's function and local density of states in mean field theory	107
References	115

1 Introduction

Studies of systems of magnetic impurities in a metal host have been done for many decades both experimentally as well as theoretically. In the early thirties, measurements in gold with iron impurities revealed some peculiar behaviour of the electrical resistance when a minimal value was found at a finite temperature rather than a constant decrease toward a saturation point, as had been expected. In the simple picture of a lattice in which all atomic vibrations are frozen out if the system is cooled down, only lattice defects prevent the conduction electrons from moving unresistant, so the resistivity should simply decrease with the temperature approaching a finite value at $T = 0$. It was a long standing problem to explain the increase of the resistivity for low temperatures, and it was not until 1964 that Jun Kondo was able to give a microscopic explanation. He showed, that a $s-d$ model describing the interaction of the spin of a magnetic impurity with the spins of the surrounding conduction electrons led to a logarithmic increase of the resistivity for low temperatures in second order perturbation theory in the coupling of the localised spin to the itinerant spins. Since this model correctly predicted the existence of the resistivity minimum, the low temperature increase of the electrical resistance was explained to be caused by scattering of the conduction electrons off a magnetic impurity.

A simple but quite general model to describe impurities in a metal host was proposed by Anderson in 1961. In this model, the impurity has only one electron level and its electron can quantum mechanically tunnel into the Fermi sea of the surrounding metal and vice versa. This model is also going to be the starting point of our studies in this work. The Anderson model allows for exchange processes that lead to a spin-flip in the impurity and a spin excitation in the Fermi sea. These processes are due to very short lived virtual excitations, in which the impurity electron can tunnel into the Fermi sea occupying a state above the Fermi level. Classically, this process is forbidden because of the conservation of energy, but due to quantum fluctuations such a state can exist for a very short time period, within which an electron must tunnel from the Fermi sea back to the impurity. However, the spin of this electron can be opposite to that of the original electron, so that the impurity undergoes a spin-flip process.

The Kondo effect, that is the increase of the resistivity of a dilute alloy of a metal and magnetic impurities, is the result of many such spin-flipping processes, due to which a many body state called the Kondo resonance state is created which has exactly the Fermi energy. This state enhances the scattering of conduction electrons near the Fermi level, which determine the low temperature behaviour of the resistivity. It is therefore increased at temperatures below the one for which the Kondo resonance state is formed. This temperature is called the Kondo temperature and it is determined by the parameters of the Anderson model (the impurity energy, the Coulomb energy, the tunnelling strength), which therefore can be replaced by a single parameter (namely said Kondo temperature) characterising the system completely.

In the Kondo state, the spin of the impurity is screened by the spins of the surrounding conduction electrons. At temperatures well below the Kondo temperature, the impurity spin can be seen as being bound into a singlet with a conduction electron, while the other electrons behave like a free gas. Today, one refers to this formation of a Kondo cloud of itinerant spins screening the magnetic moment of the impurity as "the Kondo effect" rather than to the unusual behaviour of the resistivity in dilute alloys.

1 Introduction

The Kondo effect has been studied extensively in theory for four decades and it is seen as being completely understood in the case of a single magnetic impurity on a metal host. Experimentally, however, the Kondo effect could only be observed indirectly until the late nineties, since no device existed to access single magnetic impurities. Instead, measurements of the thermodynamical properties of an impurity studded metal and their behaviour with varying temperature or their dependence on magnetic fields were the only ways to get experimental evidence of the Kondo effect. With the recent developments in nanotechnology, these restrictions could be overcome. During the past decade, many Kondo systems were studied by means of scanning tunnelling spectroscopy using a scanning tunnelling microscope (STM) or by conductance measurements in a quantum dot. While STM experiments yield direct access on the atomic scale to a metallic sample with impurities, quantum dots can be used to mimic such systems.

In STM measurements, the tip of the microscope is placed upon a certain location of the sample and the tunnelling current between tip and sample with varying voltage bias is measured. If such dI/dV measurements are made at low temperatures, the conductance is essentially proportional to the local density of states (LDOS) of the substrate electrons. If one aims for predicting the outcome of such STM experiments (which we do in this work), the local density of states therefore is the quantity which has to be computed.

If the STM tip is placed over an isolated magnetic impurity and dI/dV spectra are taken, indications of the Kondo effect can be seen. If the system is in the Kondo resonance state, a sharp dip will occur in the dI/dV curve which is centered at the Fermi energy. This shape of the differential conductance in the Kondo state is often referred to as the "Kondo resonance" although this phrase also describes the resonant spin-flip scattering of the conduction electrons at the impurity. The shape of the dI/dV spectra in the Kondo case is that of a Fano resonance known from atomic physics. The formula for the Fano resonance contains a so called Fano factor which in the case of STM experiments describes the coupling of the tip to the sample (in this work, we are often going to fit the energy resolved LDOS to a Fano line shape which always has a vanishing Fano factor, so we always describe STM experiments in the limit of very weak tip-sample coupling). At external temperatures well below the Kondo temperature, the width of the dI/dV curve is proportional to the Kondo temperature. Thus, determining the width of the energy resolved LDOS in the limit of vanishing temperature yields the Kondo temperature (up to a factor).

Kondo physics becomes more involved, if one allows for more than one magnetic impurity in a system. If the distance between different magnetic impurities in a metal sample gets small enough, other effects apart from the Kondo effect will influence the system's behaviour. Among these effects are, for example, direct exchange couplings of the impurities or the RKKY effect (named after Rudermann, Kittel, Kasuya and Yosida). The latter is an indirect interaction between the spins of the impurities which is mediated by the electrons in the substrate. This effective interaction can couple the impurity spins ferromagnetically as well as antiferromagnetically depending on their mutual distance. Compared to other effects like direct inter atomic hopping, the RKKY coupling is quite long ranged (decreasing with the inverse distance between two impurities in two dimensional systems). In this work, we are going to neglect effects that require a greater proximity of the magnetic impurities. This means, that we will only describe more "loosely" arranged magnetic clusters. A system investigated at the location of an impurity is therefore expected to be in the Kondo state, which is just slightly (or sometimes not so slightly) changed by the influence of the other impurities. We are going to quantify these changes by means of determining the Kondo temperature at a given cluster site. A higher Kondo temperature compared to that of an isolated impurity means, that the Kondo effect is enhanced

1 Introduction

while a lower Kondo temperature suggests a suppression of the Kondo effect. This approach is different from recent studies of magnetic trimers on metallic substrates in so far that those dealt with more compact structures.

In the following chapter, we give a brief overview over the literature connected to Kondo physics and its application to magnetic dimers and trimers. In chapter 3 we are going to present the model Hamiltonian and give a short outlook on how we will deal with the system in the following. Moreover, we are going to present the model for a magnetic trimer, which we will concentrate on as a concrete example for a magnetic cluster. Using mean field theory, the partition function and the local density of states for an N atomic cluster will be computed formally in chapter 4, and we are going to state the mean field equations. In chapter 5, we are going to consider the magnetic cluster to be an isosceles trimer and determine the variation of the Kondo temperature with varying trimer geometry. We will end the main part of this work with conclusions and an outlook on how the model could be generalised. In the appendix, you will find some preliminary mathematical considerations which we made use of describing the system and detailed calculations for the N atomic magnetic cluster.

In this work we will only enumerate equations, which either will be referred to later or which are central results of the preceding calculations. For the sake of readability, we will sometimes write down an equation repeatedly although it has already been stated earlier.

2 Literature survey

In this section we give a brief literature overview of the developments in Kondo physics during the past decades. We are going to start with Kondo's explanation of the resistance minimum that can be observed in dilute alloys and then turn to the theoretical solution of the Kondo problem during the late sixties and early seventies. In the late nineties the Kondo effect became subject to extensive studies again after it had not been for twenty years. This was due to developments in nano-physics which allowed to detect the Kondo resonance directly by means of STM experiments or in artificially fabricated atoms, say quantum dots. We will give a brief overview of the important experiments and the related theoretical works. Here, we are also going to present more recent works in which systems were investigated both theoretically and experimentally, which were expected to show interplay of the Kondo effect and inter-impurity effects (like the RKKY interaction), such as coupled quantum dots or magnetic trimers. In the last part of this overview, we will concentrate on the more technical issue of dealing with spin Hamiltonians in so called semi-fermionic representations.

It has been well known for a long time that the resistance of pure metals like copper and gold drops when they are cooled down, since electrons can travel through the metal more quickly if the atomic vibrations (the phonon-number) get smaller. However, due to static defects in the metal the resistance of gold and copper always stays finite and does not approach zero if the temperature vanishes. Instead, it saturates at a finite value which depends on the number of defects, even for the lowest accessible temperatures. In 1934, de Haas *et al.* observed an unexpected low temperature behaviour of the resistance in gold (see [1]). It developed a minimum at a finite temperature and rose again if the metal was cooled down further. At that time, no explanation could be found for this anomaly. In 1964, Sarachik *et al.* studied the resistance in dilute alloys of Fe in Nb-Mo alloys as host metals (see [2]). The outcome was that the depth of the minimum depended on the Nb-Mo alloys that were considered. Since Fe has a varying magnetic moment depending on the composition of the alloy, it was suggested that the magnetic moment of the iron was responsible for the resistance minimum.

The first satisfactory explanation of the resistance minimum was given by Kondo in 1964 (see [3]). He considered an s - d model describing the scattering from a magnetic ion which interacts with the spins of the conduction electrons and made a perturbative approach, computing the system's quantities up to second order perturbation theory in the s - d interaction. His discovery was that the second order term could be much larger than the leading term (at the Fermi surface), which resulted in a logarithmic increase of the resistance of the metal if the external temperature was lowered below a certain value. Kondo therefore was able to predict the increase of the resistance at very low temperatures after it had reached a minimal value. However, the logarithmic low-temperature behaviour led to a diverging resistance at vanishing temperature, which was apparently not correct. Nevertheless, Kondo was able to explain the resistance anomaly of metals hosting magnetic impurities as being the result of the interaction between the spins of the localised and the conduction electrons rather than being due to any other properties of the impurities like their charge. Moreover, he predicted that the depth of the minimum relative to the resistance value at vanishing temperature should roughly be proportional to the

impurity concentration. The conclusion was, that the minimum was basically due to a single impurity effect and not so much the result of interactions among the impurities.

In the aftermath of Kondo's discovery, many theoreticians began to study s - d models with regard to the Kondo effect. Using a self-consistent approach rather than perturbation theory at low temperatures, Nagaoka (see [4]) was able to show that perturbation theory has to break down below a certain temperature and that near the Fermi surface a quasi-bound state between the localised spin and the conduction electron spin appears. He concluded that this state was responsible for the resistance minimum. Suhl and Abrikosov derived similar results in [5] and [6], showing that for low temperature the singularity could be replaced by resonant scattering. The overall outcome in [4, 5, 6] was that for sufficiently low temperatures an s - d model lead to a condensation in which a localised conduction-electron spin polarisation compensates the magnetic moment of the impurity.

While Kondo was considering an s - d model to characterise the interaction between an impurity spin with the conduction band of the metal host, Anderson in 1961 proposed a different model describing magnetic impurities embedded in a metal (see [7]). His model Hamiltonian contained a free term for the conduction electrons as well as for the impurity electrons, a Hubbard interaction term modelling the Coulomb repulsion of impurity electrons and an interaction term, which described tunnelling of electrons from the band to the impurity and vice versa.

The Anderson model in a way is more general than the Kondo model, but because of that it is even harder to solve. So far, no general solution is known. However, in 1966 Schrieffer and Wolff showed in [8] that the Anderson model can be mapped to the Kondo model via a canonical transformation in the regime of small s - d mixing (when the tunnelling amplitude between the conduction band and the impurity is small), assuming that the energy of the (single) impurity d -orbital is below the Fermi level, while the energy of a doubly occupied impurity (being the sum of the d -orbital energy and the contribution of the Coulomb repulsion) is above it. The outcome was that at low energy scales the more general Anderson model essentially is the same as the Kondo model, and that it can be expected to develop a Kondo effect at low temperatures. It thus cannot lead to a localised magnetic moment at vanishing temperature.

In the late sixties it was known that Kondo's results were correct only above a certain temperature below which perturbation theory broke down. This temperature was by then called the Kondo temperature. In 1970, Anderson proposed a framework in which the physics of the Kondo model could be described below the Kondo temperature (see [9]). He introduced a method of scaling the problem, which meant a renormalisation of the cutoff given by the bandwidth of the conduction electrons. In this approach, high energy degrees of freedom of the conduction band were integrated out successively (so reducing the cutoff energy) in favour of an effective interaction. This method leads to scaling equations for the interaction parameters, which show that each step of the successive reduction of the band width results in an increased effective interaction strength. Anderson stated, that if this scaling process is performed repeatedly, the low-temperature limit of the Kondo Hamiltonian evolves toward a fixed point in which the effective exchange coupling of the impurity with the itinerant electrons becomes infinitely strong. In Anderson's approach, the energy scale of the Kondo temperature is a so called scaling invariant, it does not change its value during the scaling process. For the method to be valid, one has to assume that a low-temperature system is represented by a coarse-grained model, meaning that the model becomes coarser if the temperature gets smaller so that the number of degrees of freedom is reduced.

2 Literature survey

In [10] Nozières showed that, assuming the propositions of Anderson, all low temperature properties of a Kondo system can be phenomenologically described in the same way as in Fermi liquid theory. He stated that, taking for granted that below the Kondo temperature the "effective coupling" between the localised electron and the itinerant ones was diverging, the impurity spin was frozen into a singlet so that the magnetic impurity was replaced by a non-magnetic one. However, said singlet still remained in a sense polarisable (due to virtual excitations), so that an indirect interaction between the conduction electrons was induced. Using this simple picture, Nozières was able to describe thermodynamic properties of the system in the spirit of Fermi liquid theory.

In 1975, Wilson dealt with the Kondo problem (see [11]) adopting the scaling ideas of Anderson. The method he used was numerical renormalisation group theory. In renormalisation group theory, a Hamiltonian which depends on certain interaction parameters is mapped by some (generally non-linear) transformation into another Hamiltonian of the same form with an altered set of interactions (as outlined, Anderson used such a renormalisation to reduce the energy scale of the conduction band). With his renormalisation group approach, Wilson was able to overcome the problems of perturbation theory (which breaks down at energy scales of the order of the Kondo temperature) using an iterative method involving numerical diagonalisation. He was able to completely predict the behaviour of an s - d system well below the Kondo temperature. He proved that below the Kondo temperature, the magnetic moment of the impurity is completely screened by the spins of the conduction electrons by spin-flip scattering processes. Oversimplifying, one might say, the impurity and a band electron are glued together (thus confining the impurity spin) while the other electrons behave like a free gas.

After the appearance of [11], several theoreticians took up Wilson's numerical renormalisation group method and investigated different physical systems related to the Anderson or Kondo model ([12, 13, 14, 15]). With Wilson's work, the Kondo problem for single magnetic impurities in metallic hosts was finally solved for all temperature ranges. Since then, several theoreticians were able to solve the s - d model or limiting cases of the Anderson model analytically. In 1980, Andrei [16] and Wiegmann [17] independently of each other were able to solve the s - d model by means of a Bethe-Ansatz (however, this approach cannot be extended to the case of more than one magnetic impurity). The same year, Wiegmann used the Bethe-Ansatz to solve the Anderson model in [18], assuming that all occurring energies were small compared to the Fermi level and that the tunnelling amplitude did not depend on the wave vector (so that the problem was reduced to a one-dimensional one). Moreover, he neglected all electron states far from the Fermi surface.

[19] gives a very comprehensive overview of the theoretical work concerning the Anderson and the Kondo model done up to 1983.

In 1981 Jayakaprash *et al.* were the first to study a two impurity Kondo model by means of Wilson's renormalisation group (see [20]). In this work, the main contribution to the physics apart from the Kondo effect was assumed to be the RKKY effect, which was discovered in the mid to late fifties by Rudermann, Kittel (see [21]), Kasuya ([22]) and Yosida ([23]), who stated that in a metallic system with several magnetic impurities that can be described by s - d coupling, an effective spin-spin interaction between the distinct impurities arises. This indirect spin coupling is mediated by the conduction electrons, and its amplitude and sign depend on the distance between the impurities. Moreover, it shows an oscillating behaviour and can therefore couple the impurity spins ferromagnetically as well as antiferromagnetically (for another illuminating presentation of the RKKY interaction see [24] and the textbook of Yosida [25]). Antiferromagnetic RKKY interactions tend to counteract the Kondo spin screening, since

2 Literature survey

they result in the spin system getting more localised. Jayakaprash *et al.* showed that in the regime of strong antiferromagnetic RKKY interactions, the spins of the two impurities are bound to a singlet state, so that the Kondo effect is suppressed (since the itinerant electrons cannot spin-flip scatter with a vanishing magnetic moment).

After the low temperature problems with the Kondo model had been theoretically solved in [11], no new results seemed to be obtainable by the study of Kondo physics, and from the early eighties to the mid- to late nineties, no new exceptional results were made. This was mostly due to the lack of an experimental device which allowed to study the Kondo effect on a microscopic scale. Up to then, the only way to access Kondo systems was an indirect one. The usual way was to analyse the thermodynamic and transport properties of a dilute alloy of a metal with magnetic impurities and to study their dependence on the temperature or an external magnetic field. With the advances in nanotechnology in the late nineties, other possibilities to study the Kondo effect arose.

A scanning tunnelling microscope (STM) measures the tunnelling current flowing between the tip of the microscope and the sample under examination if a voltage is applied to the system. Moving the sample, the STM can measure the conductance at different locations of the sample. Since the conductance at very low temperatures essentially is proportional to the local density of states, STM experiments are able to determine the coordinate resolved LDOS in atomic resolution. Moreover, the STM allows to manipulate the sample by moving impurities directly with the tip (for example to form dimers and trimers). The possibility to resolve the LDOS on an atomic scale was expected to allow studies of the Kondo effect on a microscopic scale.

The first results were being reported quite simultaneously in 1998 by Crommie's group (see [26], for further reading also [27]) and by the group around Schneider (see [28]). Both groups considered systems of single magnetic impurities on metal hosts and measured tunnelling spectra, say dI/dV curves. Crommie *et al.* measured individual Co atoms on gold (at 4 K) while Schneider *et al.* took spectra of isolated Ce impurities on silver (at 5 K). The outcome was quite similar. The dI/dV curves developed an antiresonance at the Fermi level if the voltage was swept through. This resonance was interpreted as a Fano resonance (see [29]) showing the "footprint" of the Kondo effect.

The results of these experiments motivated experimentalists as well as theoreticians to renew their studies of Kondo systems. In [30], Schiller and Hershfield presented a theoretical treatise of scanning tunnelling spectroscopy of magnetic adatoms on metal hosts. They considered an Anderson model in the sample, but also took into account terms that described the tip and the tunnelling between tip and sample. Using self-consistent perturbation theory, they were able to compute the Green's function (and therefore the density of states) of the problem in the limit of infinite Coulomb repulsion in the impurity. They correctly predicted the antiresonance and showed that the features discovered in [26] and [28] were in fact due to a Fano resonance between tip and impurity, in which the Fano factor was connected to the coupling of the tip to the sample. They were also able to reproduce the rapid decay of the dip seen as the tip is moved away from the impurity.

Quite simultaneously, Újsághy *et al.* also predicted the Fano line shape in dI/dV spectra taken at the location of magnetic impurities on a metal host (see [31]). Using local spin density approximation and a strong correlation method (see [32]) they computed the system's Green's function and showed that the local density of states develops a Fano resonance, on which small Friedel oscillations are superimposed. Moreover, they predicted the dependence of the line shape on the distance of the tip from the impurity, emphasizing that the concrete results were strongly depending on the band structure of the metal host.

2 Literature survey

In 2005 Lin, Castro Neto and Jones developed a similar theory of a Kondo resonance in an STM experiment (see [33]) using an Anderson model in the sample. They computed the hybridisation energies and found, that those were strongly depending on the directions of the conduction electron momenta, leading to different line shapes as the impurity is pushed further from the surface into the bulk of the metal.

The STM results in [26] and [28] also motivated other experimentalists to consider systems in which some kind of Kondo physics was expected to be involved. In 2000 Eigler *et al.* investigated a quantum corral system (see [34]). Using the STM tip for sliding atoms, they constructed a corral of elliptic form using Co atoms on copper. Afterwards they placed a single Co atom in one of the focal points of the ellipse to serve as a magnetic impurity and measured dI/dV spectra, using the STM. Remarkably, a Kondo resonance was detected not only at the position of the Co impurity, but also at the other focal point despite the absence of an impurity there. This behaviour was explained as being the result of the symmetry of the corral, since electron waves passing through one focus had to converge at the second one. The authors called that peculiar situation a "quantum mirage".

In 2002, Nagaoka *et al.* measured the broadening of a the Kondo resonance when the sample is heated (see [35]). They used a STM to investigate isolated Ti atoms on silver and varied the external temperature between a sixth of and the full Kondo temperature. They saw that the Kondo resonance broadened rapidly with increasing temperature in very good accordance to the predicted Fermi liquid behaviour of a Kondo impurity (see [10]).

In [36] and [37] the subject of the dependence of the Kondo temperature of a system on its parameters was tackled. It is well known that the Kondo temperature is proportional to an exponential term, which depends on the inverse of the unperturbed density of states of the conduction electrons and the inverse of the Kondo coupling (see [38]). [36] was able to measure the scaling of the Kondo temperature with the host electron density for Co adatoms on two sorts of copper. For Cu(100) the Kondo temperature is higher than for Cu(111) which can be explained by a higher bulk electron density at the adatom. In [37] cobalt adatoms were measured in several metallic hosts like copper, silver and gold. A large range of Kondo temperatures for the different systems was observed. It was explained as being due to different hybridisations of the adatom with the substrate. Systems with smaller hybridisations had smaller Kondo temperatures compared to those with larger hybridisations as it is expected if the Kondo coupling is shifted from weak to strong.

Another development in nanotechnology that allows for more direct measurements of the Kondo effect was the ability to construct so called artificial atoms or quantum dots. Those are very small semi conducting boxes that can hold a small number of electrons adjustable by varying the voltage applied to the dot. If the number of electrons confined in the dot is odd, the artificial atom has a non-zero total spin. This localised spin embedded between the two large electron seas of the leads can be seen as a magnetic impurity in a metallic substrate. Several theoretical works predicted, that phenomena related to the Kondo effect could be observed in such quantum dot systems (see [39, 40, 41, 42, 43, 44]). The approach to tackle Kondo physics in a quantum dot is to measure the conductance through the dot (as one would do in a STM experiment). However, the difference between a quantum dot and an impurity in a metal host is the geometry of the system. In a quantum dot system, all conduction electrons have to travel through the dot, while in a metal they are described as plane waves scattering off the impurity. In a quantum dot, the Kondo resonance makes it easier for two states belonging to opposite electrodes to mix, which results in a higher conductance. In the case of an impurity in a metal, the conductance was lowered due to the Kondo resonance.

2 Literature survey

The first experimental results that showed the hint of a Kondo effect in a quantum dot were achieved by Goldhaber-Gordon *et al.* in 1998 (see [45]). They measured several narrow peaks in the conductance of the dot, which they interpreted as being the result of a Kondo resonance.

In the same year, Cronenwett *et al.* also discovered narrow peaks in the conductivity in a GaAs/AlGaAs quantum dot device, connected to the Kondo effect (see [46]). They measured the temperature and magnetic field dependence of the dot. The results were in good agreement with the theoretical predictions for a Kondo quantum dot. Moreover, they were able to switch a quantum dot from a Kondo to a non-Kondo system by changing the number of the confined electrons from odd to even (however, there were other experiments that showed that in some situations a Kondo quantum dot can deviate from this odd-even behaviour, see [47]).

In 1999, Simmel *et al.* observed an anomalous Kondo effect, also in a GaAs/AlGaAs quantum dot ([48]) with asymmetric barriers. The outcome was that the conductance developed an offset of the Kondo resonance at zero magnetic field. The Kondo resonance was only observed in the negative bias regime, while it was suppressed for bias of the opposite direction. Theory predicts, that the Kondo resonance occurs at the chemical potential of the leads. In the case of an asymmetric barrier, the Kondo resonance was pinned to the Fermi level of the more strongly coupled lead.

Another quantum dot experiment in very good agreement with the theoretical predictions was performed by van der Wiel *et al.*. They observed a strong Kondo effect when a small magnetic field was applied to the dot (see [49]).

Although usually no Kondo effect can occur in quantum dots with an even number of electrons (since there is no net magnetic moment the lead electrons can interact with), Sasaki *et al.* were able to detect a large Kondo effect for an even number of electrons confined in a so-called "vertical" multi-level dot (see [50], for theory of the Kondo effect in multi-level dots see [51, 52, 53]). In such devices, the spacing of the discrete levels is comparable to the Coulomb interaction strength. Due to Hund's rule, two electrons put into nearly degenerate levels will favor a spin triplet over a spin singlet, so that there is a net magnetic moment and a Kondo resonance can occur. Eto and Nazarov theoretically investigated such systems in mean field theory (see [54]). They showed that the competition of spin singlet and triplet states leads to a Kondo effect, which is suppressed if a perpendicular magnetic field is applied to the system.

Due to the experimental accessibility of the Kondo effect on an atomic scale by STM measurements or quantum dots, an interest to study coupled Kondo systems arose. If a single magnetic impurity on a metal host developed a Kondo effect, what would happen if one coupled two such impurities, for example by spin-spin interactions? Before the development of the STM and quantum dots, there was no way to study such phenomena directly, since there was no simple way to verify the existence of a magnetic dimer or trimer in a sample. Instead, one had to rely on more indirect methods. For example, Kumar *et al.* predicted a change in the low temperature behaviour of the specific heat due to competition of the Kondo effect and RKKY interactions between the impurities, see [55]. With help of an STM, such coupled structures as dimers and trimers can not only be measured, but also assembled by moving single impurity atoms on the surface of the metal with the STM tip. It is also possible to mimic two proximal magnetic impurities using two quantum dots which are coupled by an open conducting region.

In 1999 Chen *et al.* of the Crommie group investigated dI/dV spectra of Co dimers on gold (see [56]) at 6 K. They measured dimers of different lengths (meaning the inter atomic Co-Co spacing) and saw an abrupt disappearance of the Kondo resonance for dimers less than 6 Å long. As feasible explanations of this phenomenon, they gave three alternatives: the magnetic moment of the dimer could be quenched, which was not supported by some weak localisation measurements,

2 Literature survey

the dimer interaction could be antiferromagnetic or the exchange coupling between the dimer magnetic moment could be reduced. Antiferromagnetic dimer interactions were excluded, since Chen *et al.* assumed the energy scale of the RKKY interaction being far too small compared to the Kondo effect and because weak localisation measurements showed ferromagnetic coupling between the dimer atoms. The authors favoured the explanation that the Kondo exchange coupling was reduced by the ferromagnetic dimer interactions, which led to a decrease of the Kondo temperature below 6 K. The abruptness of the disappearance of the Kondo resonance was thus said to be due to the exponential dependence of the Kondo temperature on the exchange coupling.

Also quantum dot systems of two coupled dots were investigated experimentally. In [57] Jeong *et al.* measured dI/dV spectra of two coupled GaAs/AlGaAs quantum dots. For weak enough coupling between the dots, the system developed Kondo peaks in different regions of the voltage bias which were connected to both dots being in the spin- $\frac{1}{2}$ case (each dot containing one unpaired electron). In those regions, the Kondo resonance showed a splitting into two peaks. This splitting was interpreted as the result of the two dots being in molecular bonding or antibonding states (for such states, a splitting of the Kondo resonance was theoretically predicted in [58, 59, 60]), since its energy was comparable to that of the molecular bonding-antibonding splitting measured before (see [61]).

In 2004, Craig *et al.* investigated a system of two coupled quantum dots in which they were able to control the inter-dot coupling and the electron number in each dot (see [62]). If not coupled, the dots showed the typical Kondo peaks in the dI/dV spectra if they had non-vanishing total spin (an odd number of electrons in them). If one dot contained an even number of electrons and was coupled to the other dot (which was in a Kondo state), no significant changes in the Kondo shaped spectrum of that dot were observed (which was expected, since no spin-spin interactions could take place). If one dot contained an odd number of electrons and was coupled to the other dot, the Kondo features of that dot were suppressed. This was interpreted as being the result of strong RKKY coupling between the two dots, which led to an overall spin-zero state for which no Kondo effect could occur, or an overall spin-one state for which the Kondo temperature was assumed to be so small, that no Kondo effect could be observed at the given external temperature of the experiment (in [63] and [64], Simon *et al.* and Vavilov and Glazman independently of each other suggested a method to distinguish between ferromagnetic and antiferromagnetic RKKY couplings and therefore between the spin-zero and spin-one state).

Several theoretical groups have studied two Anderson impurities in a metal or systems of coupled quantum dots mimicking those. Various inter-impurity (inter-dot) interactions were considered, such as direct exchange coupling or RKKY interaction. In [65] a two impurity system was investigated using a variational approach in which doublet interactions of the Kondo impurities lead to ferromagnetic impurity coupling (which was not due to the RKKY interaction) enhancing the Kondo effect. In [63] and [64], the RKKY interaction was explicitly taken into account to describe the experimental situation of a double quantum dot given in [62]. Other theoretical works being concerned with coupled quantum dots can be found in [58, 59, 60, 66, 67].

In the last decade the attention of several theoretical and experimental groups has been drawn to the investigation of compact magnetic trimers on metallic substrates, since those are the minimal magnetic clusters to show frustration effects. The question was, whether some trimer geometries allowed for the development of the features of a Kondo effect while others did not.

In 1999 Uzdin *et al.* calculated the ground state properties of a compact chromium trimer on a non-magnetic surface using a modified Anderson model in Hartree-Fock approximation (see

[68]). They stated that the spins in a linear trimer will be collinear while other geometries lead to non-collinear spin arrangements which can either have a non-vanishing net-magnetic moment or a vanishing one. The net magnetic moment of an equilateral trimer, for example, should be zero, while an isosceles trimer should have a non-vanishing one. Similar results were found in [69] using local spin-density theory and Monte-Carlo methods.

In 2001 Jamneala *et al.* experimentally investigated compact triangular chromium trimers on gold (see [70]) by means of scanning tunnelling spectroscopy. They placed Cr atoms on an otherwise clean gold surface at 7 K and manipulated them with the tip of an STM to form artificial dimers and trimers. Then the low-energy excitation spectra were measured using STM spectroscopy. Single Cr atoms as well as dimers did not reveal any hints of a Kondo resonance in their dI/dV graph, their spectra being basically featureless. The conclusion was that the external temperature was significantly higher than the Kondo temperature connected to those configurations, so that no Kondo screening cloud could be formed. However, compact trimers showed a different behaviour. The experiments revealed that there were two different states a compact trimer could be in, one in which the dI/dV spectrum displayed no structure at all, as for single impurities and dimers, and one where the STM measurements showed a sharp dip around the Fermi energy. The latter was interpreted as being the result of a Kondo resonance. Jamneala *et al.* were able to switch reversibly between those two trimer states by manipulation of the geometry with the STM tip. While the featureless dI/dV spectrum in the first case implied that the Kondo temperature of the corresponding trimer configuration was still well below the external temperature, rearranging the geometry to a resonance showing trimer considerably increased the Kondo temperature (the line width implied a Kondo temperature of 50 ± 10 K compared to 7 K external temperature). Jamneala *et al.*'s explanation is, that the non-Kondo state is connected to the most symmetric case of an equilateral trimer in which the atomic spins align non-collinearly, so that the net magnetic moment of the trimer vanishes. This state should be a singlet, which does not allow any spin-flip scattering of the substrate electrons, and therefore no Kondo effect can occur. If the trimer is isosceles rather than equilateral, it gains a net magnetic moment (due to the separation of one of the atoms from the other two) which allows spin-flip scattering with the conduction electrons and therefore results in a Kondo effect. Thus, this geometric configuration was seen as being connected to the Kondo trimer state. Jamneala *et al.* also investigated more “loose” trimers, which showed no Kondo resonance though.

In the aftermath of [70], several theoretical works dealt with compact Cr trimer systems to reproduce the experimental results. Several different technical approaches were considered to tackle the problem, including variational methods, renormalisation group analysis, Monte-Carlo methods and mapping the trimer system to a single impurity model. Kudasov and Uzdin (see [71]) considered a Coqblin-Schrieffer model ([72]) to describe a Cr trimer on a metallic surface and provided it with an additional direct inter atomic exchange term. They dealt with this system by using a variational approach which allowed them to take into account superpositions of states in which some trimer atoms were in a Kondo singlet state while others kept their magnetic moment. Computing the ground state energies for several different geometric configurations of the trimer, they were able to estimate the corresponding Kondo temperature. However, the outcome was different from the interpretations of the results in [70]. The Kondo temperature of an equilateral Cr trimer was found to be always higher than that of a single impurity (up to two orders of magnitude higher), while a slight change of the geometry to isosceles form strongly suppressed the Kondo effect.

A different approach was chosen in 2005 by Lanzarovits *et al.* to describe an equilateral Cr trimer on gold (see [73]). Their starting point was a Hamiltonian taking into account spin-

2 Literature survey

spin interactions of the trimer (basically Heisenberg like with antiferromagnetic coupling) plus a term describing the Kondo coupling between trimer spins and the surrounding conduction electrons. The energy scale of the Kondo term was assumed to be much smaller than that of the inter-atomic interactions, so to describe the system in the low energy regime (where a Kondo effect could take place) they used a perturbative ansatz to transform the original Hamiltonian to an effective one (describing quantum fluctuations from the cluster spins). To determine the low-energy dynamics of the system and the Kondo temperature, they did a perturbative renormalisation group analysis, in which high energy conduction electrons are integrated out and the original bandwidth of the conduction band gradually becomes smaller and smaller. The outcome was that for large cluster spins the Kondo temperature of an equilateral trimer could be magnitudes higher than that of a single magnetic impurity (while the enhancement was not as large for smaller cluster spins), and that this increase was due to orbital fluctuations. Distortions from the equilateral shape of the trimer led to a lift of the ground state degeneracy of the spin-spin part of the Hamiltonian, thus suppressing orbital fluctuations and resulting in a much lower Kondo temperature. Contrary to the interpretation of the experimental results given in [70], isosceles trimers therefore were expected to exhibit no Kondo effect at the Kondo energy scale of the equilateral case.

Also in 2005, Savkin *et al.* tackled the trimer problem in [74] using the numerical continuous-time quantum Monte-Carlo method (see [75]). In this approach a random walk in the space of terms of the perturbation expansion for the Green's function is performed and the contributions are computed in terms of a path integral. Savkin *et al.* considered an effective exchange term for the trimer atoms, being modelled by a Kondo-lattice (since the trimer is the smallest non-trivial Kondo lattice). They investigated two different types of this effective interaction, namely a Heisenberg like one and an Ising like one, where spin-flip exchange terms are neglected. In an equilateral trimer, the latter type of interactions lead to no significantly different behaviour of the Kondo resonance in the antiferromagnetic case compared to the resonance of a single impurity. On the other hand, the Kondo peak in the density of states was strongly suppressed if the effective interactions were assumed to be Heisenberg like. In that case, the Kondo effect will thus be reduced in an equilateral trimer. If the geometry was slightly changed from an equilateral to an isosceles trimer, the Kondo resonance at the more weakly bonded adatom was restored, while it still did not appear at the other two atoms. Qualitatively, this is in good accordance with the results in [70].

A different ansatz to describe a compact magnetic chromium trimer on a gold surface was made by Aligia in [76]. The main idea in this approach is to map the trimer model to a single impurity Kondo model with an effective exchange interaction that depends on the geometry of the magnetic trimer. Aligia used a Hubbard-Anderson model that included a hopping term for the trimer atoms. He solved the part of the Hamiltonian which consists only of the trimer degrees of freedom exactly, retaining only the ground state doublet in the subspace of three particles. Then he made a generalised Schrieffer-Wolff transformation (see [8]), which mapped the full Hamiltonian to a single impurity Kondo model, in which the localised spin is given by the spin of said ground state doublet. The effective exchange interaction of the resulting s-d model depends on the geometry of the trimer. This interaction was computed for a two- and a three-dimensional band assuming that mostly itinerant electrons near the Fermi energy are involved in the relevant scattering processes. With the exchange coupling being known, the Kondo temperature can be estimated using its well known formula for a single magnetic impurity (see [11]). Aligia investigated the Kondo temperature for several isosceles geometries of the trimer. He found out that starting with the single impurity case (where the apex is

2 Literature survey

infinitely far away from the basis) the Kondo temperature increased up to a maximum at a certain configuration where the distance between the apex and any basis atom was still larger than the length of the basis, but then decreased again if an equilateral shape of the trimer was approached. Beyond this, when the trimer got more chain like, the Kondo temperature dropped down quickly. This behaviour was qualitatively in good accordance with [70]. Two scenarios were considered to explain the variation of the Kondo temperature. In the first, the decrease after reaching the maximum is due to symmetry effects, in the second, where the energy level of the trimer atoms has to be closer to the Fermi energy, the ground state of an equilateral trimer is a singlet which prevents the system from developing a Kondo effect.

In the last part of this literature survey we want to give a brief overview over the development of a more technical method to describe spin systems in terms of fermions which is called "semi-fermionic".

In the present work, we want to compute the partition function of the system in terms of a fermionic path integral. If one wants to do so, there arises the well known problem of how to treat the spin parts of the Hamiltonian. The interacting part of the Hamiltonian modelling the present system of a given number of magnetic impurities embedded on the surface of a metallic host has the form of an s - d model with a localised spin describing each impurity. Since a spin is not given by a fermionic operator, it is not quite obvious how the partition function could be written as a fermionic path integral. Although spin operators can be represented in terms of bilinear forms of fermionic construction operators (see [77], here the fermionic representation is given for general $SU(N)$ operators and spin- $\frac{1}{2}$ operators are two-dimensional representations of $SU(2)$ generators), one has to accept some ambiguities to arise. The problem is that representing spins in a fermionic way leads to a dimensionality problem, since the state space constructed by the fermionic operators is always larger than the spin space (the dimensionality of the spin representation matrices). It is a non-trivial question how to eliminate these superfluous states and it is usually quite complicated to establish diagrammatic techniques ([78, 79, 80, 81]). In [82] Popov and Fedotov suggested a method of cancelling the contributions of these superfluous states in spin- $\frac{1}{2}$ and spin-1 Hamiltonians by introducing a purely imaginary chemical potential term into the partition function in which moreover the spin Hamiltonian is replaced by the one in which the spin operators are being given in fermionic form. The original partition function is thus given by a partition function of a fermionic system with an imaginary chemical potential which can be computed in terms of a fermionic path integral, since only fermionic operators appear. When computing these integrals and the corresponding unperturbed Green's function, it turns out that the Matsubara frequencies (see [83]) are neither fermionic nor bosonic, which is not unexpected since the original spin system is neither. Due to this fact, the method is sometimes called "semi-fermionic".

We are going to use this ansatz of Popov and Fedotov in the present work. The method was generalised to arbitrary spin by Veits et al. (see [84]) and even to any $SU(N)$ pseudo spin with arbitrary occupation by Kiselev et al. (see [85]). These cases are more complicated but still follow the idea that contributions of unphysical states in the partition function are cancelled by introducing (several) imaginary chemical potentials. The original partition function is then given in a more complicated way, namely as a weighted sum of partition functions of fermionic systems with imaginary chemical potential. But still, each such partition function can be computed as a fermionic path integral with a well known related diagrammatic expansion, although the corresponding Matsubara frequencies are neither fermionic nor bosonic anymore. We will not have to make use of any of this more advanced methods here. However, for generalising the presented model to impurity clusters with a total occupation differing from the cluster size, the

2 Literature survey

knowledge of treating $SU(N)$ pseudo spin Hamiltonians is necessary (see chapter 7). [86] gives a very comprehensive overview on how to deal with $SU(N)$ pseudo spin Hamiltonians (which of course includes the case of the ordinary spin) in equilibrium and non-equilibrium systems.

3 The model

We consider a system consisting of N magnetic impurities on a metallic substrate. The impurities shall be one-level, all with energy ε_d . Moreover, we assume the total occupation of the magnetic cluster to be N at all times and that each impurity is singly occupied. In chapter 4 we will compute the partition function and the local density of states for such a system in mean field theory for an unspecified N , while in chapter 5 we will consider a trimer of isosceles geometry, say $N = 3$, and present concrete results. We are going to present the trimer system in more detail in section 3.2.

3.1 N atomic cluster

A system of N magnetic impurities on a metallic substrate is quite well described by the Anderson model (see [38]) for which the Hamiltonian reads

$$\hat{H} = \sum_{\mathbf{k}\sigma} \varepsilon_{\mathbf{k}} N_{\mathbf{k}\sigma} + \sum_{j\sigma} \varepsilon_d n_{j\sigma} + \sum_{j=1}^N U n_{j\uparrow} n_{j\downarrow} + \sum_{j=1}^N \sum_{\mathbf{k}\sigma} \left(T_{j\mathbf{k}} c_{j\sigma}^\dagger a_{\mathbf{k}\sigma} + \text{h.c.} \right). \quad (3.1.1)$$

Here, $a_{\mathbf{k}\sigma}$ is the annihilation operator in the substrate, $c_{j\sigma}$ is the one for the j -th atom, $N_{\mathbf{k}\sigma}$ and $n_{j\sigma}$ are the particle number operators in the substrate and in the j -th atom respectively, ε_d is the energy level of the cluster atoms, U the Hubbard interaction and $T_{j\mathbf{k}}$ is proportional to the tunnelling amplitude $|T(\mathbf{k})|$. Moreover, the absolute value of $T_{j\mathbf{k}}$ should be the same for all j and

$$\sum_j |T_{j\mathbf{k}}|^2 = |T(\mathbf{k})|^2.$$

This justifies to write

$$\begin{aligned} T_{j\mathbf{k}} &= \frac{1}{\sqrt{N}} e^{-i\mathbf{R}_j \mathbf{k}} |T(\mathbf{k})| \\ &= t_{j\mathbf{k}} |T(\mathbf{k})|, \end{aligned}$$

where \mathbf{R}_j is the position of the j -th atom and where we defined

$$t_{j\mathbf{k}} = \frac{1}{\sqrt{N}} e^{-i\mathbf{R}_j \mathbf{k}}. \quad (3.1.2)$$

The dominating scattering processes will involve substrate electrons in the vicinity of the Fermi level, so that we can approximately neglect the \mathbf{k} -dependence of $|T(\mathbf{k})|$ and write

$$|T(\mathbf{k})| \approx |T(\mathbf{k}_{Fermi})| = T_F.$$

To simplify our notation, we combine the position dependent part of the tunnelling amplitude with the substrate operators to a new quantity

$$\psi_{j\sigma}(\mathbf{k}) = t_{j\mathbf{k}} a_{\mathbf{k}\sigma}.$$

3 The model

Moreover, we define the 2-dimensional vectors

$$\Phi_i = (c_{i\uparrow}, c_{i\downarrow})^T$$

and

$$\Psi_i(\mathbf{k}) = (\psi_{i\uparrow}(\mathbf{k}), \psi_{i\downarrow}(\mathbf{k}))^T.$$

The interacting part of the Anderson Hamiltonian can thus be written as

$$\hat{H}_T = \sum_{j=1}^N \sum_{\mathbf{k}\sigma} \left(T_{j\mathbf{k}} c_{j\sigma}^\dagger a_{\mathbf{k}\sigma} + \text{h.c.} \right) = \sum_{\mathbf{k}} \sum_{j=1}^N T_F \left(\Phi_i^\dagger \cdot \Psi_i(\mathbf{k}) + \Psi_i(\mathbf{k})^\dagger \cdot \Phi_i \right).$$

If the tunnelling amplitudes are small compared to the other occurring energies, one can expand the Hamiltonian (3.1.1) in terms of the interaction constant

$$J \propto \frac{T_F^2}{N} \left(\frac{1}{\varepsilon_d + U} - \frac{1}{\varepsilon_d} \right) \ll 1 \quad (3.1.3)$$

using a Schrieffer-Wolff transformation (see [8]). The proper Kondo regime is given for

$$\varepsilon_d < 0 < \varepsilon_d + U,$$

where we set the Fermi energy $\varepsilon_F = 0$. We perform the Schrieffer-Wolff transformation in detail in appendix A.4. In first order approximation in J , the Anderson Hamiltonian (3.1.1) is transformed into

$$H = H'_0 + N \cdot J \sum_{\mathbf{k}\mathbf{k}'} \sum_{i=1}^N \sum_{\nu=1}^3 \left[\Phi_i^\dagger \sigma^\nu \Phi_i \right] \cdot \left[\Psi_i^\dagger(\mathbf{k}) \sigma^\nu \Psi_i(\mathbf{k}') \right], \quad (3.1.4)$$

with the Pauli spin matrices σ^ν and where

$$H'_0 = \sum_{\mathbf{k}\sigma} \varepsilon_{\mathbf{k}} N_{\mathbf{k}\sigma} + \sum_{j\sigma} \varepsilon'_d n_{j\sigma} + \sum_j U' n_{j\uparrow} n_{j\downarrow}.$$

The primed quantities ε'_d and U' are just slightly shifted in energy compared to ε_d and U respectively. We assume the energy ε'_d to be large compared to J . The term

$$\sum_{j=1}^N \varepsilon'_d n_{j\sigma}$$

does not play an important role to describe the physics of the system and we will skip it. Moreover, we want each of the impurities to be singly occupied at any time, which means $U' \rightarrow \infty$. Thus, we can also omit the Hubbard term. The resulting model Hamiltonian is

$$H = \sum_{\mathbf{k}\sigma} \varepsilon_{\mathbf{k}} N_{\mathbf{k}\sigma} + N \cdot J \sum_{\mathbf{k}\mathbf{k}'} \sum_{i=1}^N \sum_{\nu=1}^3 \left[\Phi_i^\dagger \sigma^\nu \Phi_i \right] \cdot \left[\Psi_i^\dagger(\mathbf{k}) \sigma^\nu \Psi_i(\mathbf{k}') \right] \quad (3.1.5)$$

with the additional constraint that each impurity is singly occupied, meaning that the cluster always stays in a most spinfull state. This constraint is implemented into the model by the semi-fermionic Popov-Fedotov method of imaginary chemical potentials, which will be discussed

3 The model

in the next paragraph. The interacting part of the resulting s - d model Hamiltonian (3.1.5) has the form of a Kondo Hamiltonian for each cluster site. However, since there is more than one impurity, additional effects apart from the Kondo effect will occur. Expanding (3.1.5) to second order perturbation theory in J will yield cross-over terms connecting different impurity sites, which will give rise to the RKKY effect.

We turn to the constraint that each impurity is singly occupied. The quantity which we have to compute for describing the physics of the system is the partition function, which without any constraints would be

$$Z = \text{Tr} \exp(-\beta H). \quad (3.1.6)$$

However, this expression is not the partition function of the problem presented here, since it does not comply with the constraint that each magnetic impurity is singly occupied. If we simply performed the trace, we would get contributions of states which correspond to empty or doubly occupied impurity sites. It is necessary to eliminate those contributions from the partition function. Popov and Fedotov suggested a method that does so, introducing imaginary chemical potentials. We will give a more detailed outline of the method in appendix A.5. A full presentation can be found in [82] and [85]. Using this method, the proper partition function of the system is given as

$$Z = i^N \cdot \text{Tr} \exp \left(-\beta \left[H - \mu \sum_{j\sigma} n_{j\sigma} \right] \right), \quad (3.1.7)$$

where $n_{j\sigma}$ as in (3.1.1) is the particle number operator of the cluster sites, and where

$$\mu = -\frac{i\pi}{2\beta}$$

is a purely imaginary chemical potential. Equation (3.1.7) yields no contributions of states which correspond to empty or doubly occupied sites. On the physical space of all states describing singly occupied impurities, it coincides with (3.1.6). Since we will compute the partition function via a path integral approach, we will have to add such an imaginary chemical potential term to the action of the system.

We are going to approach the problem by a mean field approximation. The "mean field" is the mean hybridisation between the itinerant and the localised degrees of freedom. In chapter 4 (and in more detail in appendix B.1) we are going to perform a Hubbard-Stratonovich transformation (see [87]) of the interacting part of the model Hamiltonian (3.1.5). If we fix the auxiliary bosonic fields related to this transformation, the Kondo term in (3.1.5) becomes

$$\frac{1}{NJ} \sum_{j=1}^N b_j^2 + \sum_{\mathbf{k}} \sum_{j=1}^N b_j t_{j\mathbf{k}}^* a_{\mathbf{k}\sigma}^\dagger c_{j\sigma} + \sum_{\mathbf{k}} \sum_{j=1}^N b_j t_{j\mathbf{k}} c_{j\sigma}^\dagger a_{\mathbf{k}\sigma},$$

where the b_j are the mean field parameters, say the mean hybridisations of the degrees of freedom of the substrate and the cluster. Using this altered interaction term, we can compute the partition function and the local density of states of the problem (chapter 4). The parameters b_j are determined by the mean field equations

$$\frac{\partial \log Z}{\partial b_j} = 0$$

3 The model

which means minimisation of the free energy. The most important quantity which we are going to compute is the local density of states. At low temperatures, it is proportional to the differential conductance dI/dV , which can be measured in STM experiments. In the Kondo regime, the width of the energy resolved local density of states (and thus the one of the differential conductance) is proportional to the Kondo temperature, which characterises the system completely, since it determines below which temperature the Kondo cloud is formed. For a single magnetic impurity, the Kondo temperature is known to be given as

$$T_0 = \Delta e^{-\frac{1}{2J\rho_0}}$$

(see [38]), where Δ is the bandwidth of the substrate and ρ_0 is the unperturbed density of states of the substrate at the Fermi level. We will see, that this case is contained in the model presented here, if the effective interactions between distinct magnetic impurities vanish. For non-vanishing effective inter-impurity interactions, the idea still is to determine the Kondo temperature by computing the width of the differential conductance. However, at distinct sites the widths could be different, thus giving rise to a varying Kondo temperature. At a given external temperature, the Kondo effect could already occur at some sites of the cluster while it would not at some other.

The key to determining the width of the differential conductance (or the corresponding local density of states) in the Kondo regime is to fit it to the shape of a Kondo-Fano resonance (see [29])

$$\rho(\omega) = \rho_0 \frac{(q\pi\Gamma + \omega)^2}{\omega^2 + (\pi\Gamma)^2},$$

where q is the Fano factor (which depends on the coupling of the STM tip to the sample).

3.2 Magnetic isosceles trimer

As a concrete example of a cluster composed of magnetic impurities, we will consider an isosceles trimer. In general, this can be described like any other N -atomic cluster, so that we will be able to make use of all formulas for the case of N impurities, especially the ones for the mean field equations and the local density of states. As for N atoms, there will occur effective interactions between the spins of the distinct trimer atoms, which have to comply with the geometry of the trimer. Figure 3.1 shows a schematic of the magnetic isosceles trimer. The effective interaction between the basis atoms is determined by the coupling g_2 while the coupling g_1 gives rise to the effective interactions between the basis atoms and the apex atom. g_0 is the on-site coupling. These effective couplings are determined by scattering processes of the substrate electrons. g_0 is proportional to the unperturbed density of states of the underlying substrate at the Fermi level by $g_0 = \rho_0/3$, while g_1 and g_2 reflect the RKKY interaction. In general, the couplings decrease with increasing inter atomic distances (up to a superimposed oscillation).

The effective inter impurity interactions can be ferromagnetic as well as antiferromagnetic leading to a corresponding alignment of the impurity spins. In this work, we are only interested in ground state properties, since we are going to perform the calculations for vanishing temperature. If g_2 corresponds to ferromagnetic interaction, there is a stable ground state which is non-degenerate up to switching of all spins. The basis atoms then will align ferromagnetically and the apex spin will either align ferromagnetically (if g_1 is ferromagnetic) or antiferromagnetically (if g_1 gives rise to antiferromagnetic interactions). If g_2 entails an effective antiferromagnetic coupling, the ground state is degenerate. In this case, the apex spin cannot align ferromagnetically or antiferromagnetically with both spins of the basis. Hence, two of the three trimer

3 The model

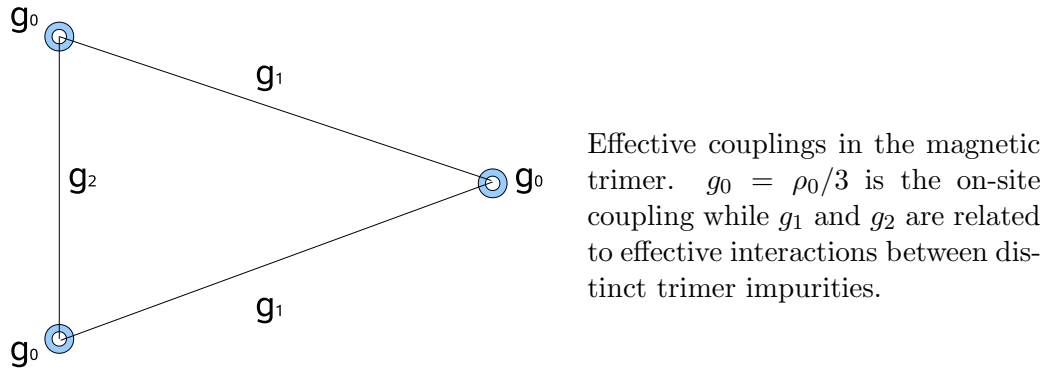


Figure 3.1: Schematic of isosceles trimer

spins are always frustrated, if they have non-vanishing projections on each other. One could expect that this frustration of spins has an effect on the geometrical behaviour of the Kondo temperature at a certain site. However, the results show that the influence of frustration on the system has to be rather small if all couplings are antiferromagnetic. In the case of mixed interactions (with g_2 being antiferromagnetic and g_1 ferromagnetic), frustration seems to have a strong influence on the geometric behaviour of the Kondo temperature.

4 Cluster of N atoms

In this chapter, we are going to perform the mean field calculations for a cluster of arbitrary size and structure (being composed of N arbitrarily arranged impurities). However, we will only be able to derive formal results. For a given cluster of a specific geometry, certain N -dimensional matrices have to be diagonalised, which in general is of course not manageable analytically. We will give an example in the next chapter, where we consider an isosceles trimer.

In the present chapter we will start performing a Hubbard-Stratonovich transformation to achieve an action which is at most quadratic in the fermionic construction operators. Then, we will compute the partition function in a static mean field approximation and derive the mean field equations. After that, we will formally calculate the Matsubara Green's function of the system and its local density of states, the latter being the crucial quantity for the scope of describing the outcome of an STM experiment at low temperatures.

Some insight can already be gained from the formal calculations done in this chapter. We will see that a system of isolated cluster atoms behaves like a combination of pure Kondo systems, which one would expect in this limiting case. Moreover, we are going to prove a theorem on the local density of states which implies that our model is only valid if the inter atomic distances are sufficiently large.

4.1 Hubbard-Stratonovich transformation and mean field approximation of the interaction

To compute the partition function of the system under consideration here, we use the path integral approach (see [87] or [90]). To this end, one has to determine the action of the problem which contains the Hamiltonian of the system with all fermionic operators being replaced by Grassman numbers. In general, it is only possible to analytically perform path integrals of Gaussian type, i.e. those in which the action is at most quadratic in the Grassman variables. However, after the Schrieffer-Wolff transformation, the action of the present system also includes quartic Grassman terms and can thus not be treated via a path integral approach as it stands.

The Hubbard-Stratonovich transformation (see [87]) decouples terms being quartic in the fermionic operators and reduces them to quadratic ones. The fermionic path integrals then become of Gaussian type and can be computed analytically. In exchange, certain auxiliary bosonic fields have to be introduced, which also have to be integrated over; this integration still cannot be done analytically. However, in a static mean field approach, the auxiliary fields are fixed at specific values, thus omitting the final integration over them. In this section, we are going to give the main results of the Hubbard-Stratonovich transformation of the interacting parts of the action. Moreover, we will determine their forms in a static mean field approach. For detailed calculations, see appendix B.1.

After a Schrieffer-Wolff transformation of the Anderson model to the low energy sector, the

4 Cluster of N atoms

interaction between cluster fermions and the substrate becomes

$$H_I = N J' \sum_{i=1}^N \sum_{\nu=1}^3 \sum_{\mathbf{k}\mathbf{k}'} \left(\Phi_i^\dagger \sigma^\nu \Phi_i \right) \left(\Psi_i^\dagger(\mathbf{k}) \sigma^\nu \Psi_i(\mathbf{k}') \right)$$

(see A.4.8). This term is quartic in the fermionic operators and therefore, the corresponding path integral cannot be analytically performed. Via a Hubbard-Stratonovich transformation, we can reduce the fermionic terms to second order but in exchange have to introduce auxiliary bosonic fields. These fields $Q_{\sigma\rho}^{i\tau}$ (with Greek indices referring to the spin and τ to the imaginary time) define hermitian 2×2 -matrices $\underline{Q}^{i\tau}$ for each $i = 1 \dots N$ which can be represented as

$$\underline{Q}^{i\tau} = \sum_{\mu} q_{\mu}^{i\tau} \sigma^{\mu} \quad (4.1.1)$$

(see section A.2), where the coefficients $q_{\mu}^{i\tau}$ are real valued. The Hubbard-Stratonovich transformation essentially is a transformation of the variable of integration combined with a completion of the square. Using the representation (4.1.1), the Hubbard-Stratonovich transformation yields for each (imaginary) time τ

$$e^{-H_I} = C' \int d\underline{Q}^{i\tau} \exp \left\{ \frac{1}{2} \frac{1}{N J'} \sum_{i\mu} (q_{\mu}^{i\tau})^2 - \frac{2}{N J'} \sum_i (q_0^{i\tau})^2 + \sum_{i\mathbf{k}} \overline{\Psi}_i^{\tau}(\mathbf{k}) \left(\frac{1}{2} \underline{Q}^{i\tau} - 2 q_0^{i\tau} \sigma^0 \right) \Phi_i^{\tau} \right. \\ \left. + \sum_{i\mathbf{k}} \overline{\Phi}_i^{\tau} \left(\frac{1}{2} \underline{Q}^{i\tau} - 2 q_0^{i\tau} \sigma^0 \right) \Psi_i^{\tau}(\mathbf{k}) \right\}.$$

C' is a (physically irrelevant) constant. Up to now, we did not gain any advantages with regard to path integration. If we perform either the fermionic or the bosonic integration first, the remaining integration still will not be accomplishable analytically. In order to be able to perform the path integration, we have to use some approximation. We will choose the most simple one and do some static mean field theory.

In a static mean field approximation, the bosonic fields $\underline{Q}^{i\tau}$ are fixed to certain, time independent values (determined by the mean field equations). They act as fields describing the (mean) interaction between the degrees of freedom of the fixed and the itinerant electrons. Since the model does not prefer a specific direction of the spin, we adopt the form

$$\underline{Q}^{i\tau} = \frac{2}{3} b_i \mathbb{1}_2 = q_0^i \sigma^0 \quad (4.1.2)$$

for the auxiliary fields in the mean field approach. Here, b_i is real valued (the factor $2/3$ is just for convenience, see appendix B.1). For the sake of a simple notation, we define

$$J = \frac{3}{4} J'$$

and the matrix

$$\underline{b} = \text{diag}(b_i | i = 1 \dots N). \quad (4.1.3)$$

Moreover we introduce the $2N$ -dimensional vectors

$$\Phi = (\Phi_i | i = 1 \dots N)^{\text{T}} \quad \text{and} \quad \Psi(\mathbf{k}) = (\Psi_i(\mathbf{k}) | i = 1 \dots N)^{\text{T}}.$$

Using (4.1.2) and the latter definitions, we arrive at

$$e^{-H_I} = C' \exp \left\{ -\frac{1}{N J} \text{Tr} \underline{b}^2 - \sum_{\mathbf{k}} \overline{\Psi}^{\tau}(\mathbf{k}) (\underline{b} \otimes \mathbb{1}_2) \Phi^{\tau} - \sum_{\mathbf{k}} \overline{\Phi}^{\tau} (\underline{b} \otimes \mathbb{1}_2) \Psi^{\tau}(\mathbf{k}) \right\} \quad (4.1.4)$$

for each (imaginary) time τ .

4.2 Partition function in mean field theory

In this section we are going to present the main steps of computing the partition function of the problem in mean field theory. We will first state the path integral of the problem and then calculate it approximately. For further details of the calculations, see appendix B.2.

We will start with writing down the partition function in mean field in terms of a path integral. We will use the Hubbard-Stratonovich transformed terms (4.1.4) in mean field and we will Fourier transform the occurring Grassman fields from (imaginary) time space to frequency space

$$\phi_{i\sigma}^\tau \rightarrow \phi_{i\sigma}^{i\omega_n}, \quad a_{\mathbf{k}\sigma}^\tau \rightarrow a_{\mathbf{k}\sigma}^{i\omega_n}.$$

We recall that

$$\psi_{i\sigma}(\mathbf{k}) = t_{i\mathbf{k}} a_{\mathbf{k}\sigma} = \frac{1}{\sqrt{N}} e^{-i\mathbf{R}_i \mathbf{k}} a_{\mathbf{k}\sigma}.$$

The $2N$ -dimensional vector $\Psi(\mathbf{k})$ can thus be written as

$$\Psi(\mathbf{k}) = t_{\mathbf{k}} \otimes a_{\mathbf{k}},$$

where $t_{\mathbf{k}}$ is a N -dimensional vector composed of the $t_{i\mathbf{k}}$, and $a_{\mathbf{k}}$ is a two-dimensional vector composed of $a_{\mathbf{k}\uparrow}, a_{\mathbf{k}\downarrow}$. For the localised degrees of freedom, we will use the Popov-Fedotov method of imaginary chemical potentials, which for singly occupied cluster sites means, that one has to include a term

$$-\frac{i\pi}{2\beta} \bar{\Phi} \cdot \Phi$$

in the action. For the sake of a brief notation and more clarity, we define the unperturbed Green's function $G_{i\omega_n}(\mathbf{k})$ of the itinerant degrees of freedom by

$$G_{i\omega_n}^{-1}(\mathbf{k}) = i\omega_n - \varepsilon_{\mathbf{k}} \quad (4.2.1)$$

and the unperturbed Green's function $D_{i\omega_n}$ of the localised degrees of freedom by

$$D_{i\omega_n}^{-1} = i\omega_n - \frac{i\pi}{2\beta}. \quad (4.2.2)$$

The partition function in static mean field theory is then given as

$$\begin{aligned} Z_{MF} = C e^{-\frac{\beta}{N} \text{Tr} \mathbf{b}^2} \int \mathcal{D}(\bar{\Phi}, \Phi, \bar{a}, a) \exp \left(- \sum_{i\omega_n} \left[\sum_{\mathbf{k}} \bar{a}_{\mathbf{k}}^{i\omega_n} G_{i\omega_n}^{-1}(\mathbf{k}) \mathbb{1}_2 a_{\mathbf{k}}^{i\omega_n} + \bar{\Phi}^{i\omega_n} D_{i\omega_n}^{-1} \mathbb{1}_{2N} \Phi^{i\omega_n} \right. \right. \\ \left. \left. - \sum_{\mathbf{k}} (t_{\mathbf{k}}^\dagger \otimes \bar{a}_{\mathbf{k}}^{i\omega_n})(\mathbf{b} \otimes \mathbb{1}_2) \Phi^{i\omega_n} - \sum_{\mathbf{k}} \bar{\Phi}^{i\omega_n} (\mathbf{b} \otimes \mathbb{1}_2) (t_{\mathbf{k}} \otimes a_{\mathbf{k}}^{i\omega_n}) \right] \right). \end{aligned} \quad (4.2.3)$$

We denote the prefactor of the path integral as $C Z_0$. C is a constant, but it is of no importance to us, since all quantities of interest are derivatives of logarithms of the partition function, so that C never has to be taken into account. One can rewrite the integral (4.2.3) by defining the vector

$$\chi^{i\omega_n} = \left(\phi_{1\uparrow}^{i\omega_n}, \phi_{1\downarrow}^{i\omega_n}, \dots, \phi_{3\uparrow}^{i\omega_n}, \phi_{3\downarrow}^{i\omega_n}, \left\{ a_{\mathbf{k}\uparrow}^{i\omega_n}, a_{\mathbf{k}\downarrow}^{i\omega_n} | \mathbf{k} \right\} \right)^T,$$

4 Cluster of N atoms

so that

$$\begin{aligned} Z_{MF} &= C Z_0 \int D(\bar{\chi}, \chi) \exp \left(- \sum_{i\omega_n} \bar{\chi}^{i\omega_n} (\underline{M}_{i\omega_n} \otimes \mathbb{1}_2) \chi^{i\omega_n} \right) \\ &= C Z_0 \prod_{i\omega_n} (\det \underline{M}_{i\omega_n})^2 = C Z_0 \exp \left(2 \sum_{i\omega_n} \text{Tr} \log \underline{M}_{i\omega_n} \right), \end{aligned}$$

where the matrix $\underline{M}_{i\omega_n}$ is defined by (4.2.3). For details, see appendix B.2. The matrix $\underline{M}_{i\omega_n}$ can be unitarily transformed into another matrix $\tilde{\underline{M}}_{i\omega_n}$ such that

$$\det \underline{M}_{i\omega_n} = \det \tilde{\underline{M}}_{i\omega_n} = \exp \text{Tr} \log \tilde{\underline{M}}_{i\omega_n}.$$

This matrix $\tilde{\underline{M}}_{i\omega_n}$ has the form

$$\tilde{\underline{M}}_{i\omega_n} = \begin{pmatrix} \hat{\underline{X}}_{i\omega_n} & 0 \\ \underline{A} & \text{diag} (G_{i\omega_n}^{-1}(\mathbf{k}) | \mathbf{k}) \end{pmatrix}$$

with \underline{A} being irrelevant for the determinant and with the $N \times N$ -matrix $\hat{\underline{X}}_{i\omega_n}$ being defined as

$$\begin{aligned} (\hat{\underline{X}}_{i\omega_n})_{ij} &= D_{i\omega_n}^{-1} \delta_{ij} - \sum_{\mathbf{k}} (t_{\mathbf{k}}^\dagger \underline{b}^*)_{i\mathbf{k}} (\underline{b} t_{\mathbf{k}})_j G_{i\omega_n}(\mathbf{k}) \\ &= D_{i\omega_n}^{-1} \delta_{ij} - \sum_{i'j'} \underline{b}_{ii'} \left(\frac{1}{N} \sum_{\mathbf{k}} \frac{e^{i(\mathbf{R}_{i'} - \mathbf{R}_j) \mathbf{k}}}{i\omega_n - \varepsilon_{\mathbf{k}}} \right) \underline{b}_{j'j} \end{aligned} \quad (4.2.4)$$

$$= D_{i\omega_n}^{-1} \delta_{ij} - b_i \left(\frac{1}{N} \sum_{\mathbf{k}} \frac{e^{i(\mathbf{R}_i - \mathbf{R}_j) \mathbf{k}}}{i\omega_n - \varepsilon_{\mathbf{k}}} \right) b_j, \quad (4.2.5)$$

where we used the definition of $t_{i\mathbf{k}}$ as well as the fact that \underline{b} is diagonal. The partition function is thus given as

$$Z_{MF} = C Z_0 e^{2 \sum_{i\omega_n} \sum_{\mathbf{k}} \log G_{i\omega_n}^{-1}(\mathbf{k})} \exp \left(2 \sum_{i\omega_n} \text{Tr} \log \hat{\underline{X}}_{i\omega_n} \right). \quad (4.2.6)$$

The exponential term consisting of unperturbed Green's functions of substrate electrons only, will not have to be taken into account if we look at derivatives of logarithms of the partition function with respect to the auxiliary fields. Thus, we absorb it into the prefactor C . To compute the partition function more explicitly, we obviously have to diagonalise the matrices $\hat{\underline{X}}_{i\omega_n}$ to get the eigenvalues. To this end, we define the matrix $\tilde{\underline{g}}(i\omega_n)$ by

$$(\tilde{\underline{g}}(i\omega_n))_{ij} = \frac{1}{N} \sum_{\mathbf{k}} \frac{e^{i(\mathbf{R}_i - \mathbf{R}_j) \mathbf{k}}}{i\omega_n - \varepsilon_{\mathbf{k}}} \quad (4.2.7)$$

so that

$$\hat{\underline{X}}_{i\omega_n} = D_{i\omega_n}^{-1} \mathbb{1}_N - \underline{b} \tilde{\underline{g}}(i\omega_n) \underline{b}.$$

One can compute the sum (which of course is meant as an integral) in (4.2.7) approximately if the band structure is known. However, for the following, the explicit form is not as important as the general structure of the matrix. By taking the adjoint, we see

$$(\tilde{\underline{g}}(i\omega_n))_{ji}^* = \frac{1}{N} \sum_{\mathbf{k}} \frac{e^{-i(\mathbf{R}_j - \mathbf{R}_i) \mathbf{k}}}{-i\omega_n - \varepsilon_{\mathbf{k}}} = (\tilde{\underline{g}}(-i\omega_n))_{ij}.$$

4 Cluster of N atoms

Moreover, writing down the integral

$$(\tilde{\mathbf{g}}(i\omega_n))_{ij} = \int dk \int d\phi f(k, \phi) \frac{e^{i|\mathbf{R}_i - \mathbf{R}_j|k \cos \phi}}{i\omega_n - \varepsilon_k} \quad (4.2.8)$$

for two or three dimensions, where k is the absolute value of \mathbf{k} and ϕ the angle between $\mathbf{R}_i - \mathbf{R}_j$ and \mathbf{k} , one can see that

$$(\tilde{\mathbf{g}}(i\omega_n))_{ji} = (\tilde{\mathbf{g}}(i\omega_n))_{ij}.$$

For a broad and flat band the diagonal elements of $\tilde{\mathbf{g}}$ can be computed to

$$[\tilde{\mathbf{g}}(i\omega_n)]_{ii} = -i\pi \operatorname{sgn}(\omega_n) \frac{\rho_0}{N} = -i\pi \operatorname{sgn}(\omega_n) g_0,$$

where ρ_0 is the unperturbed electronic density of states (for the case without impurities) and where we defined g_0 . Computing also the off-diagonal terms, one arrives at the general formula

$$\tilde{\mathbf{g}}(i\omega_n) = -i\pi \operatorname{sgn}(\omega_n) [\mathbf{g}^R + i \operatorname{sgn}(\omega_n) \mathbf{g}^I] = -i\pi \operatorname{sgn}(\omega_n) \mathbf{g}(i\omega_n), \quad (4.2.9)$$

where \mathbf{g}^R and \mathbf{g}^I are real valued symmetric matrices (not depending on ω_n) and where we defined the matrix $\mathbf{g}(i\omega_n)$. The diagonal elements of \mathbf{g}^R are all given by g_0 and \mathbf{g}^I has a vanishing diagonal. We remark that always

$$\left| (\mathbf{g}^{R/I})_{ij} \right| \leq g_0,$$

for all i, j . The derivation of (4.2.9) is given in more detail in appendix B.2. We remark that in a two-dimensional substrate the coordinate dependence of the off-diagonal entries of $\mathbf{g}(i\omega_n)$ is that of Bessel functions with arguments $z = k_F |\mathbf{R}_i - \mathbf{R}_j|$. Since the Fermi wave vector is the inverse Fermi wavelength, z measures distance as multiples of the Fermi wavelength. For large arguments z (that is $z > 1$), the $[\mathbf{g}(i\omega_n)]_{ij}$ decay like $\sqrt{2/\pi z} \cdot \cos(z - \pi/4)$.

The matrix $\hat{\mathbf{X}}_{i\omega_n}$ can be written as

$$\hat{\mathbf{X}}_{i\omega_n} = D_{i\omega_n}^{-1} \mathbb{1}_N + i\pi \operatorname{sgn}(\omega_n) \underline{\mathbf{b}} \mathbf{g}(i\omega_n) \underline{\mathbf{b}}.$$

In order to diagonalise the matrix $\hat{\mathbf{X}}_{i\omega_n}$, we have to diagonalise the matrix $\underline{\mathbf{b}} \mathbf{g}(i\omega_n) \underline{\mathbf{b}}$. The way this is done depends on the size and geometric configuration of the cluster. We are going to give the result of the diagonalisation in the case of an isosceles trimer in chapter 5. The matrix $\underline{\mathbf{b}} \mathbf{g}(i\omega_n) \underline{\mathbf{b}}$ is connected to the RKKY interaction which depends on the geometry of the trimer. We are going to discuss the physical meaning of the matrix in section 4.2.1.

Let us assume the matrix $\underline{\mathbf{b}} \mathbf{g}(i\omega_n) \underline{\mathbf{b}}$ has been diagonalised. Because of the structure of $\mathbf{g}(i\omega_n)$, the eigenvalues are of the form

$$\hat{T}_j(i\omega_n) = T_j^R + i \operatorname{sgn}(\omega_n) T_j^I \quad (4.2.10)$$

for $j = 1 \dots N$ and with real valued $T_j^{R/I}$. We denote the eigenvectors as $\hat{u}_j(i\omega_n)$, and it holds

$$\hat{u}_j(i\omega_n) = \hat{u}_j(i \operatorname{sgn}(\omega_n)) = u_j^R + i \operatorname{sgn}(\omega_n) u_j^I \quad (4.2.11)$$

with real valued vectors u_j^R and u_j^I . Depending on the geometry of the cluster it is possible that some of the eigenvalues are degenerate. However, this does not affect the general results. But

in concrete calculations, when a fixed geometry is given, possible degeneracy of the eigenvalues has to be taken into account. Knowing the eigenvalues of $\underline{\hat{X}}_{i\omega_n}$, we can now give a more explicit form of the partition function (4.2.6). It is

$$Z_{MF} = \hat{C} Z_0 \exp \left(2 \sum_{i\omega_n} \sum_{j=1}^N \log \left[i\omega_n - \frac{i\pi}{2\beta} + i\pi \operatorname{sgn}(\omega_n) T_j^R - \pi T_j^I \right] \right). \quad (4.2.12)$$

Here, we absorbed the exponential factor depending only on the free electronic Green's function into the prefactor \hat{C} , and Z_0 is given as

$$Z_0 = \exp \left(-\frac{\beta}{NJ} \operatorname{Tr} \underline{\mathbf{b}}^2 \right) \quad (4.2.13)$$

The partition function (4.2.12) fixes all other quantities of interest. It determines the mean field equations, which specify the values of the mean field parameters $\underline{\mathbf{b}}$. Having the value of those parameters for a specific geometry, the local density of states (the quantity we are interested in most) can be explicitly computed.

4.2.1 RKKY interaction

Up to now, we have defined the matrix $\underline{\mathbf{b}} \mathbf{g}(i\omega_n) \underline{\mathbf{b}}$ but so far have not attached to it any physical content. It turns out, that this matrix is connected to the RKKY interaction.

After the Hubbard Stratonovich transformation, the interacting part of the s - d model Hamiltonian becomes

$$\frac{1}{NJ} \sum_{j=1}^N b_j^2 + \sum_{\mathbf{k}} \sum_{j=1}^N b_j t_{j\mathbf{k}}^* a_{\mathbf{k}\sigma}^\dagger c_{j\sigma} + \sum_{\mathbf{k}} \sum_{j=1}^N b_j t_{j\mathbf{k}} c_{j\sigma}^\dagger a_{\mathbf{k}\sigma}. \quad (4.2.14)$$

We fix the hybridisations b_i to their mean values in mean field theory. Therefore, the first term in (4.2.14) only gives rise to a constant. When computing the partition function, each term

$$b_j t_{j\mathbf{k}} c_{j\sigma}^\dagger a_{\mathbf{k}\sigma}$$

(or its hermitian conjugate) gives rise to a diagram shown on the left hand side in figure 4.1. The solid line corresponds to the itinerant degrees of freedom, the dashed line to the located cluster electrons and the vertex is given by $b_j t_{j\mathbf{k}}$. The RKKY interaction is an effective interaction

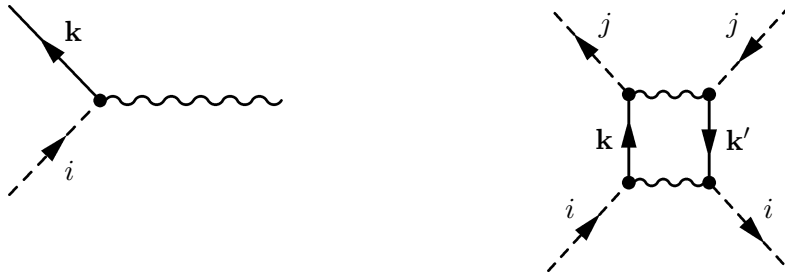


Figure 4.1: Interacting part after Hubbard-Stratonovich transformation, R.H.S.: RKKY interaction. Solid line correspond to itinerant degrees of freedom, dashed lines to localised ones, the vertex is given by $b_j t_{j\mathbf{k}}$.

4 Cluster of N atoms

between distinct located spins of the cluster. It is given as a diagram in fourth order perturbation in the bosonic auxiliary fields (see [38]). The diagram is shown on the right hand side of figure 4.1, and it has negative weight. The diagram includes a fermionic loop which gives an additional sign. Therefore its contribution to the RKKY interaction computes to

$$\begin{aligned}
& \left(b_i \sum_{\mathbf{k}} t_{i\mathbf{k}} t_{j\mathbf{k}}^* G_{i\omega_n}(\mathbf{k}) b_j \right) \left(b_j \sum_{\mathbf{k}'} t_{j\mathbf{k}'} t_{i\mathbf{k}'}^* G_{i\omega_n}(\mathbf{k}') b_i \right) \\
&= \left(b_i \sum_{\mathbf{k}} \frac{e^{-i|\mathbf{R}_i - \mathbf{R}_j|k}}{i\omega_n - \varepsilon_{\mathbf{k}}} b_j \right) \left(b_j \sum_{\mathbf{k}'} \frac{e^{-i|\mathbf{R}_j - \mathbf{R}_i|k'}}{i\omega_n - \varepsilon_{\mathbf{k}'}} b_i \right) \\
&= \left(-i\pi \operatorname{sgn}(\omega_n) b_i [\underline{\mathbf{g}}(i\omega_n)]_{ij} b_j \right) \left(-i\pi \operatorname{sgn}(\omega_n) b_j [\underline{\mathbf{g}}(i\omega_n)]_{ji} b_i \right) \\
&= -\pi^2 \left(b_i [\underline{\mathbf{g}}(i\omega_n)]_{ij} b_j \right)^2 \\
&= -\pi^2 (\underline{\mathbf{b}} \underline{\mathbf{g}}(i\omega_n) \underline{\mathbf{b}})_{ij}^2.
\end{aligned}$$

Here, we used the definitions (4.2.7) and (4.2.9). Thus, the RKKY interaction is connected to the matrix $\underline{\mathbf{b}} \underline{\mathbf{g}}(i\omega_n) \underline{\mathbf{b}}$. The matrix $\underline{\mathbf{b}}$ is always real-valued while the matrix $\underline{\mathbf{g}}(i\omega_n)$ can be real-valued or imaginary. Hence, the RKKY interaction between the i -th and the j -th site is ferromagnetic if $[\underline{\mathbf{g}}(i\omega_n)]_{ij}$ is real-valued (since its contribution to the Hamiltonian lowers the free energy in this case), and it is antiferromagnetic if $[\underline{\mathbf{g}}(i\omega_n)]_{ij}$ is imaginary.

4.3 Mean field equations

The partition function Z of a given system is connected to its free energy F by the relation

$$Z = e^{-\beta F}.$$

The value of the mean field parameters is determined by minimising the free energy. The auxiliary fields b_i , the entries of the diagonal matrix $\underline{\mathbf{b}}$, are therefore fixed by the system of equations given by

$$\frac{\partial \log Z_{MF}}{\partial b_i} = 0$$

for each i . Recalling the form of the prefactor Z_0 in (4.2.13)

$$Z_0 = \exp\left(-\frac{\beta}{NJ} \operatorname{Tr} \underline{\mathbf{b}}^2\right) = \exp\left(-\frac{\beta}{NJ} \sum_i b_i^2\right),$$

the mean field equations are given as

$$\begin{aligned}
\frac{\partial \log Z_{MF}}{\partial b_i} &= -\frac{2\beta}{NJ} b_i + 2 \sum_{j=1}^N \left[\frac{\partial T_j^R}{\partial b_i} \sum_{\omega_n} \frac{i\pi \operatorname{sgn}(\omega_n)}{i\omega_n - \frac{i\pi}{2\beta} + i\pi \operatorname{sgn}(\omega_n) T_j^R - \pi T_j^I} \right. \\
&\quad \left. - \frac{\partial T_j^I}{\partial b_i} \sum_{\omega_n} \frac{\pi}{i\omega_n - \frac{i\pi}{2\beta} + i\pi \operatorname{sgn}(\omega_n) T_j^R - \pi T_j^I} \right] = 0.
\end{aligned}$$

The frequency summations in the latter formula can be performed using the bandwidth Δ as energy cut-off, which is done in detail in appendix B.3. It is

$$\sum_{i\omega_n} \frac{i\pi \operatorname{sgn}(\omega_n)}{i\omega_n - \frac{i\pi}{2\beta} + i\pi \operatorname{sgn}(\omega_n) T_j^R - \pi T_j^I} = \frac{\beta}{2} \left[\Psi \left(\frac{\beta}{2} \Delta + \frac{\beta}{2} T_j^* + \frac{1}{4} \right) - \Psi \left(\frac{\beta}{2} T_j^* + \frac{1}{4} \right) \right. \\ \left. + \Psi \left(\frac{\beta}{2} \Delta + \frac{\beta}{2} T_j + \frac{3}{4} \right) - \Psi \left(\frac{\beta}{2} T_j + \frac{3}{4} \right) \right] \quad (4.3.1)$$

and

$$\sum_{i\omega_n} \frac{-\pi}{i\omega_n - \frac{i\pi}{2\beta} + i\pi \operatorname{sgn}(\omega_n) T_j^R - \pi T_j^I} = -i \frac{\beta}{2} \left[\Psi \left(\frac{\beta}{2} T_j^* + \frac{1}{4} \right) - \Psi \left(\frac{\beta}{2} T_j + \frac{3}{4} \right) \right], \quad (4.3.2)$$

where we defined

$$T_j = T_j^R - iT_j^I \quad \text{and} \quad T_j^* = T_j^R + iT_j^I \quad \text{respectively,} \quad (4.3.3)$$

and where Ψ denotes the Digamma function. For arguments of large absolute value, the Digamma function takes the form of the logarithm (see [88]):

$$\Psi(z) \approx \log(z) \quad \text{for} \quad |z| \gg 1.$$

Since we want to investigate the mean field equations in the limit of low temperatures, we assume $\beta \gg 1$ so that (4.3.1) and (4.3.2) get much simpler. In this limit, the mean field equations take the form

$$\sum_{j=1}^N \left[\frac{\partial T_j^R}{\partial b_i} \log \left(\frac{(T_j^R)^2 + (T_j^I)^2}{\Delta^2} \right) - 2 \frac{\partial T_j^I}{\partial b_i} \arctan \left(\frac{T_j^I}{T_j^R} \right) \right] = -\frac{2}{NJ} b_i \quad (4.3.4)$$

Here, we assumed $|T_j| \ll \Delta$. We are going to see in section 4.5 that this assumption means

$$J\rho_0 \ll 1 \quad (4.3.5)$$

(ρ_0 being the unperturbed density of states) in the case of isolated impurities. Relation (4.3.5) means, that we always are in the regime of small s - d coupling. In our model, J was assumed to be small compared to all other occurring energies of the model, and (4.3.5) simply states that the Fermi energy is much larger than the energy scale of the s - d coupling.

4.4 Green's function and local density of states

In this section we are going to state the formula for the electronic Green's function in mean field theory. Moreover, we will determine the local density of states, the quantity we are mostly interested in, since it is connected to the conductance at low temperatures. Again, mostly we are just going to present final results here, while more detailed computations are performed in appendix B.4. To get the Green's function one introduces a source term

$$S_{Source} = \sum_{i\omega_n} \sum_{\mathbf{k}} \left(\eta_{i\omega_n}^{\mathbf{k}} a_{\mathbf{k}}^{i\omega_n} + \bar{a}_{\mathbf{k}}^{i\omega_n} \eta_{i\omega_n}^{\mathbf{k}} \right) \quad (4.4.1)$$

4 Cluster of N atoms

into the action of the model. This leads to a modified partition function

$$\hat{Z}_{MF} = Z_{MF} \exp \left(\sum_{i\omega_n} \bar{\Theta}_{i\omega_n} [\underline{\mathbf{M}}_{i\omega_n}^{-1} \otimes \mathbb{1}_2] \Theta_{i\omega_n} \right), \quad (4.4.2)$$

where the vector $\Theta_{i\omega_n}$ is defined by

$$\Theta_{i\omega_n} = \left(\underbrace{0, 0, \dots, 0}_{N\text{-times}}, \left\{ \eta_{i\omega_n}^{\mathbf{k}} | \mathbf{k} \right\} \right)^{\text{T}}$$

and where the matrix $\underline{\mathbf{M}}_{i\omega_n}$ is the same as in section 4.2. The electronic Green's function is then defined as

$$\hat{G}(i\omega_n; \mathbf{k}, \mathbf{k}') = \frac{\partial^2 \log \hat{Z}_{MF}}{\partial \bar{\eta}_{i\omega_n}^{\mathbf{k}} \partial \eta_{i\omega_n}^{\mathbf{k}'}} \Big|_{\bar{\eta}=\eta=0}. \quad (4.4.3)$$

Inverting the matrix $\underline{\mathbf{M}}_{i\omega_n}$, the Green's function is actually given as

$$\hat{G}(i\omega_n; \mathbf{k}, \mathbf{k}') = G_{i\omega_n}(\mathbf{k}) \delta_{\mathbf{k}\mathbf{k}'} + G_{i\omega_n}(\mathbf{k}) D_{i\omega_n} t_{\mathbf{k}}^\dagger \underline{\mathbf{b}} \sum_{n=0}^{\infty} D_{i\omega_n}^n \left[-i\pi \text{sgn}(\omega_n) \underline{\mathbf{b}} \underline{\mathbf{g}}(i\omega_n) \underline{\mathbf{b}} \right]^n \underline{\mathbf{b}} t_{\mathbf{k}'} G_{i\omega_n}(\mathbf{k}'). \quad (4.4.4)$$

Here, the matrix $\underline{\mathbf{b}} \underline{\mathbf{g}}(i\omega_n) \underline{\mathbf{b}}$ appears again. As in section 4.2, we denote the eigenvalues of this matrix as $\hat{T}_j(i\omega_n)$ and its eigenvectors as $\hat{u}_j(i\omega_n)$. Let the matrix $\underline{\mathbf{U}}_{i\omega_n}$ diagonalise the matrix $\underline{\mathbf{b}} \underline{\mathbf{g}}(i\omega_n) \underline{\mathbf{b}}$ so that

$$\underline{\mathbf{U}}_{i\omega_n} \underline{\mathbf{b}} \underline{\mathbf{g}}(i\omega_n) \underline{\mathbf{b}} \underline{\mathbf{U}}_{i\omega_n}^\dagger = \text{diag}(\hat{T}_j(i\omega_n) | j = 1 \dots N).$$

Then

$$(\underline{\mathbf{b}} \underline{\mathbf{g}}(i\omega_n) \underline{\mathbf{b}})^n = \underline{\mathbf{U}}_{i\omega_n}^\dagger \left[\text{diag}(\hat{T}_j(i\omega_n) | j = 1 \dots N) \right]^n \underline{\mathbf{U}}_{i\omega_n}$$

and

$$\begin{aligned} D_{i\omega_n} \sum_{n=0}^{\infty} D_{i\omega_n}^n \left[-i\pi \text{sgn}(\omega_n) \underline{\mathbf{b}} \underline{\mathbf{g}}(i\omega_n) \underline{\mathbf{b}} \right]^n \\ = \underline{\mathbf{U}}_{i\omega_n}^\dagger \text{diag} \left(\frac{1}{D_{i\omega_n}^{-1} + i\pi \text{sgn}(\omega_n) \hat{T}_j(i\omega_n)} \Big| j = 1 \dots N \right) \underline{\mathbf{U}}_{i\omega_n}. \end{aligned}$$

Using the eigenvectors of $\underline{\mathbf{b}} \underline{\mathbf{g}}(i\omega_n) \underline{\mathbf{b}}$ we can thus write the Green's function (4.4.4) as

$$\hat{G}(i\omega_n; \mathbf{k}, \mathbf{k}') = G_{i\omega_n}(\mathbf{k}) \delta_{\mathbf{k}\mathbf{k}'} + \sum_{j=1}^N \frac{G_{i\omega_n}(\mathbf{k}) \left[t_{\mathbf{k}}^\dagger \underline{\mathbf{b}} \hat{u}_j(i\omega_n) \right] \cdot \left[\hat{u}_j^\dagger(i\omega_n) \underline{\mathbf{b}} t_{\mathbf{k}'} \right] G_{i\omega_n}(\mathbf{k}')}{D_{i\omega_n}^{-1} + i\pi \text{sgn}(\omega_n) \hat{T}_j(i\omega_n)}. \quad (4.4.5)$$

Since our overall goal is to get the coordinate resolved local density of states, we perform a Fourier transformation of (4.4.5) to coordinate space. It is

$$\tilde{G}(i\omega_n; \mathbf{r}) = \sum_{\mathbf{k}\mathbf{k}'} \hat{G}(i\omega_n; \mathbf{k}, \mathbf{k}') e^{-i\mathbf{r}(\mathbf{k}-\mathbf{k}')}.$$

The integrals involved here are the same as for the computation of the matrix $\tilde{\underline{\mathbf{g}}}(i\omega_n)$ in section 4.2. The coordinate resolved Green's function is thus given as

$$\tilde{G}(i\omega_n; \mathbf{r}) = -i\pi \text{sgn}(\omega_n) \rho_0 - \frac{\pi^2 \rho_0^2}{N} \sum_{j=1}^N \frac{\left[\hat{v}_{\mathbf{r}}^{\text{T}}(i\omega_n) \underline{\mathbf{b}} \hat{u}_j(i\omega_n) \right] \cdot \left[\hat{u}_j^\dagger(i\omega_n) \underline{\mathbf{b}} \hat{v}_{\mathbf{r}}(i\omega_n) \right]}{D_{i\omega_n}^{-1} + i\pi \text{sgn}(\omega_n) \hat{T}_j(i\omega_n)}. \quad (4.4.6)$$

4 Cluster of N atoms

The vector $\hat{v}(i\omega_n)$ is defined by the Fourier transformation

$$\sum_{\mathbf{k}} G_{i\omega_n}(\mathbf{k}) t_{\mathbf{k}} e^{i\mathbf{k}\mathbf{r}} = -i\pi \operatorname{sgn}(\omega_n) \frac{\rho_0}{\sqrt{N}} \hat{v}_{\mathbf{r}}(i\omega_n).$$

It is of the form

$$\hat{v}_{\mathbf{r}}(i\omega_n) = v_{\mathbf{r}}^R + i \operatorname{sgn}(\omega_n) v_{\mathbf{r}}^I$$

with some real-valued vectors v^R and v^I , and we remark that

$$(\hat{v}_{\mathbf{R}_j}(i\omega_n))_i = \frac{[\underline{\mathbf{g}}(i\omega_n)]_{ij}}{g_0}.$$

We emphasise that \hat{v}^T means transposed and not hermitian conjugate. The $i\omega_n$ -dependence of \hat{v} and \hat{v}^T is the same, their entries are not complex conjugate to each other.

The local density of states is related to the imaginary part of the advanced electronic Green's function by the formula

$$\rho(\omega, \mathbf{r}) = \frac{1}{\pi} \operatorname{Im} G^{adv}(\omega, \mathbf{r}). \quad (4.4.7)$$

Therefore, one needs to know the advanced Green's function which can be derived from (4.4.6) by the usual technique of complex continuation to the lower half plane:

$$G^{adv}(\omega, \mathbf{r}) = \lim_{\delta \rightarrow 0} \tilde{G} \left(i\omega_n - \frac{i\pi}{2\beta} \rightarrow \omega - i\delta; \mathbf{r} \right).$$

The continuation

$$i\omega_n - \frac{i\pi}{2\beta} \rightarrow \omega - i\delta$$

also means

$$i \operatorname{sgn}(\omega_n) \rightarrow -i.$$

Using this relations and the definitions (4.2.10) and (4.2.11) of the eigenvalues and eigenvectors of $\underline{\mathbf{b}}\underline{\mathbf{g}}(i\omega_n)\underline{\mathbf{b}}$, one gets

$$D_{i\omega_n}^{-1} \rightarrow \omega, \quad i\pi \operatorname{sgn}(\omega_n) \hat{T}_j(i\omega_n) \rightarrow -i\pi T_j^R - \pi T_j^I, \quad \hat{v}_{\mathbf{r}}(i\omega_n) \rightarrow v_{\mathbf{r}} = v_{\mathbf{r}}^R - i v_{\mathbf{r}}^I$$

and

$$\hat{u}_j(i\omega_n) \rightarrow u_j = u_j^R - i u_j^I.$$

The advanced Green's function therefore is

$$G^{adv}(\omega, \mathbf{r}) = i\pi \rho_0 - \pi^2 \rho_0 g_0 \sum_{j=1}^N \frac{[v_{\mathbf{r}}^T \underline{\mathbf{b}} u_j] \cdot [u_j^\dagger \underline{\mathbf{b}} v_{\mathbf{r}}]}{\omega - i\pi T_j^R - \pi T_j^I}, \quad (4.4.8)$$

where we replaced $g_0 = \rho_0/N$. To get the local density of states we use (4.4.7) and therefore have to determine the imaginary part of (4.4.8), where we have to take the structure of $v_{\mathbf{r}}$ and u_j into account, using that due to the symmetry of a real scalar product, it is

$$v^T \underline{\mathbf{b}} u = u^T \underline{\mathbf{b}} v$$

4 Cluster of N atoms

for any real-valued vectors v and u . In order to keep the formulas manageable, we define

$$B_{XY}^{j\mathbf{r}} = (v_{\mathbf{r}}^X)^T \underline{\mathbf{b}} u_j^Y \quad (4.4.9)$$

where $X, Y \in \{R, I\}$. Using this abbreviation, the local density of states is given as

$$\rho(\omega, \mathbf{r}) = \rho_0 \left(1 - \pi g_0 \sum_{j=1}^N \frac{\pi T_j^R [(B_{RR}^{j\mathbf{r}})^2 - (B_{II}^{j\mathbf{r}})^2 - (B_{IR}^{j\mathbf{r}})^2 + (B_{RI}^{j\mathbf{r}})^2] - 2(\omega - \pi T_j^I) [B_{RI}^{j\mathbf{r}} B_{II}^{j\mathbf{r}} + B_{IR}^{j\mathbf{r}} B_{RR}^{j\mathbf{r}}]}{(\omega - \pi T_j^I)^2 + (\pi T_j^R)^2} \right). \quad (4.4.10)$$

In the low temperature limit, the local density of states is essentially proportional to the conductivity at a certain point \mathbf{r} and the voltage bias related to the energy ω .

4.4.1 The "touching ground" theorem for the local density of states

In this section we are going to prove a theorem on the local density of states, which implies that the present mean field model can only be applied to magnetic clusters with sufficiently large inter atomic distances. The theorem reads:

The local density of states observed at any cluster atom vanishes at the Fermi level.

(4.4.11)

$$\rho(0, \mathbf{R}_i) = 0 \quad \text{for} \quad i = 1 \dots N.$$

Before proving (4.4.11), we discuss its consequences. Given an arbitrary cluster, the local density of states taken at any cluster atom always shows a dip at the Fermi level. As this dip is an indicator of the Kondo effect, we can conclude that the model treated here always is in the regime of the Kondo effect which cannot be destroyed by any other occurring effects. It can be enhanced or reduced but it cannot be completely destroyed.

This behaviour can be explained by the terms of the model itself. We described the system by using mean field theory for the hybridisation of the substrate spins and the localised ones at each site. However, this approach will fail if the distances of the cluster atoms become smaller than the Fermi wavelength, since then the cluster atoms should be collectively hybridised with the substrate. The mean field approach presented here is only valid if the inter-atomic distances are large enough - and this means the Kondo effect will be the most important.

We will now turn to the proof of (4.4.11). Afterwards, we are going to show that the necessary requirement for the validity of (4.4.11) is the absence of fluctuations of the hybridisations, so the theorem will only hold true in mean field theory.

The starting point of the proof of (4.4.11) is the advanced Green's function given in equation (4.4.8).

$$T_j = T_j^R - i T_j^I$$

and

$$u_j = u_j^R - i u_j^I$$

are the eigenvalues and eigenvectors of the matrix $\underline{\mathbf{b}} \underline{\mathbf{g}} \underline{\mathbf{b}}$ with

$$\underline{\mathbf{g}} = \underline{\mathbf{g}}^R - i \underline{\mathbf{g}}^I.$$

This simply follows by complex continuation from $\hat{T}_j(i\omega_n)$ and $\hat{u}_j(i\omega_n)$ to the lower half-plane, since those are the eigenvalues and eigenvectors of $\underline{\mathbf{b}} \underline{\mathbf{g}}(i\omega_n) \underline{\mathbf{b}}$. As stated in section 4.4 it is

$$(\hat{v}_{\mathbf{R}_i}(i\omega_n))_j = \frac{[\underline{\mathbf{g}}(i\omega_n)]_{ji}}{g_0}$$

4 Cluster of N atoms

and therefore

$$(v_{\mathbf{R}_i})_j = \frac{\mathbf{g}_{ji}}{g_0}.$$

So

$$\begin{aligned} \rho(0, \mathbf{R}_i) &= \rho_0 \left(1 - \pi g_0 \operatorname{Im} \left[\sum_{j=1}^N \frac{[v_{\mathbf{R}_i}^\top \underline{\mathbf{b}} u_j] \cdot [u_j^\dagger \underline{\mathbf{b}} v_{\mathbf{R}_i}]}{-i\pi (T_j^R - iT_j^I)} \right] \right) \\ &= \rho_0 \left(1 - g_0 \operatorname{Im} \left[i \sum_{l_1 l_2 l_3 l_4} \frac{\mathbf{g}_{il_1}}{g_0} \underline{\mathbf{b}}_{l_1 l_2} \sum_{j=1}^N \frac{(u_j)_{l_2} (u_j)_{l_3}^*}{T_j} \underline{\mathbf{b}}_{l_3 l_4} \frac{\mathbf{g}_{l_4 i}}{g_0} \right] \right). \end{aligned}$$

Since u_j are the eigenvectors of $\underline{\mathbf{b}} \mathbf{g} \underline{\mathbf{b}}$ with eigenvalues T_j , they also are the eigenvectors of $(\underline{\mathbf{b}} \mathbf{g} \underline{\mathbf{b}})^{-1}$ with T_j^{-1} being the corresponding eigenvalues. Hence

$$\sum_{j=1}^N \frac{(u_j)_{l_2} (u_j)_{l_3}^*}{T_j} = (\underline{\mathbf{b}} \mathbf{g} \underline{\mathbf{b}})^{-1}_{l_2 l_3}.$$

So

$$\begin{aligned} \rho(0, \mathbf{R}_i) &= \rho_0 \left(1 - \frac{1}{g_0} \operatorname{Im} \left[i \sum_{l_1 l_2 l_3 l_4} \mathbf{g}_{il_1} \underline{\mathbf{b}}_{l_1 l_2} (\underline{\mathbf{b}} \mathbf{g} \underline{\mathbf{b}})^{-1}_{l_2 l_3} \underline{\mathbf{b}}_{l_3 l_4} \mathbf{g}_{l_4 i} \right] \right) \\ &= \rho_0 \left(1 - \frac{1}{g_0} \sum_l \mathbf{g}_{il} \delta_{li} \right) \\ &= \rho_0 \left(1 - \frac{\mathbf{g}_{ii}}{g_0} \right) \\ &= 0, \end{aligned}$$

since $\mathbf{g}_{ii} = g_0$. This proves (4.4.11).

In the following we show, that the theorem 4.4.11 is only valid in mean field theory. The main reason for this is, that the Dyson series given in (4.4.4) does not converge toward the limit of a geometric series if the hybridisations are fluctuating. Therefore, the Green's function does not have the form (4.4.8) in that case, which was crucial for proving the theorem (4.4.11).

If we consider the hybridisation matrices $\underline{\mathbf{b}}$ to be fluctuating rather than being fixed to a mean value, the partition function is not given by (4.2.3) anymore, but by a similar expression, in which also the integration over all possible values of $\underline{\mathbf{b}}$ has to be performed. In the fluctuating case, the matrices $\underline{\mathbf{b}}$ are arbitrary, hermitian, complex-valued matrices which also depend on the Matsubara frequencies $i\omega_n$. Rather than (4.2.12), the partition function would therefore be given as

$$\begin{aligned} Z &= \int \mathcal{D}(b_{i\omega_n}) \mathcal{D}(b_{i\omega_n}^*) \hat{C} e^{-\frac{1}{\mathcal{J}N} \sum_{i\omega_n} \operatorname{Tr} \underline{\mathbf{b}}_{i\omega_n}^\dagger \underline{\mathbf{b}}_{i\omega_n}} \times \\ &\quad \times \exp \left(2 \sum_{i\omega_n} \sum_{j=1}^N \log \left[i\omega_n - \frac{i\pi}{2\beta} + i\pi \operatorname{sgn}(\omega_n) T_j^R(i\omega_n) - \pi T_j^I(i\omega_n) \right] \right), \end{aligned} \quad (4.4.12)$$

4 Cluster of N atoms

where $b_{i\omega_n}$ and $b_{i\omega_n}^*$ denote all possible values of the hybridisations and their complex conjugate and where the eigenvalues $T_j^{R/I}$ now have to depend on $i\omega_n$, since they depend on the hybridisations. We denote the integrand of 4.4.12 as $\tilde{z}(b, b^*)$. The Matsubara Green's function of the system still can be computed by introducing a source term as defined in (4.4.1) into the partition function, thus altering it from Z as given in (4.4.12) to \tilde{Z} fulfilling

$$\tilde{Z}\Big|_{\tilde{\eta}=\eta=0} = Z.$$

The Green's function is given as already defined in (4.4.3):

$$\hat{G}(i\omega_n; \mathbf{k}, \mathbf{k}') = \frac{\partial^2 \log \tilde{Z}}{\partial \tilde{\eta}_{i\omega_n}^{\mathbf{k}} \partial \tilde{\eta}_{i\omega_n}^{\mathbf{k}'}} \Big|_{\tilde{\eta}=\eta=0}.$$

Contrary to the mean field result (4.4.4), the Green's function for fluctuating hybridisations is

$$\begin{aligned} \hat{G}(i\omega_n; \mathbf{k}, \mathbf{k}') &= G_{i\omega_n}(\mathbf{k}) \delta_{\mathbf{k}\mathbf{k}'} + G_{i\omega_n}(\mathbf{k}) D_{i\omega_n} t_{\mathbf{k}}^\dagger \sum_{n=0}^{\infty} [-i\pi \text{sgn}(\omega_n) D_{i\omega_n}]^n \times \\ &\times \frac{1}{Z} \left(\int db db^* \tilde{z}(b, b^*) \underline{b}_{i\omega_n}^\dagger \left[\underline{b}_{i\omega_n} \underline{g}(i\omega_n) \underline{b}_{i\omega_n}^\dagger \right]^n \underline{b}_{i\omega_n} \right) t_{\mathbf{k}'} G_{i\omega_n}(\mathbf{k}'). \end{aligned} \quad (4.4.13)$$

The Dyson series in (4.4.13) does not converge to the limit of a geometric series in general. Instead, it is given as the sum over all connected diagrams in \underline{b} , which of course does not only contain the mean field part. The Dyson series in (4.4.13) will only coincide with the geometric series, if the (slightly altered) n -point function

$$\langle b^* b^* \dots b b \rangle = \frac{1}{Z} \left(\int db db^* \tilde{z}(b, b^*) [b^* b]^n \right)$$

has the property

$$\langle \underline{b}^\dagger \underline{b}^\dagger \dots \underline{b} \underline{b} \rangle = \langle \underline{b} \rangle \langle \underline{b} \rangle \dots \langle \underline{b} \rangle \langle \underline{b} \rangle,$$

which is the definition of the mean field approach. For fluctuating hybridisations, the Green's function (4.4.13) will thus not take a form similar to (4.4.8), which would be necessary in order that theorem (4.4.11) would still hold true.

This means, that theorem (4.4.11) will not be valid anymore, if fluctuations of the hybridisation are taken into account. It is therefore linked to the mean field approach used throughout this work. Since (4.4.11) implies, that the model will always develop a Kondo effect, one can draw the conclusion that mean field theory will only be valid for systems in the Kondo regime.

We want to conclude this section with a remark on the outcome of an STM experiment described by the present model. In the domain of the Kondo effect the differential conductance dI/dV (and thus for small temperatures the local density of states) taken at an impurity will be of Fano-Kondo resonance shape (see for example [31] or [30])

$$\rho(\omega, \mathbf{R}_i) = \frac{(q \pi \Gamma + \omega)^2}{\omega^2 + (\pi \Gamma)^2}.$$

Here, q is the Fano factor and $\omega = 0$ is the Fermi level. The theorem $\rho(0, \mathbf{R}_i) = 0$ then implies $q = 0$. In the model presented here, the Fano shape fit to the local density of states will always be one of vanishing Fano factor, which means that we always are in the regime where the coupling between STM tip and the substrate is weak. This is not very surprising, since the present model does not take into account any terms describing the tip of the STM or its coupling to the sample.

4.5 Single impurity limit

As outlined in the last subsection, the model presented here mostly starts from a Kondo case which then can be altered by geometric effects. Of course, it is mandatory for the model to contain the pure Kondo effect as a limiting case. The pure Kondo case will be given if the cluster consists of isolated atoms which do not interact with each other. In our model, this corresponds to diverging inter atomic distances:

$$|\mathbf{R}_i - \mathbf{R}_j| \rightarrow \infty \quad \text{for all } i, j = 1 \dots N.$$

In this case the integrals in (4.2.8) vanish if $i \neq j$ and the matrix $\underline{\mathbf{g}}(i\omega_n)$ defined in (4.2.9) becomes proportional to the unity:

$$\underline{\mathbf{g}}(i\omega_n) = g_0 \mathbb{1}_N.$$

The matrix $\underline{\mathbf{b}} \underline{\mathbf{g}}(i\omega_n) \underline{\mathbf{b}}$ then already is diagonal

$$\underline{\mathbf{b}} \underline{\mathbf{g}}(i\omega_n) \underline{\mathbf{b}} = \text{diag}(b_j^2 g_0 | j = 1 \dots N)$$

with the real-valued eigenvalues

$$T_j(i\omega_n) = T_j = T_j^R = b_j^2 g_0.$$

The mean field equations (4.3.4) are given as

$$2 b_i g_0 \log \frac{b_i^2 g_0}{\Delta} = -\frac{1}{NJ} b_i$$

with the non-trivial solution

$$b_i^2 g_0 = \Delta \exp\left(-\frac{1}{2N g_0 J}\right) = \Delta \exp\left(-\frac{1}{2\rho_0 J}\right) = T_j, \quad (4.5.1)$$

for every $i = 1 \dots N$. We used $g_0 = \rho_0/N$. So all T_j and b_j respectively coincide, and we remark that

$$T_0 = \Delta \exp\left(-\frac{1}{2J\rho_0}\right) \quad (4.5.2)$$

has the usual form of a Kondo temperature known for a single magnetic impurity (see [38]). The local density of states (4.4.10) becomes strikingly simple:

$$\rho(\omega, \mathbf{r}) = \rho_0 \left(1 - \pi g_0 \sum_{j=1}^N \frac{\pi T_j [(v_{\mathbf{r}})^T \underline{\mathbf{b}} u_j]^2}{\omega^2 + (\pi T_j)^2} \right).$$

The eigenvectors u_j here simply are

$$(u_j)_l = \delta_{il}.$$

At the position \mathbf{R}_i of any cluster atom, the vectors $v_{\mathbf{R}_i}$ are given as

$$(v_{\mathbf{R}_i})_l = \frac{\underline{\mathbf{g}}_{li}}{g_0} = \delta_{il}.$$

So in this case

$$(v_{\mathbf{r}})^T \underline{\mathbf{b}} u_j = b_j \delta_{ij}$$

and

$$\begin{aligned}\rho(\omega, \mathbf{R}_i) &= \rho_0 \left(1 - \pi g_0 \frac{\pi T_i b_i^2}{\omega^2 + (\pi T_i)^2} \right) \\ &= \rho_0 \left(1 - \frac{\pi^2 T_0^2}{\omega^2 + \pi^2 T_0^2} \right).\end{aligned}$$

This is the Fano-Kondo form of a Kondo dip with width πT_0 and vanishing Fano factor. The case of isolated atoms leads to the formation of a Kondo peak at each atom with same Kondo temperature T_0 given in (4.5.2).

4.6 Summary

In this section we considered a cluster of N magnetic impurities sufficiently far from each other. The interacting part of the Hamiltonian was given by a Kondo term at each site. We formally computed the partition function of the problem in mean field theory, the mean field here being the mean hybridisation of each cluster atom with the surrounding substrate atoms. Using the partition function as a starting point, we calculated the mean field equations of the problem as well as the Green's function and the local density of states in coordinate space. During the calculations, the quantity $\underline{\mathbf{b}}\underline{\mathbf{g}}(i\omega_n)\underline{\mathbf{b}}$ arose. The eigenvalues of this matrix determine the values of the mean field parameters. It was outlined that the squares of the entries of $\underline{\mathbf{b}}\underline{\mathbf{g}}(i\omega_n)\underline{\mathbf{b}}$ are related to the RKKY interaction, which acts ferromagnetically for real-valued entries of $\underline{\mathbf{g}}(i\omega_n)$ and antiferromagnetically for imaginary ones. The influence of the cluster geometry on the system is therefore encoded in the matrix $\underline{\mathbf{g}}(i\omega_n)$.

It was proven, that the local density of states taken at any cluster site vanishes at the Fermi level. As a result, the LDOS at a cluster site (as a function of energy) always develops a dip around the Fermi energy. Since this is what one would expect from a system with dominating Kondo effect, we concluded that only such cases are to be considered here. For dominating RKKY effect, the inter atomic distances have to be small (less than a Fermi wavelength) which is not compatible with the mean field ansatz used here.

We considered the limiting case of a completely isolated cluster, where no interactions between the distinct atoms occur. In this case, the system develops a normal Kondo effect at each cluster site. The Kondo temperature then is

$$T_0 = \Delta \exp\left(-\frac{1}{2J\rho_0}\right)$$

with Δ the bandwidth of the substrate, J the strength of the s - d coupling and ρ_0 the substrate density of states at the Fermi level. We are going to use this system in the following chapter as a reference system.

The problem of a cluster consisting of N magnetic impurities cannot be treated analytically in general, since the $N \times N$ matrix $\underline{\mathbf{b}}\underline{\mathbf{g}}(i\omega_n)\underline{\mathbf{b}}$ has to be diagonalised for solving the mean field equations. We are going to restrict ourselves in the following to a trimer so that $N = 3$. To make things even simpler, we will assume the trimer to be isosceles. However, the case of an N -dimensional cluster can be treated in principle, though a numerical approach would then be appropriate.

5 Isosceles Trimer

In this chapter, we are going to look at an actual example of a magnetic cluster. We are going to consider three single level magnetic impurities that form an isosceles trimer. As we have stated in the latter chapter, geometrical effects are completely encoded in the eigenvalues and eigenvectors of the matrix $\underline{h}\underline{g}\underline{h}$. We will have to solve the mean field equations (4.3.4) for a given geometry and compute the local density of states (4.4.10) at a certain point. We are going to consider several limiting cases of the geometry of an isosceles trimer, which can be treated analytically to a large extent, for example an equilateral triangle and a chain. Yet, we are also going to deal with more general geometries, whose corresponding mean field equations will then have to be solved using numerical methods. In all cases, we are going to determine the local density of states given at the cluster atoms and interpret its behaviour with varying geometry.

5.1 General case

We start with the general case of an isosceles trimer. To model it, we consider the related \underline{g} -matrix to be given as

$$\underline{g} = \begin{pmatrix} g_0 & g_1 & g_2 \\ g_1 & g_0 & g_1 \\ g_2 & g_1 & g_0 \end{pmatrix}. \quad (5.1.1)$$

This is due to the isosceles form, where we consider the apex to be located at \mathbf{R}_2 . We recall that $g_0 = \rho_0/3$ is positive real-valued but g_1 and g_2 are complex. It is

$$\underline{g} = \underline{g}^R - i\underline{g}^I,$$

and we use the notation

$$g_j = g_j^R - ig_j^I$$

with real-valued $g_j^{R/I}$ for the entries of the matrix. Since the hybridisation at the cluster atoms opposite the apex should be of the same kind (due to symmetry considerations) we assume the matrix \underline{h} to be of the form

$$\underline{h} = \begin{pmatrix} b & 0 & 0 \\ 0 & \hat{b} & 0 \\ 0 & 0 & b \end{pmatrix}. \quad (5.1.2)$$

So $b_1 = b_3 = b$ and $b_2 = \hat{b}$. Since there are only two distinct mean field parameters left, the mean field equations (4.3.4) are slightly altered. Their right hand side computes to

$$-\frac{1}{3J} \frac{\partial}{\partial b_i} \text{Tr} \underline{h}^2 = -\frac{2}{3J} (2b \delta_{b_i b} + \hat{b} \delta_{b_i \hat{b}}).$$

Since the mean field parameter b appears twice in the matrix \underline{h} , the right hand side of its mean field equation is multiplied by 2. As outlined earlier, the main tasks are to diagonalise the matrix

5 Isosceles Trimer

$\underline{\mathbf{b}}\underline{\mathbf{g}}\underline{\mathbf{b}}$ formally, solve the mean field equations and compute the local density of states. Assuming (5.1.1) and (5.1.2), the matrix $\underline{\mathbf{b}}\underline{\mathbf{g}}\underline{\mathbf{b}}$ is given as

$$\underline{\mathbf{b}}\underline{\mathbf{g}}\underline{\mathbf{b}} = \begin{pmatrix} b^2 g_0 & b \hat{b} g_1 & b^2 g_2 \\ b \hat{b} g_1 & \hat{b}^2 g_0 & b \hat{b} g_1 \\ b^2 g_2 & b \hat{b} g_1 & b^2 g_0 \end{pmatrix} \quad (5.1.3)$$

For the sake of a brief notation, we define

$$z_0 = b^2 g_0, \quad \hat{z}_0 = \hat{b}^2 g_0, \quad z_1 = b \hat{b} g_1 \quad \text{and} \quad z_2 = b^2 g_2. \quad (5.1.4)$$

The characteristic polynomial of the matrix (5.1.3) is

$$\begin{aligned} \det(\underline{\mathbf{b}}\underline{\mathbf{g}}\underline{\mathbf{b}} - T \mathbb{1}_3) &= (z_0 - T)[(\hat{z}_0 - T)(z_0 - T) - z_1^2] \\ &\quad - z_1[z_1(z_0 - T) - z_1 z_2] + z_2[z_1^2 - z_2(\hat{z}_0 - T)] \\ &= [(z_0 - T)^2 - z_2^2](\hat{z}_0 - T) - 2(z_0 - T)z_1^2 + 2z_1^2 z_2 \\ &= (T - z_0 + z_2)(T - z_0 - z_2)(\hat{z}_0 - T) + 2z_1^2(T - z_0 + z_2) \\ &= -(T - z_0 + z_2)[T^2 - (z_0 + \hat{z}_0 + z_2)T + \hat{z}_0 z_0 + \hat{z}_0 z_2 - 2z_1^2]. \end{aligned} \quad (5.1.5)$$

The roots of the characteristic polynomial are

$$T_1 = b^2(g_0 - g_2), \quad (5.1.6)$$

$$T_2 = \frac{1}{2} \left[b^2(g_0 + g_2) + \hat{b}^2 g_0 + \sqrt{(b^2(g_0 + g_2) - \hat{b}^2 g_0)^2 + 8 b^2 \hat{b}^2 g_1^2} \right], \quad (5.1.7)$$

$$T_3 = \frac{1}{2} \left[b^2(g_0 + g_2) + \hat{b}^2 g_0 - \sqrt{(b^2(g_0 + g_2) - \hat{b}^2 g_0)^2 + 8 b^2 \hat{b}^2 g_1^2} \right]. \quad (5.1.8)$$

The square roots in the latter equations are meant to be complex, since g_1 and g_2 are. There are two different square roots of any given complex number z which differ by sign. However, switching the sign of the roots just turns T_2 into T_3 and vice versa. The normalised eigenvectors u_j are determined by the equations

$$\underline{\mathbf{b}}\underline{\mathbf{g}}\underline{\mathbf{b}} u_j = T_j u_j, \quad |u_j|^2 = 1.$$

Using the notation (5.1.4), this reads for T_1 and $u_1 = (x, y, z)^T$

$$\begin{aligned} z_0 x + z_1 y + z_2 z &= (z_0 - z_2) x, \\ z_1 x + \hat{z}_0 y + z_1 z &= (z_0 - z_2) y, \\ z_2 x + z_1 y + z_0 z &= (z_0 - z_2) z, \end{aligned}$$

which means $z = -x, y = 0$ and therefore

$$u_1 = \frac{1}{\sqrt{2}} \begin{pmatrix} 1 \\ 0 \\ -1 \end{pmatrix}. \quad (5.1.9)$$

For $T_{2/3}$ and $u_{2/3}$ it is

$$\begin{aligned} z_0 x + z_1 y + z_2 z &= \frac{1}{2} \left[z_0 + z_2 + \hat{z}_0 \pm \sqrt{(z_0 + z_2 - \hat{z}_0)^2 + 8 z_1^2} \right] x, \\ z_1 x + \hat{z}_0 y + z_1 z &= \frac{1}{2} \left[z_0 + z_2 + \hat{z}_0 \pm \sqrt{(z_0 + z_2 - \hat{z}_0)^2 + 8 z_1^2} \right] y, \\ z_2 x + z_1 y + z_0 z &= \frac{1}{2} \left[z_0 + z_2 + \hat{z}_0 \pm \sqrt{(z_0 + z_2 - \hat{z}_0)^2 + 8 z_1^2} \right] z. \end{aligned}$$

5 Isosceles Trimer

Adding the first and the last of these equations, one arrives at

$$2 z_1 y = \frac{1}{2} \left[\hat{z}_0 - z_0 - z_2 \pm \sqrt{(z_0 + z_2 - \hat{z}_0)^2 + 8z_1^2} \right] (x + z). \quad (5.1.10)$$

Using this relation, the second equation is trivially solved and does not yield any new information. By subtracting the third equation from the first, one gets

$$(z_0 - z_2)(x - z) = \frac{1}{2} \left[z_0 + z_2 + \hat{z}_0 \pm \sqrt{(z_0 + z_2 - \hat{z}_0)^2 + 8z_1^2} \right] (x - z)$$

which is solved for $x = z$. Using (5.1.10), we get

$$\begin{aligned} y &= \frac{T_j - z_0 - z_2}{z_1} x \\ &= \frac{2z_1}{T_j - \hat{z}_0} \frac{T_j^2 - T_j(z_0 + \hat{z}_0 + z_2) + \hat{z}_0 z_0 + \hat{z}_0 z_2}{2z_1^2} x \\ &= \frac{2z_1}{T_j - \hat{z}_0} x, \end{aligned} \quad (5.1.11)$$

where we used, that T_j is a root of the characteristic polynomial (5.1.5). With the requirement $|u_j|^2 = 1$, it is

$$u_{2/3} = \frac{1}{\sqrt{2 + |y_{2/3}|^2}} \begin{pmatrix} 1 \\ y_{2/3} \\ 1 \end{pmatrix}, \quad (5.1.12)$$

with

$$y_{2/3} = \frac{2 b \hat{b} g_1}{T_{2/3} - \hat{b}^2 g_0}. \quad (5.1.13)$$

The case $T_{2/3} = \hat{b}^2 g_0$ could apparently be problematic. It is equivalent to $g_1 = 0$ (see (5.1.11)) which describes the splitting of the trimer into a dimer and an isolated atom, since $g_1 = 0$ means that the apex atom is infinitely far away from the remaining two (see the definition of the matrix $\tilde{\mathbf{g}}(i\omega_n)$, (4.2.7)). A priori it is unclear what the outcome of y_j will be, since both nominator and denominator are vanishing. We are going to deal with this case in section 5.2.

Knowing the form of the eigenvalues of the matrix $\underline{\mathbf{b}} \underline{\mathbf{g}} \underline{\mathbf{b}}$, we can solve the mean field equations (4.3.4) in principle. For certain geometric configurations of the cluster this is doable analytically, for others one would like to consider a numerical approach. Since we have the eigenvalues u_j as well, the local density of states (4.4.10) can be computed at a given position, preferably at an atomic site. The main point we are interested in, is the influence of the geometry on the Kondo behaviour. Hence, we determine the width of the density peak at an atomic site, since this is proportional to the Kondo temperature, and investigate its behaviour with varying geometry.

Varying the geometry will be implemented by varying the value of the entries of the matrix $\underline{\mathbf{g}}$. Here, we will abstain from considering arbitrary values of g_1 and g_2 but concentrate on either real-valued or purely imaginary ones, corresponding to ferromagnetic and antiferromagnetic coupling respectively.

5.1.1 Useful formulas for the isosceles trimer

As mentioned earlier, we are mostly interested in the local density of states at the position of the trimer atoms. Due to the symmetry of the trimer, the LDOS should be the same for \mathbf{R}_1 and \mathbf{R}_3 . Since in the LDOS equation (4.4.10) the real and imaginary parts of the eigenvalues and eigenvectors appear, we will give more explicit formulas for those to make computations or numerical implementations simpler. Moreover, we will compute the $B_{XY}^{j\mathbf{R}_i}$, as defined in (4.4.9), for the impurity positions \mathbf{R}_i .

This section is rather a formulary for further computations or numerical implementations. It is not necessarily needed for the understanding of the following sections, though we will make use of the formulas given here.

We start with the eigenvalues T_j . As we have defined the matrix $\underline{\mathbf{g}}$ as

$$\underline{\mathbf{g}} = \underline{\mathbf{g}}^R - i \underline{\mathbf{g}}^I$$

with real-valued symmetric matrices $\underline{\mathbf{g}}^R$ and $\underline{\mathbf{g}}^I$, we will stick to the same structure for the entries of that matrix:

$$g_{1/2} = g_{1/2}^R - i g_{1/2}^I. \quad (5.1.14)$$

The diagonal values $g_0 = \rho_0/3$ are strictly positive. The eigenvalue T_1 given in (5.1.6) thus simply is

$$T_1 = b^2(g_0 - g_2^R) - i(-b^2 g_2^I) = T_1^R - i T_1^I. \quad (5.1.15)$$

For dealing with T_2 and T_3 we first bring the square root to a more manageable form. It is

$$\begin{aligned} (b^2(g_0 + g_2) - \hat{b}^2 g_0)^2 + 8b^2 \hat{b}^2 g_1^2 &= (b^2(g_0 + g_2^R) - \hat{b}^2 g_0 - i b^2 g_2^I)^2 + 8b^2 \hat{b}^2 (g_1^R - i g_1^I)^2 \\ &= (b^2(g_0 + g_2^R) - \hat{b}^2 g_0)^2 - b^4 (g_2^I)^2 + 8b^2 \hat{b}^2 \left[(g_1^R)^2 - (g_1^I)^2 \right] \\ &\quad - i \left[2b^2 g_2^I (b^2(g_0 + g_2^R) - \hat{b}^2 g_0) + 16b^2 \hat{b}^2 g_1^R g_1^I \right] \\ &= z^R - i z^I \end{aligned} \quad (5.1.16)$$

Here, we defined z^R and z^I . We need the square root of $z^R - i z^I$. To get it explicitly, we transform $z^R - i z^I$ to polar form. It is

$$z^R - i z^I = \text{sgn}(z^R) \sqrt{(z^R)^2 + (z^I)^2} \exp\left(-i \arctan \frac{z^I}{z^R}\right).$$

Rewriting the sign-function as

$$\text{sgn}(x) = e^{-i\pi \Theta(-x)}$$

with the Heaviside-function Θ , we get

$$\begin{aligned} \sqrt{z^R - i z^I} &= \left((z^R)^2 + (z^I)^2 \right)^{1/4} \exp\left(-i \frac{1}{2} \arctan \frac{z^I}{z^R} - \frac{i\pi}{2} \Theta(-z^R)\right) \\ &= \left((z^R)^2 + (z^I)^2 \right)^{1/4} \cos\left(\frac{1}{2} \arctan \frac{z^I}{z^R} + \frac{\pi}{2} \Theta(-z^R)\right) - \\ &\quad - i \left((z^R)^2 + (z^I)^2 \right)^{1/4} \sin\left(\frac{1}{2} \arctan \frac{z^I}{z^R} + \frac{\pi}{2} \Theta(-z^R)\right). \end{aligned}$$

5 Isosceles Trimer

There is another complex square root with changed sign due to the invariance of the exponential function under translations by $2\pi i$. However, changing the sign of the root just switches the meaning of the eigenvalues T_2 and T_3 , which has no physical effect. Putting this relation into the formulas (5.1.7) and (5.1.8) for the eigenvalues and using $T_2 = T_2^R - i T_2^I$ and $T_3 = T_3^R - i T_3^I$, one gets

$$T_2^R = \frac{1}{2} \left[b^2(g_0 + g_2^R) + \hat{b}^2 g_0 + \left((z^R)^2 + (z^I)^2 \right)^{1/4} \cos \left(\frac{1}{2} \arctan \frac{z^I}{z^R} + \frac{\pi}{2} \Theta(-z^R) \right) \right], \quad (5.1.17)$$

$$T_2^I = \frac{1}{2} \left[b^2 g_2^I + \left((z^R)^2 + (z^I)^2 \right)^{1/4} \sin \left(\frac{1}{2} \arctan \frac{z^I}{z^R} + \frac{\pi}{2} \Theta(-z^R) \right) \right], \quad (5.1.18)$$

$$T_3^R = \frac{1}{2} \left[b^2(g_0 + g_2^R) + \hat{b}^2 g_0 - \left((z^R)^2 + (z^I)^2 \right)^{1/4} \cos \left(\frac{1}{2} \arctan \frac{z^I}{z^R} + \frac{\pi}{2} \Theta(-z^R) \right) \right], \quad (5.1.19)$$

$$T_3^I = \frac{1}{2} \left[b^2 g_2^I - \left((z^R)^2 + (z^I)^2 \right)^{1/4} \sin \left(\frac{1}{2} \arctan \frac{z^I}{z^R} + \frac{\pi}{2} \Theta(-z^R) \right) \right]. \quad (5.1.20)$$

As mentioned in the latter section, the eigenvector corresponding to the eigenvalue T_1 is

$$u_1 = \frac{1}{\sqrt{2}} \begin{pmatrix} 1 \\ 0 \\ -1 \end{pmatrix} = u_1^R - i u_1^I, \quad (5.1.21)$$

so $u_1^I = 0$. To get the real and imaginary parts of the eigenvectors u_2 and u_3 given in (5.1.12), we have to know those of y_j . According to (5.1.13) it is

$$\begin{aligned} y_j &= \frac{2b\hat{b}g_1}{T_{2/3} - \hat{b}^2 g_0} \\ &= \frac{2b\hat{b}(g_1^R - i g_1^I)}{T_{2/3}^R - \hat{b}^2 g_0 - i T_{2/3}^I} \\ &= \frac{2b\hat{b}(g_1^R - i g_1^I) (T_{2/3}^R - \hat{b}^2 g_0 + i T_{2/3}^I)}{(T_{2/3}^R - \hat{b}^2 g_0)^2 + (T_{2/3}^I)^2} \\ &= \frac{2b\hat{b} \left[g_1^R (T_{2/3}^R - \hat{b}^2 g_0) + g_1^I T_{2/3}^I \right]}{(T_{2/3}^R - \hat{b}^2 g_0)^2 + (T_{2/3}^I)^2} - i \frac{2b\hat{b} \left[g_1^I (T_{2/3}^R - \hat{b}^2 g_0) - g_1^R T_{2/3}^I \right]}{(T_{2/3}^R - \hat{b}^2 g_0)^2 + (T_{2/3}^I)^2} \\ &= y_{2/3}^R - i y_{2/3}^I, \end{aligned} \quad (5.1.22)$$

where we defined $y_{2/3}^{R/I}$. The eigenvectors of T_2 and T_3 are therefore given as

$$\begin{aligned} u_{2/3} &= \frac{1}{\sqrt{2 + (y_{2/3}^R)^2 + (y_{2/3}^I)^2}} \begin{pmatrix} 1 \\ y_{2/3}^R \\ 1 \end{pmatrix} - i \frac{1}{\sqrt{2 + (y_{2/3}^R)^2 + (y_{2/3}^I)^2}} \begin{pmatrix} 0 \\ y_{2/3}^I \\ 0 \end{pmatrix} \\ &= u_{2/3}^R - i u_{2/3}^I. \end{aligned} \quad (5.1.23)$$

In (4.4.9) we introduced the quantities

$$B_{XY}^{j\mathbf{r}} = (v_{\mathbf{r}}^X)^{\mathbf{T}} \underline{\mathbf{b}} u_j^Y$$

5 Isosceles Trimer

to keep the formula for the LDOS (4.4.10) manageable. We compute those quantities for $\mathbf{r} = \mathbf{R}_i$ to get the LDOS at the respective trimer site. As mentioned earlier, it is

$$[v_{\mathbf{R}_i}]_j = \frac{g_{ij}}{g_0}$$

at any cluster site \mathbf{R}_i . Hence, we get

$$v_{\mathbf{R}_1} = \begin{pmatrix} 1 \\ g_1^R/g_0 \\ g_2^R/g_0 \end{pmatrix} - i \begin{pmatrix} 0 \\ g_1^I/g_0 \\ g_2^I/g_0 \end{pmatrix} = v_{\mathbf{R}_1}^R - i v_{\mathbf{R}_1}^I, \quad (5.1.24)$$

$$v_{\mathbf{R}_2} = \begin{pmatrix} g_1^R/g_0 \\ 1 \\ g_1^R/g_0 \end{pmatrix} - i \begin{pmatrix} g_1^I/g_0 \\ 0 \\ g_1^I/g_0 \end{pmatrix} = v_{\mathbf{R}_2}^R - i v_{\mathbf{R}_2}^I \quad (5.1.25)$$

and

$$v_{\mathbf{R}_3} = \begin{pmatrix} g_2^R/g_0 \\ g_1^R/g_0 \\ 1 \end{pmatrix} - i \begin{pmatrix} g_2^I/g_0 \\ g_1^I/g_0 \\ 0 \end{pmatrix} = v_{\mathbf{R}_3}^R - i v_{\mathbf{R}_3}^I. \quad (5.1.26)$$

At $\mathbf{r} = \mathbf{R}_2$, we thus get

$$\begin{aligned} B_{RR}^{1\mathbf{R}_2} &= B_{RI}^{1\mathbf{R}_2} = B_{IR}^{1\mathbf{R}_2} = B_{II}^{1\mathbf{R}_2} = 0, \\ B_{RR}^{2/3\mathbf{R}_2} &= \frac{1}{\sqrt{2 + (y_{2/3}^R)^2 + (y_{2/3}^I)^2}} \left(2b \frac{g_1^R}{g_0} + \hat{b} y_{2/3}^R \right), \quad B_{II}^{2/3\mathbf{R}_2} = 0, \\ B_{RI}^{2/3\mathbf{R}_2} &= \frac{\hat{b} y_{2/3}^I}{\sqrt{2 + (y_{2/3}^R)^2 + (y_{2/3}^I)^2}}, \quad B_{IR}^{2/3\mathbf{R}_2} = \frac{2b \frac{g_1^I}{g_0}}{\sqrt{2 + (y_{2/3}^R)^2 + (y_{2/3}^I)^2}}, \end{aligned} \quad (5.1.27)$$

and at $\mathbf{r} = \mathbf{R}_1$ and $\mathbf{r} = \mathbf{R}_3$ respectively

$$\begin{aligned} B_{RR}^{1\mathbf{R}_1} &= \frac{1}{\sqrt{2}} b \left(1 - \frac{g_2^R}{g_0} \right) = -B_{RR}^{1\mathbf{R}_3}, \quad B_{RI}^{1\mathbf{R}_1} = B_{RI}^{1\mathbf{R}_3} = 0 \\ B_{IR}^{1\mathbf{R}_1} &= -\frac{1}{\sqrt{2}} b \frac{g_2^I}{g_0} = -B_{IR}^{1\mathbf{R}_3}, \quad B_{II}^{1\mathbf{R}_1} = B_{II}^{1\mathbf{R}_3} = 0, \\ B_{RR}^{2/3\mathbf{R}_1} &= \frac{1}{\sqrt{2 + (y_{2/3}^R)^2 + (y_{2/3}^I)^2}} \left(b \left[1 + \frac{g_2^R}{g_0} \right] + \hat{b} y_{2/3}^R \frac{g_1^R}{g_0} \right) = B_{RR}^{2/3\mathbf{R}_3}, \\ B_{II}^{2/3\mathbf{R}_1} &= \frac{1}{\sqrt{2 + (y_{2/3}^R)^2 + (y_{2/3}^I)^2}} \hat{b} y_{2/3}^I \frac{g_1^I}{g_0} = B_{II}^{2/3\mathbf{R}_3}, \\ B_{RI}^{2/3\mathbf{R}_1} &= \frac{1}{\sqrt{2 + (y_{2/3}^R)^2 + (y_{2/3}^I)^2}} \hat{b} y_{2/3}^I \frac{g_1^R}{g_0} = B_{RI}^{2/3\mathbf{R}_3}, \\ B_{IR}^{2/3\mathbf{R}_1} &= \frac{1}{\sqrt{2 + (y_{2/3}^R)^2 + (y_{2/3}^I)^2}} \left(b \frac{g_2^I}{g_0} + \hat{b} y_{2/3}^R \frac{g_1^I}{g_0} \right) = B_{IR}^{2/3\mathbf{R}_3}. \end{aligned} \quad (5.1.28)$$

Plugging (5.1.28) in (4.4.10) one can see that

$$\rho(\omega, \mathbf{R}_1) = \rho(\omega, \mathbf{R}_3)$$

5 Isosceles Trimer

as expected. We can now give a more explicit formula for the local density of states taken at \mathbf{R}_2 and \mathbf{R}_1 respectively. At the apex atom, one gets

$$\begin{aligned} \rho(\omega, \mathbf{R}_2) = & \rho_0 - \rho_0 \pi g_0 \sum_{j=2}^3 \frac{1}{\left[(\omega - \pi T_j^I)^2 + (\pi T_j^R)^2 \right] \cdot \left[2 + (y_j^R)^2 + (y_j^I)^2 \right]} \times \\ & \times \left(\pi T_j^R \left[4b^2 \left(\left[\frac{g_1^R}{g_0} \right]^2 - \left[\frac{g_1^I}{g_0} \right]^2 \right) + \hat{b}^2 [(y_j^R)^2 + (y_j^I)^2] + 4b \hat{b} y_j^R \frac{g_1^R}{g_0} \right] - \right. \\ & \left. - 2(\omega - \pi T_j^I) \left[2b \hat{b} y_j^R \frac{g_1^I}{g_0} + 4b^2 \frac{g_1^R}{g_0} \frac{g_1^I}{g_0} \right] \right). \end{aligned} \quad (5.1.29)$$

At the basis atoms, the LDOS is

$$\begin{aligned} \rho(\omega, \mathbf{R}_{1/3}) = & \rho_0 - \rho_0 \pi g_0 \frac{1}{2} b^2 \frac{\pi T_1^R \left[\left(1 - \left[\frac{g_2^R}{g_0} \right]^2 \right) - \left[\frac{g_2^I}{g_0} \right]^2 \right] + 2(\omega - \pi T_1^I) \left(1 - \frac{g_2^R}{g_0} \right) \frac{g_2^I}{g_0}}{(\omega - \pi T_1^I)^2 + (\pi T_1^R)^2} - \\ & - \rho_0 \pi g_0 \sum_{j=2}^3 \frac{1}{\left[(\omega - \pi T_j^I)^2 + (\pi T_j^R)^2 \right] \cdot \left[2 + (y_j^R)^2 + (y_j^I)^2 \right]} \times \\ & \times \left(\pi T_j^R \left[b^2 \left(\left[1 + \frac{g_2^R}{g_0} \right]^2 - \left[\frac{g_2^I}{g_0} \right]^2 \right) + 2b \hat{b} y_j^R \frac{g_1^R}{g_0} + 2b \hat{b} y_j^R \left(\frac{g_1^R}{g_0} \frac{g_2^R}{g_0} - \frac{g_1^I}{g_0} \frac{g_2^I}{g_0} \right) + \right. \right. \\ & \left. \left. + \hat{b}^2 ((y_j^R)^2 + (y_j^I)^2) \left(\left[\frac{g_1^R}{g_0} \right]^2 - \left[\frac{g_1^I}{g_0} \right]^2 \right) \right] - \right. \\ & \left. - 2(\omega - \pi T_j^I) \left[b^2 \frac{g_2^I}{g_0} + b \hat{b} y_j^R \frac{g_1^I}{g_0} + b \hat{b} y_j^R \left(\frac{g_1^R}{g_0} \frac{g_2^I}{g_0} + \frac{g_1^I}{g_0} \frac{g_2^R}{g_0} \right) + b^2 \frac{g_2^R}{g_0} \frac{g_2^I}{g_0} + \right. \right. \\ & \left. \left. + b^2 ((y_j^R)^2 + (y_j^I)^2) \frac{g_1^R}{g_0} \frac{g_1^I}{g_0} \right] \right). \end{aligned} \quad (5.1.30)$$

The formulas (5.1.29) and (5.1.30) are rather inconvenient for analytical calculations. However, they may serve as a starting point for numerical computations. As mentioned earlier, we are only interested in cases, where g_1 and g_2 are either real-valued or imaginary. So every term of the form $g_j^R \cdot g_j^I$ does not have to be taken into account in actual computations.

5.2 Dimer

In this section, we are going to deal with the case in which the apex atom is isolated from the remaining two. The isosceles trimer then is split up into a dimer and a single atom. This limiting case is given if there is no interaction between the apex atom and the other two. Using the definition of the matrix $\tilde{\mathbf{g}}(i\omega_n)$ (4.2.7) this means $g_1 = 0$ (the apex atom is infinitely far away from the other two). Hence, the matrix $\underline{\mathbf{g}}\underline{\mathbf{g}}$ is given as

$$\underline{\mathbf{g}}\underline{\mathbf{g}} = \begin{pmatrix} b^2 g_0 & 0 & b^2 g_2 \\ 0 & \hat{b}^2 g_0 & 0 \\ b^2 g_2 & 0 & b^2 g_0 \end{pmatrix},$$

5 Isosceles Trimer

where

$$g_2 = g_2^R - i g_2^I.$$

The eigenvalues of this matrix are the solutions of

$$(T_j^2 - 2T_j b^2 g_0 + b^2 g_0 - b^2 g_2) (\hat{b}^2 g_0 - T_j) = 0.$$

Hence, one gets

$$T_1 = b^2(g_0 - g_2), \tag{5.2.1}$$

$$T_2 = b^2(g_0 + g_2), \tag{5.2.2}$$

$$T_3 = \hat{b}^2 g_0. \tag{5.2.3}$$

This also follows from last section's equations (5.1.6)-(5.1.8). The eigenvectors compute to

$$u_1 = \frac{1}{\sqrt{2}} \begin{pmatrix} 1 \\ 0 \\ -1 \end{pmatrix}, \quad u_2 = \frac{1}{\sqrt{2}} \begin{pmatrix} 1 \\ 0 \\ 1 \end{pmatrix}, \quad u_3 = \begin{pmatrix} 0 \\ 1 \\ 0 \end{pmatrix}. \tag{5.2.4}$$

The eigenvectors do not depend on any of the parameters and are always real-valued. They also can be computed by (5.1.23), but then one has to determine the quantities y_j , as given in (5.1.13), more carefully. We will come back to this subject at the end of this section.

Having the eigenvalues and eigenvectors of $\underline{b} \underline{g} \underline{b}$ we can solve the mean field equations (4.3.4) and compute the local density of states (4.4.10) at any cluster site. We consider two different cases: ferromagnetic coupling of the dimer modelled by a real-valued g_2 and antiferromagnetic coupling where g_2 is purely imaginary. However, since the apex atom is isolated from the dimer, its local density of states should be the same in either case. Before we come to the dimer itself, we will treat the isolated atom first.

Since the eigenvalues T_1 and T_2 depend only on b while the real-valued $T_3 = T_3^R$ only depends on \hat{b} , the mean field equations decouple completely into an equation for \hat{b} and one for b . The one for \hat{b} is reads

$$2 \hat{b} g_0 \cdot 2 \log \frac{\hat{b}^2 g_0}{\Delta} = -\frac{2}{3J} \hat{b}$$

which apart from $\hat{b} = 0$ has the solution

$$\hat{b}^2 g_0 = \Delta \exp\left(-\frac{1}{2J\rho_0}\right) = T_3^R = T_3, \tag{5.2.5}$$

where we used $3g_0 = \rho_0$. T_3 is the same as T_0 in (4.5.2), so \hat{b} is the same as in the pure Kondo case. We compute the local density of states at the apex position \mathbf{R}_2 . Since

$$(v_{\mathbf{R}_i})_j = \frac{g_{ij}}{g_0},$$

it is

$$v_{\mathbf{R}_2} = \begin{pmatrix} 0 \\ 1 \\ 0 \end{pmatrix}.$$

5 Isosceles Trimer

Hence, the only $B_{XY}^{j\mathbf{R}_2}$ as defined in (4.4.9) that does not vanish and has to be taken into account in the local density of states (4.4.10) is

$$B_{RR}^{3\mathbf{R}_2} = (v_{\mathbf{R}_2})^T \underline{\mathbf{h}} u_3 = \hat{b}.$$

The local density of states is therefore given as

$$\begin{aligned} \rho(\omega, \mathbf{R}_2) &= \rho_0 \left(1 - \pi g_0 \frac{\pi T_3^R \hat{b}^2}{\omega^2 + (\pi T_3^R)^2} \right) \\ &= \rho_0 \left(1 - \frac{(\pi T_0)^2}{\omega^2 + (\pi T_0)^2} \right), \end{aligned} \quad (5.2.6)$$

where we used (5.2.5). The local density of states has the same form as in the completely isolated case which we treated in section 4.5. T_0 , as defined in (4.5.2), is the Kondo temperature of a single magnetic impurity. As expected, a pure Kondo effect occurs at the apex site, since it is completely isolated from the rest of the trimer so that geometric effects do not play any role.

We turn to treating the dimer, considering first ferromagnetic coupling between the dimer atoms corresponding to real-valued g_2 , and afterwards antiferromagnetic coupling corresponding to imaginary g_2 . Before we come to the mean field equations, we will compute the LDOS formally at the dimer atom \mathbf{R}_1 . As we have seen in section 5.1.1, we would get the same result if we computed the LDOS at \mathbf{R}_3 . Using the eigenvectors (5.2.4) and

$$v_{\mathbf{R}_1} = \begin{pmatrix} 1 \\ 0 \\ g_2^R/g_0 \end{pmatrix} - i \begin{pmatrix} 0 \\ 0 \\ g_2^I/g_0 \end{pmatrix}$$

we can determine the $B_{XY}^{j\mathbf{R}_1}$ as defined in (4.4.9). The only non-vanishing $B_{XY}^{j\mathbf{R}_1}$ are

$$B_{RR}^{1\mathbf{R}_1} = \frac{1}{\sqrt{2}} b \left(1 - \frac{g_2^R}{g_0} \right), \quad B_{IR}^{1\mathbf{R}_1} = -\frac{1}{\sqrt{2}} b \frac{g_2^I}{g_0}, \quad B_{RR}^{2\mathbf{R}_1} = \frac{1}{\sqrt{2}} b \left(1 + \frac{g_2^R}{g_0} \right)$$

and

$$B_{IR}^{2\mathbf{R}_1} = \frac{1}{\sqrt{2}} b \frac{g_2^I}{g_0}.$$

The LDOS (4.4.10) then computes to

$$\begin{aligned} \rho(\omega, \mathbf{R}_1) &= \rho_0 - \rho_0 \pi g_0 \frac{\pi b^2 (g_0 - g_2^R) \frac{1}{2} b^2 \left[\left(1 - \frac{g_2^R}{g_0} \right)^2 - \left(\frac{g_2^I}{g_0} \right)^2 \right] + 2 (\omega + \pi b^2 g_2^I) \frac{1}{2} b^2 \left(1 - \frac{g_2^R}{g_0} \right) \frac{g_2^I}{g_0}}{(\omega + \pi b^2 g_2^I)^2 + (\pi b^2 [g_0 - g_2^R])^2} \\ &\quad - \rho_0 \pi g_0 \frac{\pi b^2 (g_0 + g_2^R) \frac{1}{2} b^2 \left[\left(1 + \frac{g_2^R}{g_0} \right)^2 - \left(\frac{g_2^I}{g_0} \right)^2 \right] - 2 (\omega - \pi b^2 g_2^I) \frac{1}{2} b^2 \left(1 + \frac{g_2^R}{g_0} \right) \frac{g_2^I}{g_0}}{(\omega - \pi b^2 g_2^I)^2 + (\pi b^2 [g_0 + g_2^R])^2} \\ &= \rho_0 - \rho_0 \frac{1}{2} \frac{[\pi b^2 g_0]^2 (1 - \varepsilon_R) [(1 - \varepsilon_R)^2 - \varepsilon_I^2] + 2 (\omega + \pi b^2 g_0 \varepsilon_I) \pi b^2 g_0 (1 - \varepsilon_R) \varepsilon_I}{(\omega + \pi b^2 g_0 \varepsilon_I)^2 + (\pi b^2 g_0 (1 - \varepsilon_R))^2} \\ &\quad - \rho_0 \frac{1}{2} \frac{[\pi b^2 g_0]^2 (1 + \varepsilon_R) [(1 + \varepsilon_R)^2 - \varepsilon_I^2] - 2 (\omega - \pi b^2 g_0 \varepsilon_I) \pi b^2 g_0 (1 + \varepsilon_R) \varepsilon_I}{(\omega - \pi b^2 g_0 \varepsilon_I)^2 + (\pi b^2 g_0 (1 + \varepsilon_R))^2}, \end{aligned} \quad (5.2.7)$$

where we introduced

$$\varepsilon_R = \frac{g_2^R}{g_0} \quad \text{and} \quad \varepsilon_I = \frac{g_2^I}{g_0}. \quad (5.2.8)$$

5 Isosceles Trimer

As one can see, the mean field parameter \hat{b} does not appear in the LDOS at a dimer atom site. It only depends on b , and we will have to solve the corresponding mean field equations to get explicit formulas for the local density of states.

Before we start doing so for ferromagnetic dimer interactions, we will make some remarks about the connection of the density derived here and the general LDOS formulas (5.1.29) and (5.1.30) given in section (5.1.1). One can make use of these formulas directly, but then one has to make some considerations concerning the y_j (as given in (5.1.13)) which enter the eigenvectors u_j . The y_j are

$$y_j = \frac{2b\hat{b}g_1}{T_j - \hat{b}^2 g_0}.$$

Since $T_3 = \hat{b}^2 g_0$, the denominator of y_3 vanishes, but since $g_1 = 0$ for the dimer, so does the nominator. Thus, the value of y_j at $g_1 \rightarrow 0$ is unclear up to now. To get it, we expand the general eigenvalues T_j for the isosceles trimer (5.1.6)-(5.1.8) for small g_1/g_0 up to first non-vanishing order. It is

$$\begin{aligned} T_1 &= b^2(g_0 - g_2), \\ T_2 &= b^2(g_0 + g_2) + \frac{2b^2\hat{b}^2 g_1^2}{b^2(g_0 + g_2) - \hat{b}^2 g_0}, \\ T_3 &= \hat{b}^2 g_0 - \frac{2b^2\hat{b}^2 g_1^2}{b^2(g_0 + g_2) - \hat{b}^2 g_0}. \end{aligned}$$

For $g_1 \rightarrow 0$ this gives the dimer eigenvalues (5.2.1)-(5.2.3) since $b^2(g_0 + g_2) - \hat{b}^2 g_0 \neq 0$. Using this expansion for the T_j , we can immediately see that $y_2 = 0$ for $g_1 \rightarrow 0$. On the other hand, it is

$$y_3 \propto \frac{1}{g_1},$$

so that $|y_3| \rightarrow \infty$ for $g_1 \rightarrow 0$. Putting these results along with $g_1 = 0$ into the LDOS formulas (5.1.29) and (5.1.30), one arrives at the dimer densities (5.2.6) and (5.2.7). The dimer case therefore is a continuous limit of the isosceles trimer, a special treatment (which we applied to it here) would not have been necessary. However, we decided to choose a more instructive way of deriving the dimer quantities. Moreover, it will turn out that the more general LDOS formulas (5.1.29) and (5.1.30) in some systems give rise to numerical problems if the dimer case is approached, due to the divergence of y_3 .

5.2.1 Ferromagnetic dimer coupling

If the dimer atoms are coupled ferromagnetically, the coupling g_2 is real-valued:

$$g_2 = g_2^R.$$

The eigenvalues T_1 and T_2 in this case read

$$\begin{aligned} T_1 &= b^2(g_0 - g_2^R) = b^2 g_0(1 - \varepsilon_R) = T_1^R, \\ T_2 &= b^2(g_0 + g_2^R) = b^2 g_0(1 + \varepsilon_R) = T_2^R, \end{aligned}$$

5 Isosceles Trimer

where we used ε_R as in (5.2.8). The eigenvalue T_3 is still given by (5.2.3). The mean field equation (4.3.4) for b reads in the ferromagnetic case

$$2b g_0 (1 - \varepsilon_R) \cdot 2 \log \frac{b^2 g_0 (1 - \varepsilon_R)}{\Delta} + 2b g_0 (1 + \varepsilon_R) \cdot 2 \log \frac{b^2 g_0 (1 + \varepsilon_R)}{\Delta} = -\frac{4}{3J} b.$$

Neglecting the trivial solution $b = 0$, this equation is equivalent to

$$2 \log \frac{b^2 g_0}{\Delta} + \log(1 - \varepsilon_R^2) + \varepsilon \log \frac{1 + \varepsilon_R}{1 - \varepsilon} = -\frac{1}{J\rho_0},$$

where we used $3g_0 = \rho_0$. Hence, one gets

$$\begin{aligned} b^2 g_0 &= \Delta \exp\left(-\frac{1}{2J\rho_0}\right) \exp\left(-\frac{1}{2} \log(1 - \varepsilon_R^2) - \frac{1}{2} \varepsilon_R \log \frac{1 + \varepsilon_R}{1 - \varepsilon_R}\right) \\ &= T_0 f(\varepsilon_R), \end{aligned} \quad (5.2.9)$$

where T_0 is the single-impurity Kondo temperature (4.5.2) and

$$f(\varepsilon_R) = \exp\left(-\frac{1}{2} \log(1 - \varepsilon_R^2) - \frac{1}{2} \varepsilon_R \log \frac{1 + \varepsilon_R}{1 - \varepsilon_R}\right). \quad (5.2.10)$$

Using (5.2.6), we get the LDOS

$$\rho(\omega, \mathbf{R}_1) = \rho_0 \left(1 - \frac{1}{2} \frac{[\pi T_0 f(\varepsilon_R)]^2 (1 - \varepsilon_R)^3}{\omega^2 + [\pi T_0 f(\varepsilon_R)]^2 (1 - \varepsilon_R)^2} - \frac{1}{2} \frac{[\pi T_0 f(\varepsilon_R)]^2 (1 + \varepsilon_R)^3}{\omega^2 + [\pi T_0 f(\varepsilon_R)]^2 (1 + \varepsilon_R)^2}\right). \quad (5.2.11)$$

Plotting (5.2.11), one can see that a Kondo dip appears for each ε_R . We plotted the LDOS for $\varepsilon_R = 0.3$ on the left hand side of figure 5.1 as a solid line. We are interested in the behaviour of the Kondo temperature when the geometry of the Dimer is changed, say with varying ε_R . As we know, the Kondo temperature is proportional to the width of the density dip. We can most accurately fit the density (5.2.11) with the formula of a Fano-resonance

$$\rho(\omega, \mathbf{R}_2) = \rho_0 \frac{(q\pi\Gamma + \omega)^2}{\omega^2 + (\pi\Gamma)^2}. \quad (5.2.12)$$

Here, q is the Fano factor which depends on the coupling of the STM tip to the substrate. For ε_R between 0 and 0.3, we get $q \approx 0$. We plotted the approximation (5.2.12) for $\varepsilon_R = 0.3$ as a dashed line on the right hand side of figure 5.1. As one can see, the approximation is very accurate. It is better, the smaller the coupling ε_R is. $\pi\Gamma$ is the half-width of (5.2.12). We compute it for each ε_R and compare it to πT_0 , the one of a pure Kondo system. We plot the ε_R dependence of this normalised half-width on the right hand side of figure 5.1. As T_0 was interpreted as the Kondo temperature of an isolated pure Kondo system, we can now interpret Γ as the Kondo temperature for the interacting system. We make some simple observations. As the ferromagnetic coupling ε_R gets stronger, the Kondo temperature rises, which means that the Kondo effect is enhanced: the Kondo cloud will form at a higher external temperature than it would in the case of a single magnetic impurity. This enhancement has to be due to the increase of the total magnetic moment of the dimer. Since the dimer atoms are ferromagnetically coupled, they tend to maximise the total spin of the system, which results in a higher Kondo temperature (see [50]). It is quite remarkable, that the increase of the total magnetic moment of the dimer

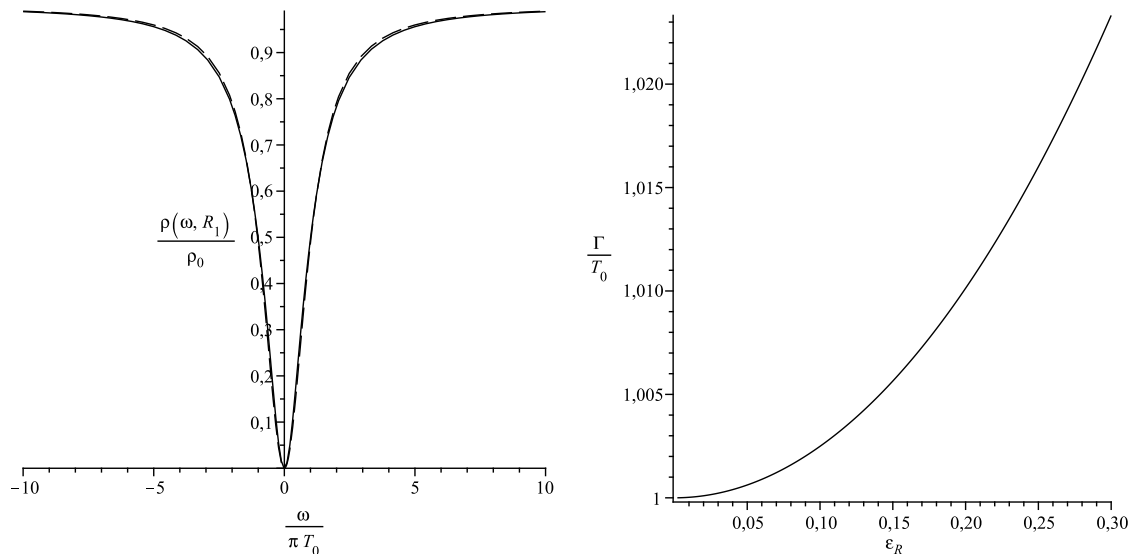


Figure 5.1: LDOS and Fano resonance fit for ferromagnetic coupling $\varepsilon_R = 0.3$. RHS: Dependence of Kondo temperature on coupling $\varepsilon_R \in [0, 0.3]$.

influences the Kondo temperature even for "loose" system, which we are considering here. The shape of the right hand side of figure 5.1 is very accurately approximated by

$$\frac{\Gamma}{T_0} = 1 + 0.258 \cdot \varepsilon_R^2. \quad (5.2.13)$$

As mentioned in section 4.2.1, the couplings g_j in lowest order enter quadratically in the RKKY-interaction, which they seem also to do in the Kondo temperature. If one takes into account only widths up to couplings $\varepsilon_R = 0.2$ and fits a parabola to the data, the prefactor in front of the quadratic term becomes 0.253. The smaller the couplings strengths ε_R are, which are taken into account for the fit, the closer this prefactor comes to 0.25. The enhancement of the Kondo temperature is therefore roughly given by

$$\Delta \frac{\Gamma}{T_0} = \frac{1}{4} \cdot \varepsilon_R^2$$

and is about 2.3 per cent at $\varepsilon_R = 0.3$. However, beyond that coupling strength, the enhancement is even stronger, but it is not clear if the system is still well described by the present mean field model at such strong couplings.

5.2.2 Antiferromagnetic dimer coupling

If the dimer atoms are coupled antiferromagnetically, g_2 is purely imaginary. As we defined $g_2 = g_2^R - i g_2^I$ we get

$$g_2 = -i g_2^I.$$

Using the abbreviation (5.2.8), the eigenvalues T_1 and T_2 read

$$\begin{aligned} T_1 &= b^2 g_0 - i(-b^2 g_0 \varepsilon_I) = T_1^R - i T_1^I \\ T_2 &= b^2 g_0 - i b^2 g_0 \varepsilon_I = T_2^R - i T_2^I. \end{aligned}$$

5 Isosceles Trimer

The mean field equation (4.3.4) for b reads

$$4 b g_0 \log \frac{[b^2 g_0]^2 (1 + \varepsilon_I^2)}{\Delta^2} - 2 \cdot (-2) b g_0 \varepsilon_I \arctan \frac{-b^2 g_0 \varepsilon_I}{b^2 g_0} - 2 \cdot 2 b g_0 \varepsilon_I \arctan \frac{b^2 g_0 \varepsilon_I}{b^2 g_0} = -\frac{4}{3J} b.$$

Excluding the trivial solution $b = 0$, this equation is equivalent to

$$2 \log \frac{b^2 g_0}{\Delta} + \log (1 + \varepsilon_I^2) - 2 \varepsilon_I \arctan \varepsilon_I = -\frac{1}{J \rho_0},$$

where we used $3 g_0 = \rho_0$. Solving this for $b^2 g_0$, one gets

$$\begin{aligned} b^2 g_0 &= \Delta \exp \left(-\frac{1}{2 J \rho_0} \right) \exp \left(\varepsilon_I \arctan \varepsilon_I - \frac{1}{2} \log (1 + \varepsilon_I^2) \right) \\ &= T_0 g(\varepsilon_I), \end{aligned} \quad (5.2.14)$$

with T_0 being the single-impurity Kondo temperature and

$$g(\varepsilon_I) = \exp \left(\varepsilon_I \arctan \varepsilon_I - \frac{1}{2} \log (1 + \varepsilon_I^2) \right). \quad (5.2.15)$$

With the formula for the local density of states (5.2.7) one gets

$$\begin{aligned} \rho(\omega, \mathbf{R}_1) &= \rho_0 \left(1 - \frac{1}{2} \frac{[\pi T_0 g(\varepsilon_I)]^2 (1 - \varepsilon_I^2) + 2 (\omega + \pi T_0 g(\varepsilon_I) \varepsilon_I) \pi T_0 g(\varepsilon_I) \varepsilon_I}{[\omega + \pi T_0 g(\varepsilon_I) \varepsilon_I]^2 + [\pi T_0 g(\varepsilon_I)]^2} - \right. \\ &\quad \left. - \frac{1}{2} \frac{[\pi T_0 g(\varepsilon_I)]^2 (1 - \varepsilon_I^2) - 2 (\omega - \pi T_0 g(\varepsilon_I) \varepsilon_I) \pi T_0 g(\varepsilon_I) \varepsilon_I}{[\omega - \pi T_0 g(\varepsilon_I) \varepsilon_I]^2 + [\pi T_0 g(\varepsilon_I)]^2} \right). \end{aligned} \quad (5.2.16)$$

For each ε_I this has the form of a Kondo dip. As in the ferromagnetic case, we fit a Fano resonance (5.2.12) to (5.2.16) for any given ε_I between 0 and 0.3. These fits are quite accurate, but not as good as in the ferromagnetic case, as one can see on the left hand side of figure 5.2, where we plotted the LDOS (solid line) and its Fano fit (dashed line) for $\varepsilon_I = 0.3$. However, the smaller the couplings are, the better the LDOS can be fitted to a Fano resonance. As in the previous case, we compute the half-width $\pi \Gamma$ of the Fano fit and compare it to the single-impurity width πT_0 . The dependence of this normalised width on the coupling ε_I is shown on the right hand side of figure 5.2. Again, we interpret Γ as the Kondo temperature of the system. As the antiferromagnetic coupling increases, the Kondo temperature gets lower. The Kondo effect is therefore suppressed, the formation of the Kondo cloud will occur at lower temperatures than it would in the case of a single magnetic impurity. This, as in the ferromagnetic case, is due to the spin interaction of the dimer atoms. Since they are antiferromagnetically coupled, they tend to minimise the total magnetic moment of the dimer, which apparently leads to a lower Kondo temperature. The shape of the Kondo temperature graph in 5.2 can quite well be fitted with a quadratic function

$$\frac{\Gamma}{T_0} = 1 - 0.234 \cdot \varepsilon_I^2.$$

This behaviour is similar to the one in the ferromagnetic case except for the sign. As in the ferromagnetic case, the prefactor of the quadratic term comes the closer to 0.25 the smaller the couplings ε_I are, which are taken into account for the fit. The influence of the dimer couplings on the Kondo temperature is therefore roughly given as

$$\Delta \frac{\Gamma}{T_0} = -\frac{1}{4} \cdot \varepsilon_I^2.$$

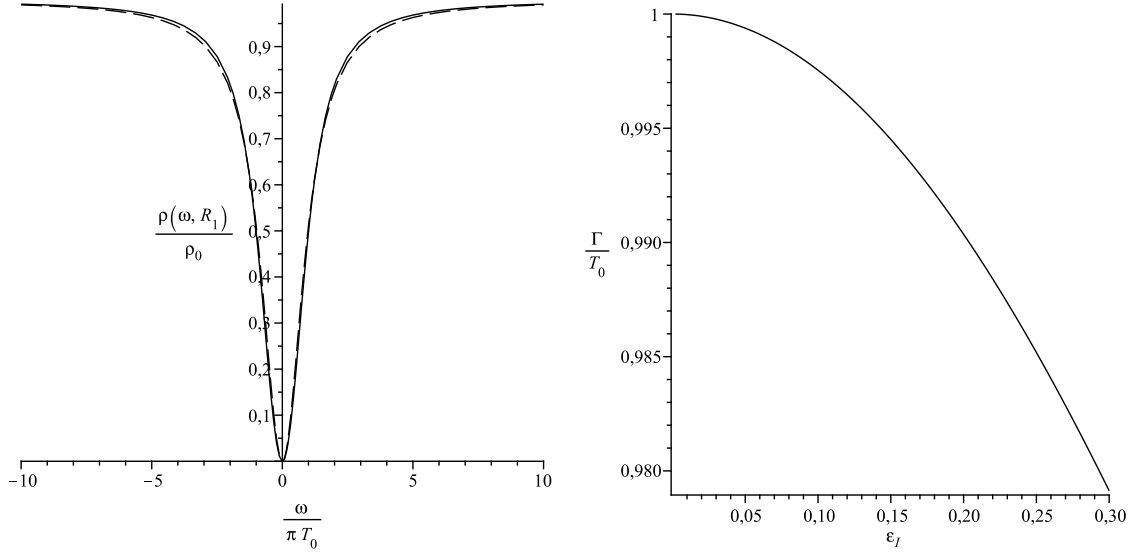


Figure 5.2: LDOS and Fano resonance fit for antiferromagnetic coupling $\varepsilon_I = 0.3$. RHS: Dependence of Kondo temperature on coupling $\varepsilon_I \in [0, 0.3]$.

5.3 Equilateral trimer

We turn to another special case of an isosceles trimer, the equilateral one. In this case the entries g_1 and g_2 in (5.1.1) coincide since all inter atomic distances $|\mathbf{R}_i - \mathbf{R}_j|$ do so for $i \neq j$. Moreover, we assume $\hat{b} = b$ in (5.1.2), since the hybridisations must be the same for each cluster site. This means, we only have to deal with one mean field parameter b instead of two and therefore only one mean field equation has to be solved. The right hand side of (4.3.4) then reads

$$-\frac{1}{3J} \frac{\partial}{\partial b} \text{Tr} \underline{b}^2 = -\frac{1}{3J} 3 \cdot 2b = -\frac{2}{J} b.$$

We therefore get the mean field equation

$$\sum_{j=1}^N \left[\frac{\partial T_j^R}{\partial b} \log \left(\frac{(T_j^R)^2 + (T_j^I)^2}{\Delta^2} \right) - 2 \frac{\partial T_j^I}{\partial b} \arctan \left(\frac{T_j^I}{T_j^R} \right) \right] = -\frac{2}{J} b. \quad (5.3.1)$$

In the following, we use the notation

$$g_1 = g_2 = g_{1/2}^R - i g_{1/2}^I = g_0 (\varepsilon_R - i \varepsilon_I), \quad (5.3.2)$$

as we have done quite similarly when we treated the dimer. The eigenvalues T_1 , T_2 and T_3 as defined in (5.1.6)-(5.1.8) are given as

$$T_1 = b^2 g_0 (1 - \varepsilon_R) - i (-b^2 g_0 \varepsilon_I) = T_1^R - i T_1^I, \quad (5.3.3)$$

$$T_2 = b^2 g_0 (1 + 2\varepsilon_R) - i 2b^2 g_0 \varepsilon_I = T_2^R - i T_2^I, \quad (5.3.4)$$

$$T_3 = b^2 g_0 (1 - \varepsilon_R) - i (-b^2 g_0 \varepsilon_I) = T_3^R - i T_3^I. \quad (5.3.5)$$

Here, we used (with $g_1 = g_2$ and $b = \hat{b}$)

$$\begin{aligned} \sqrt{(b^2 g_0 + b^2 g_2 - \hat{b}^2 g_0)^2 + 8 b^2 \hat{b}^2 g_1^2} &= \sqrt{(b^2 g_1)^2 + 8 b^4 g_1^2} \\ &= 3 b^2 g_0 (\varepsilon_R - i \varepsilon_I). \end{aligned}$$

Sign ambiguities of the square root are not relevant since both signs appear in T_2 and T_3 . As one can see, T_1 and T_3 coincide for the equilateral trimer. Before we turn to solving the mean field equations for the ferromagnetic and the antiferromagnetic case, we give the LDOS of the problem. Since it must be the same at all three trimer atoms (because the trimer is equilateral), we are free to use one of the formulas (5.1.30) or (5.1.29). The latter is easier to handle, though. To compute it, we first have to determine the $y_j^{R/I}$ as given in (5.1.22) for $g_1 = g_2$ and $b = \hat{b}$. Those become quite simple: it is

$$y_2^R = 1, \quad y_2^I = 0, \quad y_3^R = -2 \quad \text{and} \quad y_3^I = 0.$$

Using (5.1.29) we arrive at

$$\begin{aligned} \rho(\omega, \mathbf{R}_2) = & \rho_0 - \rho_0 \frac{1}{3} \frac{[\pi b^2 g_0]^2 (1+2\varepsilon_R)[(1+2\varepsilon_R)^2 - 4\varepsilon_I^2] - 2(\omega - 2\pi b^2 g_0 \varepsilon_I) 2\pi b^2 g_0 \varepsilon_I (1+2\varepsilon_R)}{[\omega - 2\pi b^2 g_0 \varepsilon_I]^2 + [\pi b^2 g_0 (1+2\varepsilon_R)]^2} \\ & - \rho_0 \frac{2}{3} \frac{[\pi b^2 g_0]^2 (1-\varepsilon_R)[(1-\varepsilon_R)^2 - \varepsilon_I^2] + 2(\omega + \pi b^2 g_0 \varepsilon_I) \pi b^2 g_0 \varepsilon_I (1-\varepsilon_R)}{[\omega + \pi b^2 g_0 \varepsilon_I]^2 + [\pi b^2 g_0 (1-\varepsilon_R)]^2}. \end{aligned} \quad (5.3.6)$$

5.3.1 Ferromagnetic trimer coupling

We start with the ferromagnetic case for which $g_{1/2}$ is real valued

$$g_{1/2} = g_0 \varepsilon_R.$$

The eigenvalues then are

$$\begin{aligned} T_1 &= b^2 g_0 (1 - \varepsilon_R) = T_3, \\ T_2 &= b^2 g_0 (1 + 2\varepsilon_R). \end{aligned}$$

The mean field equation (5.3.1) is

$$2 \cdot 2b g_0 (1 - \varepsilon_R) \cdot 2 \log \frac{b^2 g_0 (1 - \varepsilon)}{\Delta} + 2b^2 g_0 (1 + 2\varepsilon_R) \cdot 2 \log \frac{b^2 g_0 (1 + 2\varepsilon_R)}{\Delta} = -\frac{2}{J} b.$$

Excluding the trivial solution $b = 0$, this is equivalent to

$$3 \log \frac{b^2 g_0}{\Delta} + 2(1 - \varepsilon_R) \log(1 - \varepsilon_R) + (1 + 2\varepsilon_R) \log(1 + 2\varepsilon_R) = -\frac{3}{2J\rho_0},$$

where we used $3g_0 = \rho_0$. Solving for $b^2 g_0$, one arrives at

$$\begin{aligned} b^2 g_0 &= \Delta \exp\left(-\frac{1}{2J\rho_0}\right) \exp\left(-\frac{2}{3}(1 - \varepsilon_R) \log(1 - \varepsilon_R) - \frac{1}{3}(1 + 2\varepsilon_R) \log(1 + 2\varepsilon_R)\right) \\ &= T_0 f(\varepsilon_R), \end{aligned} \quad (5.3.7)$$

with T_0 the single impurity Kondo temperature (4.5.2) and with

$$f(\varepsilon_R) = \exp\left(-\frac{2}{3}(1 - \varepsilon_R) \log(1 - \varepsilon_R) - \frac{1}{3}(1 + 2\varepsilon_R) \log(1 + 2\varepsilon_R)\right). \quad (5.3.8)$$

The LDOS at any trimer atom is in this case given as

$$\rho(\omega, \mathbf{R}_2) = \rho_0 \left(1 - \frac{1}{3} \frac{[\pi T_0 f(\varepsilon_R)]^2 (1 + 2\varepsilon_R)^3}{\omega^2 + [\pi T_0 f(\varepsilon_R)]^2 (1 + 2\varepsilon_R)^2} - \frac{2}{3} \frac{[\pi T_0 f(\varepsilon_R)]^2 (1 - \varepsilon_R)^3}{\omega^2 + [\pi T_0 f(\varepsilon_R)]^2 (1 - \varepsilon_R)^2} \right). \quad (5.3.9)$$

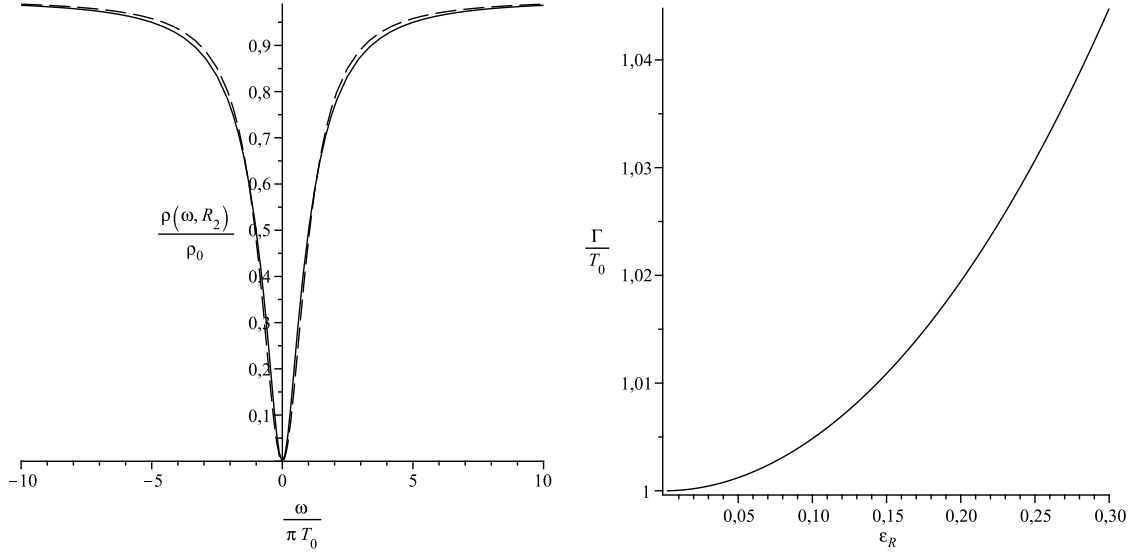


Figure 5.3: LDOS and Fano resonance fit for ferromagnetic coupling $\varepsilon_R = 0.3$. RHS: Dependence of Kondo temperature on coupling $\varepsilon_R \in [0, 0.3]$.

For each ε_R this density shows a Kondo dip. As with the dimer we fit the LDOS (5.3.9) to a Fano resonance shape (5.2.12). These fits are quite accurate for couplings ε_R between 0 and 0.3. The left hand side of figure 5.3 shows the LDOS for $\varepsilon_R = 0.3$ (solid line) and the corresponding Fano fit (dashed line). We compute the widths of the Fano fits for ε_R between 0 and 0.3 and compare them to the width πT_0 of the LDOS of a single magnetic impurity. The result is shown on the right hand side of 5.3. As for the dimer, we can interpret Γ as the Kondo temperature of the system. The Kondo effect is enhanced compared to T_0 for non-vanishing ferromagnetic coupling. This is due to the trimer tending to maximise the total spin because of the ferromagnetic interaction of the trimer spins. The ε_R -dependence of the normalised Kondo temperature is approximated quite well by

$$\frac{\Gamma}{T_0} = 1 + 0.494 \cdot \varepsilon_R^2.$$

As in the dimer case, the behaviour is quadratic for sufficiently small couplings and the approximation becomes more accurate if the couplings, which are taken into account, become smaller. The enhancement of the Kondo temperature is about twice as large as for the ferromagnetic dimer. It seems, that it can be seen as being the result of the cumulative influence of two dimers each impurity is linked to.

5.3.2 Antiferromagnetic trimer coupling

We turn to the antiferromagnetic case where $g_{1/2}$ is imaginary

$$g_{1/2} = -i g_0 \varepsilon_I.$$

The eigenvalues T_1 , T_2 and T_3 then read

$$\begin{aligned} T_1 &= b^2 g_0 - i(-b^2 g_0 \varepsilon_I) = T_1^R - iT_1^I = T_3, \\ T_2 &= b^2 g_0 - i2b^2 g_0 \varepsilon_I = T_2^R - iT_2^I. \end{aligned}$$

5 Isosceles Trimer

The mean field equation (5.3.1) is given as

$$2 \cdot 2 b g_0 \log \frac{[b^2 g_0]^2 (1 + \varepsilon_I^2)}{\Delta^2} + 2 \cdot 2 \cdot 2 b g_0 \varepsilon_I \arctan \frac{-b^2 g_0 \varepsilon_I}{b^2 g_0} + \\ + 2 b g_0 \log \frac{[b^2 g_0]^2 (1 + 4 \varepsilon_I^2)}{\Delta^2} + 2 \cdot 2 b g_0 \cdot 2 \varepsilon_I \arctan \frac{b^2 g_0 2 \varepsilon_I}{b^2 g_0} = -\frac{1}{J} b.$$

If $b \neq 0$ this equation becomes

$$3 \log \frac{b^2 g_0}{\Delta} + \log(1 + \varepsilon_I^2) + \frac{1}{2} \log(1 + 4 \varepsilon_I^2) - 2 \varepsilon_I [\arctan(\varepsilon_I) + \arctan(2 \varepsilon_I)] = -\frac{3}{2 J \rho_0},$$

where we inserted $3 g_0 = \rho_0$. We solve for $b^2 g_0$ and get

$$b^2 g_0 = \Delta \exp\left(-\frac{1}{2 J \rho_0}\right) \exp\left(-\frac{1}{3} \log(1 + \varepsilon_I^2) - \frac{1}{6} \log(1 + 4 \varepsilon_I^2) + \right. \\ \left. + \frac{2}{3} \varepsilon_I [\arctan(\varepsilon_I) + \arctan(2 \varepsilon_I)]\right) \\ = T_0 g(\varepsilon_I), \tag{5.3.10}$$

with T_0 given by (4.5.2) and where

$$g(\varepsilon_I) = \exp\left(-\frac{1}{3} \log(1 + \varepsilon_I^2) - \frac{1}{6} \log(1 + 4 \varepsilon_I^2) + \frac{2}{3} \varepsilon_I [\arctan(\varepsilon_I) + \arctan(2 \varepsilon_I)]\right). \tag{5.3.11}$$

The local density of states at any trimer atom is given as

$$\rho(\omega, \mathbf{R}_2) = \rho_0 \left(1 - \frac{1}{3} \frac{[\pi T_0 g(\varepsilon_I)]^2 (1 - 4 \varepsilon_I^2) - 2 [\omega - 2 \pi T_0 g(\varepsilon_I) \varepsilon_I] \cdot 2 \pi T_0 g(\varepsilon_I) \varepsilon_I}{[\omega - 2 \pi T_0 g(\varepsilon_I) \varepsilon_I]^2 + [\pi T_0 g(\varepsilon_I)]^2} - \right. \\ \left. - \frac{2}{3} \frac{[\pi T_0 g(\varepsilon_I)]^2 (1 - \varepsilon_I^2) + 2 [\omega + \pi T_0 g(\varepsilon_I) \varepsilon_I] \cdot \pi T_0 g(\varepsilon_I) \varepsilon_I}{[\omega + \pi T_0 g(\varepsilon_I) \varepsilon_I]^2 + [\pi T_0 g(\varepsilon_I)]^2} \right). \tag{5.3.12}$$

The LDOS is dipped around $\omega = 0$ for each coupling ε_I . We fit the LDOS (5.3.12) to a Fano shape (5.2.12). For ε_I up to 0.3 this approximation works quite well. We plotted the LDOS (solid line) and its Fano shaped fit (dashed line) for $\varepsilon_I = 0.3$ in the left hand side of figure 5.4. The fit is the more accurate the smaller the coupling strength is.

As in the ferromagnetic case, we compute the widths of the Fano fits for ε_I between 0 and 0.3 and compare them to the reference width πT_0 . The dependence of that normalised width on ε_I is plotted on the right hand side of 5.4. Since the width is proportional to the Kondo temperature in the domain of the Kondo effect, the plot shows that the Kondo temperature of the equilateral trimer compared to the one of a single magnetic impurity decreases, if the antiferromagnetic coupling ε_I gets larger. Antiferromagnetic trimer interactions therefore suppress the Kondo effect, the Kondo cloud is formed at lower temperatures. One can explain this behaviour with the tendency of the trimer to minimise its total spin as in the dimer case. However, there could be another effect which would have to be taken into account. Contrary to the dimer spins, the trimer spins are always frustrated, since no stable antiferromagnetic configuration can be achieved, if all impurities are coupled antiferromagnetically. Nevertheless ε_I dependence of the normalised Kondo temperature Γ/T_0 is approximately quadratic as for the systems described up to now. It is quite well fit by

$$\frac{\Gamma}{T_0} = 1 - 0.503 \cdot \varepsilon_I^2.$$

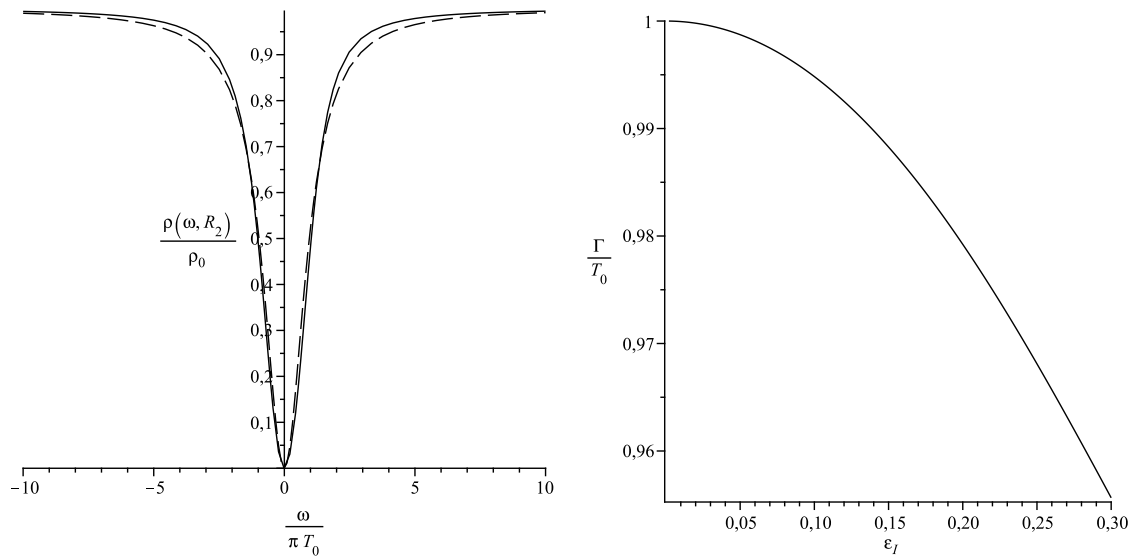


Figure 5.4: LDOS and Fano resonance fit for antiferromagnetic coupling $\epsilon_I = 0.3$. RHS: Dependence of Kondo temperature on coupling $\epsilon_I \in [0, 0.3]$.

As for the ferromagnetic trimer, the decay of the Kondo temperature is about twice as large as for the dimer case. Again, one could roughly state that each impurity is under the cumulative influence of two antiferromagnetic dimers. Therefore, frustration effects do not seem to be very large.

5.4 Linear chain

The third of the limiting cases of an isosceles trimer we are going to treat is the impurities forming a linear chain. The apex atom is the centre of the chain while the remaining two are its boundaries. We assume the chain to have only next neighbour interactions since the interaction between the boundary sites will be screened for a sufficiently large chain length. In the notation presented here, that means

$$g_2 = 0$$

in the matrix (5.1.1). The remaining inter impurity coupling is

$$g_1 = g_1^R - i g_1^I = g_0(\epsilon_R - i e_I).$$

As in the latter sections, we assume g_1 to be either real-valued or purely imaginary. The eigenvalues T_1 , T_2 and T_3 of \underline{bgb} are given by (5.1.15) and (5.1.17) - (5.1.20) as presented in section 5.1.1. To get them, we determine the quantities z^R and z^I as given in (5.1.16). Using that either $g_1^R = 0$ or $g_1^I = 0$ and that $g_2 = 0$ we get

$$z^R = (b^2 - \hat{b}^2)^2 g_0^2 + 8 b^2 \hat{b}^2 [(g_1^R)^2 - (g_1^I)^2]$$

and

$$z^I = 0$$

and thus

$$\begin{aligned} T_1 &= b^2 g_0 = T_1^R, \\ T_2 &= \frac{1}{2} \left(b^2 g_0 + \hat{b}^2 g_0 + \sqrt{(b^2 - \hat{b}^2)^2 g_0^2 + 8 b^2 \hat{b}^2 [(g_1^R)^2 - (g_1^I)^2]} \right) = T_2^R, \\ T_3 &= \frac{1}{2} \left(b^2 g_0 + \hat{b}^2 g_0 - \sqrt{(b^2 - \hat{b}^2)^2 g_0^2 + 8 b^2 \hat{b}^2 [(g_1^R)^2 - (g_1^I)^2]} \right) = T_3^R. \end{aligned}$$

The eigenvalues $T_1 - T_3$ are therefore real-valued. Although this significantly simplifies the mean field equations (4.3.4), it is still more convenient to solve them numerically, which we did using MAPLE. Afterwards we used the formulas (5.1.29) and (5.1.30) to determine the local density of states at the central impurity and the boundary impurities respectively.

5.4.1 Ferromagnetic chain interactions

If the boundary atoms interact ferromagnetically with the central atom, it is

$$g_1 = g_1^R = g_0 \varepsilon_R.$$

We solve the mean field equations for b and \hat{b} numerically and compute the local density of states at the central atom (5.1.29) and at the boundary atoms (5.1.30). In both cases the LDOS is dipped around the Fermi energy $\omega = 0$. We approximate the LDOS at \mathbf{R}_1 and \mathbf{R}_2 with a Fano resonance shape (5.2.12) for ε_R between 0 and 0.3. This approximation is better for the central atom than for the boundaries of the chain, but in both cases it is quite accurate. The LDOS at the central impurity (solid line) and its corresponding Fano fit (dashed line) are plotted on the left hand side of figure 5.5 for $\varepsilon_R = 0.3$, the fits getting the better the smaller ε_R is. As in the latter sections we compute the width of the Fano fit for each ε_R and

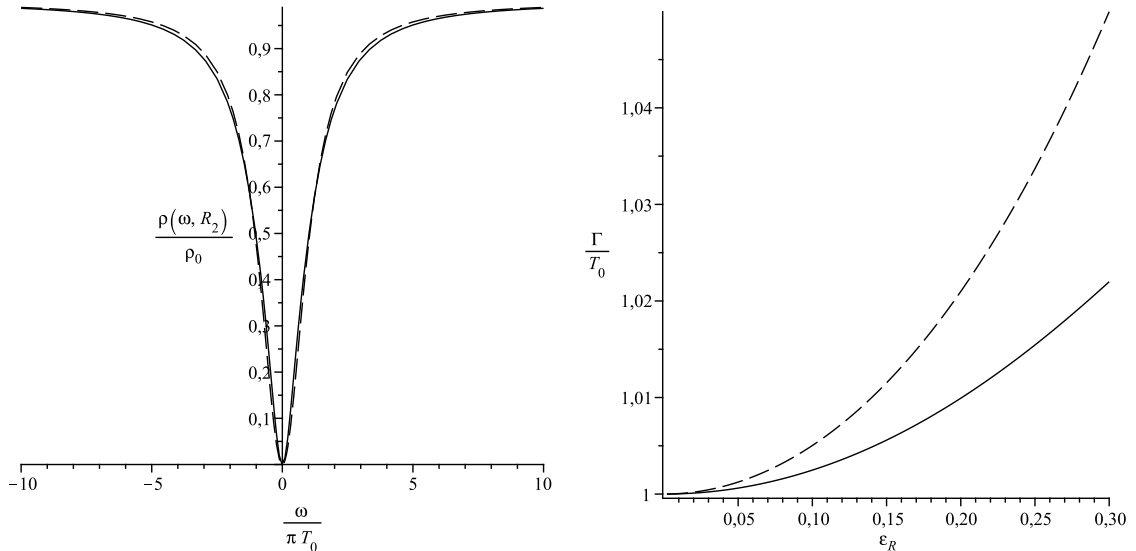


Figure 5.5: LDOS and Fano resonance fit for ferromagnetic coupling $\varepsilon_R = 0.3$ at the central atom. RHS: Dependence of Kondo temperature on coupling $\varepsilon_R \in [0, 0.3]$ for central atom (dashed line) and boundary atoms (solid line).

compare it to the single impurity width πT_0 , interpreting the fraction Γ/T_0 of those widths as the normalised Kondo temperature. The right hand side of 5.5 shows the dependence of this normalised Kondo temperature on the ferromagnetic coupling strength ε_R for the central impurity (dashed line) and the boundary impurities (solid line). At both sites, the Kondo temperature increases with ascending interaction strength, but the enhancement of the Kondo effect is larger at the central atom than it is at the boundary atoms. As with the dimer and the equilateral trimer, the dependence of the normalised Kondo temperature on the couplings ε_R is approximately quadratic and it is

$$\frac{\Gamma}{T_0}(\text{Centre}) = 1 + 0.549 \cdot \varepsilon_R^2$$

and

$$\frac{\Gamma}{T_0}(\text{Boundary}) = 1 + 0.246 \cdot \varepsilon_R^2.$$

For the boundary impurities this is about the same behaviour as for the ferromagnetic dimer, for the central impurity the dependence resembles the one of the equilateral trimer. The ferromagnetic chain can be interpreted as being composed of two dimers where the effect on the central atom, the connexional atom of the two dimers, is twice as large as for a single dimer. The increase of the Kondo effect can be explained the same way as for the dimer: each dimer tends to maximise its total magnetic moment and thus gives rise to a higher Kondo temperature. The central atom is part of two distinct dimers and thus the effect on the Kondo temperature is twice as large.

5.4.2 Antiferromagnetic chain interactions

For the boundary impurities coupling antiferromagnetically to the central atom, it is

$$g_1 = -i g_1^I = -i g_0 \varepsilon_I.$$

The mean field equations for b and \hat{b} are solved numerically, and again we compute the local density of states at the centre of the chain and at its boundaries. As in the ferromagnetic case the densities develop a dip around the Fermi energy and we approximate them by Fano resonances (5.2.12) for ε_I between 0 and 0.3. As in the latter case, these fits are quite well for both sites. We plotted the LDOS at the centre and its Fano fit for $\varepsilon_I = 0.3$ on the left hand side of figure 5.6. Computing the normalised Kondo temperature of the system depending on the coupling strength similarly to the latter cases, we see on the right hand side of figure 5.6 that the Kondo effect is suppressed at the centre (dashed line) as well as at the boundary of the chain (solid line). As for ferromagnetic couplings, the effect on the central impurity is stronger than that on the boundary atoms, but most notably, it is much stronger for both of them than in the ferromagnetic case. While the increase of the Kondo temperature for ferromagnetic interactions was about 5.0 per cent at the centre and about 2.2 per cent at the boundary, the decrease in the antiferromagnetic case is approximately 22.0 per cent at the centre and 19.4 per cent for the boundary impurities. For ferromagnetic couplings, the chain behaved like a composition of two linked dimers, which definitely does not describe the geometric behaviour in the antiferromagnetic case.

Nevertheless, the dependence of the normalised Kondo temperature on the couplings is quite accurately approximated quadratically for ε_I less than 0.3, as it was in the latter cases. It is

$$\frac{\Gamma}{T_0}(\text{Centre}) = 1 - 2.437 \cdot \varepsilon_I^2$$

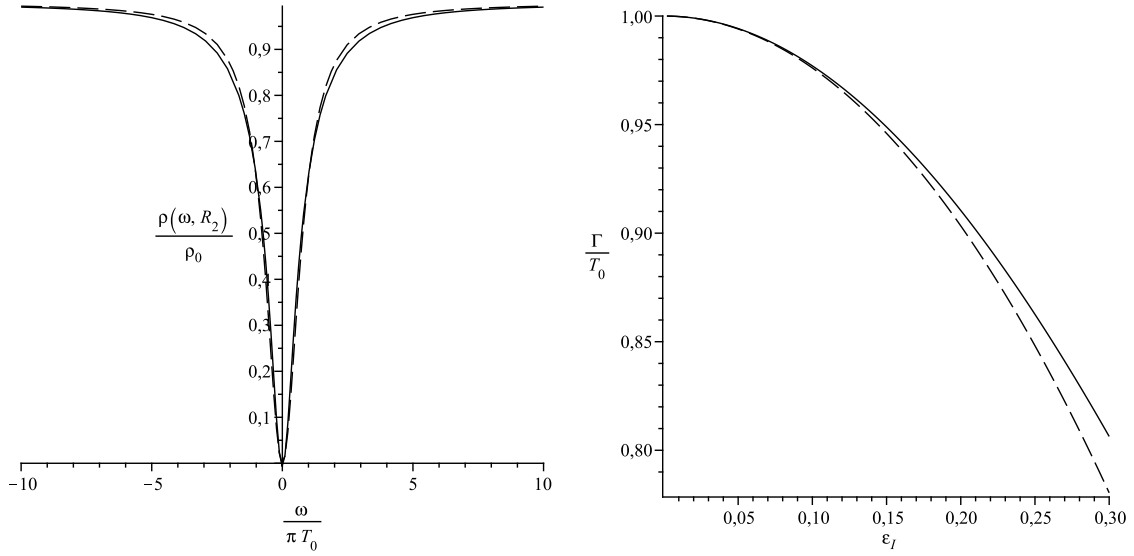


Figure 5.6: LDOS and Fano resonance fit for antiferromagnetic coupling $\varepsilon_I = 0.3$ at the central atom. RHS: Dependence of Kondo temperature on coupling $\varepsilon_I \in [0, 0.3]$ for central atom (dashed line) and boundary atoms (solid line).

and

$$\frac{\Gamma}{T_0}(\text{Boundary}) = 1 - 2.172 \cdot \varepsilon_I^2.$$

5.5 Asymmetric isosceles trimer

As a last example, we consider an actually isosceles trimer. The impurities opposite the apex are assumed to be at fixed distance from each other. Their distance to the apex atom is varied. We model this by keeping the interaction g_2 in (5.1.1) fixed while we vary g_1 . Since the mean field equations for b and \hat{b} cannot be handled easily for an arbitrary isosceles trimer, we solve them numerically using MAPLE. Afterwards, we compute the local density of states at the apex atom using (5.1.29) and at the opposite atoms using (5.1.30).

5.5.1 Ferromagnetic interactions

We consider the occurring couplings g_1 and g_2 to be ferromagnetic. In this case, they are given as

$$g_1 = g_1^R = g_0 \varepsilon_R^1 \quad \text{and} \quad g_2 = g_2^R = g_0 \varepsilon_R^2$$

and we fix

$$\varepsilon_R^2 = 0.1$$

in the following. ε_R^1 is varied between 0 and 0.3. For any ε_R^1 the LDOS at the apex or opposite of it is dipped around $\omega = 0$, and we fit it by a Fano resonance shape (5.2.12) as in the latter sections. For ε_R^1 between 0 and 0.3 these fits are quite accurate, being the better the smaller the coupling is. We plotted the LDOS (solid line) and its Fano fit (dashed line) at the apex atom for $\varepsilon_R^1 = 0.3$ on the left hand side of figure 5.7. On the right hand side of 5.7 we plotted the ε_R^1 dependence of the normalised widths for the apex atom (dashed line) and the other atoms (solid

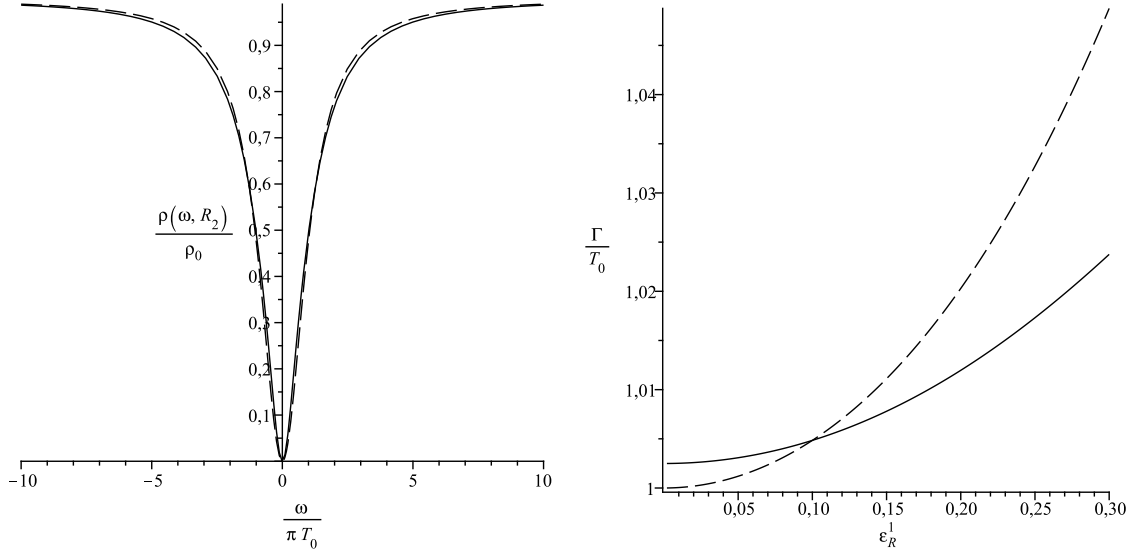


Figure 5.7: LDOS and Fano resonance fit for ferromagnetic coupling $\varepsilon_R^1 = 0.3$ and $\varepsilon_R^2 = 0.1$ at the apex atom. RHS: Dependence of Kondo temperature on coupling $\varepsilon_R^1 \in [0, 0.3]$ and $\varepsilon_R^2 = 0.1$ for apex atom (dashed line) and the other trimer atoms (solid line).

line). The normalised Kondo temperature gets higher for increasing coupling ε_R^1 in both cases. The crossing point of the two line shapes is located at $\varepsilon_R^1 = 0.1$ since this value corresponds to an equilateral trimer. Because $\varepsilon_R^2 = 0.1$, the width for the LDOS at \mathbf{R}_1 and \mathbf{R}_3 is different from πT_0 at $\varepsilon_R^1 = 0$, since those atoms already form a ferromagnetic dimer with non-vanishing coupling.

For all preceding ferromagnetic cases we saw, that the impurity atoms can be interpreted as either being part of one dimer (for the boundary impurities of a chain) or being part of two linked dimers. We will pursue this thought here. For the ferromagnetic dimer, the influence of the dimer interaction was roughly given by

$$\Delta \frac{\Gamma}{T_0} = \frac{1}{4} \varepsilon_R^2.$$

We now assume that each impurity in the present case is linked to two dimers, experiencing a cumulative influence. Since the apex impurity is linked two the remaining two atoms with a coupling strength ε_R^1 we assume its width shape to be given by

$$\frac{\Gamma}{T_0} = 1 + \frac{1}{4} (\varepsilon_R^1)^2 + \frac{1}{4} (\varepsilon_R^1)^2 = 1 + \frac{1}{2} (\varepsilon_R^1)^2. \quad (5.5.1)$$

Any other impurity of the trimer is linked to the apex by a coupling strength ε_R^1 and to the remaining atom with a coupling $\varepsilon_R^2 = 0.1$. The shape of the normalised Kondo temperature then is

$$\frac{\Gamma}{T_0} = 1 + \frac{1}{4} (\varepsilon_R^1)^2 + \frac{1}{4} (\varepsilon_R^2)^2. \quad (5.5.2)$$

Figure 5.8 shows the ε_R^1 -dependence of the normalised widths for the apex atom and the other atoms (black lines) together with the approximations (5.5.1) and (5.5.2) (red lines). The approx-

5 Isosceles Trimer

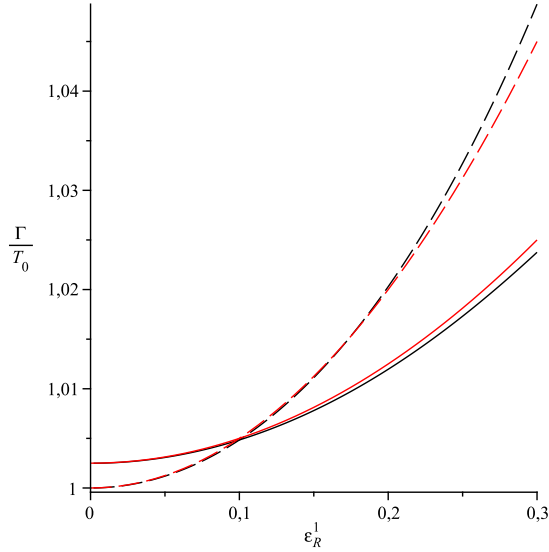


Figure 5.8: Normalised widths (black lines) and their approximations (5.5.1) and (5.5.2) (red lines) for a ferromagnetically coupled isosceles trimer. The interaction between the basis impurities is fixed at $\varepsilon_R^2 = 0.1$ while $\varepsilon_R^1 \in [0, 0.3]$. Apex atom quantities are indicated by dashed lines, those of the remaining atoms by solid lines.

imations (5.5.1) and (5.5.2) seem to be quite well. The deviations of the numerically determined influences $\Delta\Gamma/T_0$ of the couplings from the approximated ones are less than 8.4 per cent for $\varepsilon_R^1 < 0.3$. Let us recall that the idea behind the approximations is that each impurity can be described as being part of two distinct dimers, which have a cumulative effect on its normalised Kondo temperature. The influence of the dimer interactions between the other atoms is neglected. As figure 5.8 indicates, it is rather small if the couplings are.

5.5.2 Antiferromagnetic interactions

We now consider the antiferromagnetic version of the latter case. The couplings g_1 and g_2 are

$$g_1 = -i g_1^I = -i g_0 \varepsilon_I^1 \quad \text{and} \quad g_2 = -i g_2^I = -i g_0 \varepsilon_I^2$$

and we fix

$$\varepsilon_I^2 = 0.1.$$

ε_I^1 is varied between 0 and 0.3. Again, the LDOS is dipped around the Fermi energy, and we can fit it quite accurately by a Fano resonance shape for each ε_I^2 , determine the width and compare it to the single impurity width πT_0 . The normalised widths are plotted in figure 5.9 (black lines) for the apex atom (dashed line) and the other atoms (solid lines). As in the latter case, we approximate the normalised Kondo temperatures by quadratic functions composed of dimers, say

$$\frac{\Gamma}{T_0} = 1 - \frac{1}{2} (\varepsilon_I^1)^2 \quad (5.5.3)$$

at the apex atom and

$$\frac{\Gamma}{T_0} = 1 - \frac{1}{4} (\varepsilon_I^1)^2 - \frac{1}{4} (\varepsilon_I^2)^2 \quad (5.5.4)$$

5 Isosceles Trimer

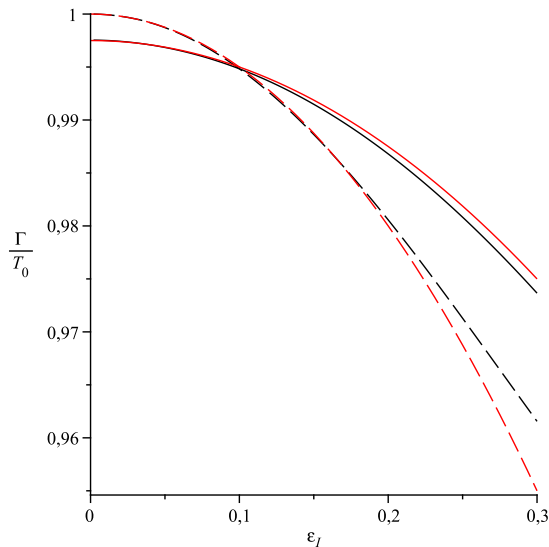


Figure 5.9: Normalised Kondo temperatures (black lines) and approximations 5.5.3 and 5.5.4 (red lines) for an antiferromagnetically coupled isosceles trimer. The AFM basis interaction is fixed at $\varepsilon_I^2 = 0.1$ and $\varepsilon_I^1 \in [0, 0.3]$. Apex atom quantities are indicated by dashed lines, those of the remaining atoms by solid lines.

at the other impurities. These approximations are plotted as red lines in figure 5.9. This approximation does not seem to be too bad, but not as good as in the ferromagnetic case. It becomes the more accurate, the larger the interaction ε_I^2 between the atoms opposite the apex is compared to ε_I^1 . For $\varepsilon_I^2 = 0.1$ the difference between the approximated $\Delta(\Gamma/T_0)$ and the numerical one is about 17.1 per cent at $\varepsilon_I^1 = 0.3$. At $\varepsilon_I^2 = 0.05$ it is already 21.5 per cent, but for $\varepsilon_I^2 = 0.15$ it is only 12.8 per cent. The smaller the quotient

$$\frac{|g_1|}{|g_2|},$$

the better are the approximations (5.5.3) and (5.5.4). The same is true for the ferromagnetic isosceles trimer, but the effect is smaller. A small quotient $|g_1|/|g_2|$ means that the trimer is acute-angled, being closer to the limiting case of a dimer and an isolated atom than to the limiting case of a chain. The more the trimer becomes a chain, the less the approximation of splitting it into distinct dimers is valid.

5.5.3 Mixed type interactions

We consider the case of a mixed type of interactions. The apex atom is assumed to interact ferromagnetically with the remaining two, which among themselves are coupled antiferromagnetically. This means

$$g_1 = g_1^R = g_0 \varepsilon_R^1$$

and

$$g_2 = -i g_2^I = -i g_0 \varepsilon_I^2.$$

We fixed the antiferromagnetic interaction between the basis impurities to values between $\varepsilon_I^2 = 0.08$ and $\varepsilon_I^2 = 0.17$ and varied the ferromagnetic coupling ε_R^1 between the apex and the basis from 0 to 0.3 (corresponding to a varying distance between those). We solved the mean field

5 Isosceles Trimer

equations using MAPLE and computed the local density of states at the apex and the position of the remaining impurities. Due to numerical problems, the LDOS could not be computed for small interactions. For $\varepsilon_I^2 = 0.08$, those problems arose for $\varepsilon_R^1 < 0.028$, at $\varepsilon_I^2 = 0.17$, the LDOS could not be computed for interactions $\varepsilon_R^1 < 0.06$. These numerical problems were due to the divergence of y_3^I when the system approaches the dimer case (see section 5.2). For all values $\varepsilon_R < 0.3$ for which it can be computed, the LDOS is dipped at all impurity sites, and it can be quite accurately fitted to a Fano-Kondo shape. As in the previous sections, we determined the normalised width of the LDOS for each interaction ε_R^1 . Figure 5.10 shows the results for the apex (dashed line) and the opposite atoms (solid lines).

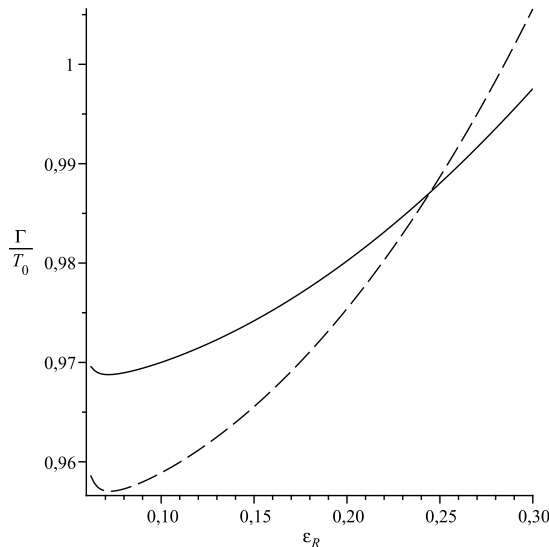


Figure 5.10: Normalised Kondo temperatures at apex site (dashed line) and remaining sites (solid lines) for $\varepsilon_I^2 = 0.17$.

In contrast to the cases treated so far, the curves cannot be fitted by quadratic ones, the geometric behaviour of the normalised Kondo temperature being in a way more complicated. For all investigated values of the antiferromagnetic basis interaction, it was qualitatively the same: For small ferromagnetic couplings, the normalised Kondo temperature is lower than that of a single magnetic impurity at all three sites, having a point of minimal value that depends on the strength of the antiferromagnetic coupling ε_I^2 . Hence, small ferromagnetic interactions ε_R^1 do not have an increasing but a decreasing effect on the Kondo temperature. At the apex atom, $\varepsilon_I^2 = 0.1$ and $\varepsilon_R^1 = 0.05$, the normalised Kondo temperature already is more than 2.5 per cent lower than that of a single magnetic impurity. For comparison: for an all-antiferromagnetic trimer with $\varepsilon_I^2 = 0.1$ the decrease of the normalised Kondo temperature at the apex was less than 0.15 per cent at $\varepsilon_I^1 = 0.05$.

This decreasing effect and the location of the minimum depends on the antiferromagnetic coupling ε_I^2 . Tabular 5.11 gives the location of the minimum and the associated decrease of the normalised Kondo temperature for several ε_I^2 .

The shape of the normalised Kondo temperature is as in figure 5.10 for all investigated ε_I^2 , although the minimum is shifted to larger values of ε_R^1 and the minimal value gets lower as the antiferromagnetic basis interaction increases.

If the ferromagnetic coupling ε_R^1 gets larger, it gains more influence on the systems behaviour,

ε_I^2	Location of minimum in interval	Decrease of normalised Kondo temperature
0.08	[0.030, 0.034]	2.2 per cent
0.10	[0.040, 0.044]	2.7 per cent
0.13	[0.052, 0.056]	3.4 per cent
0.17	[0.070, 0.074]	4.3 per cent

Figure 5.11: Location of minimum and approximated associated decrease of the normalised Kondo temperature for different antiferromagnetic basis couplings.

increasing the Kondo temperature due to the increasing tendency of the trimer impurities to maximise the total spin. For dominating ferromagnetic interaction ε_R^1 (compared to ε_I^2), the system approaches the limiting case of a ferromagnetic chain; the normalised Kondo temperature at all three sites exceeds the one of a single impurity despite the antiferromagnetic coupling of the opposite impurities.

The geometric behaviour of a trimer with mixed interactions cannot be approximated by splitting it up into distinct ferromagnetic or antiferromagnetic dimers (if ε_I^2 is not completely negligible compared to ε_R^1), even if $|g_1|/|g_2| < 1$ which means that the trimer is close to the dimer case. Each impurity "feels" the influence of the couplings between all other impurities.

On first sight, it is quite peculiar that the Kondo temperature at the apex site sinks when the ferromagnetic interaction to the basis atoms is turned on. However, this behaviour can be explained with frustration of spins. If the antiferromagnetic interaction between the basis impurities is large compared to the ferromagnetic coupling ε_R^1 , the basis atoms form an antiferromagnetic dimer. As long as there is no ferromagnetic interaction of the apex with those, the apex spin is free to point in any direction and a Kondo effect as for a single magnetic impurity is observed at this site. As the interaction is turned on, the basis atoms still form a dimer, but any non-zero z -component of the apex spin will lead to frustration of that spin. In order to avoid frustration, the apex spin will tend to minimise its z -component, thus confining itself to a plane. Therefore its possible degrees of freedom are reduced, which results in a lower Kondo temperature (see figure 5.12).

This effect gets stronger with increasing ferromagnetic coupling as the favourable orientation of the spin is more and more confined due to stronger frustration. If the coupling gets large enough, the ferromagnetic interaction tends to align all three spin parallelly and the normalised Kondo temperature will rise again with further increase of ε_R^1 .

All considerations made here are also applicable to the spins of the basis impurities. For small ferromagnetic interactions between those and the apex, the basis forms an antiferromagnetic dimer. Its spin orientation axis avoids to have a non-vanishing projection on that of the apex spin, since one of the spins would be frustrated otherwise. Hence, the spin axis of the dimer is confined, its degrees of freedom are reduced and the normalised Kondo temperature decreases. If the ferromagnetic interaction with the apex gets strong enough, it tends to gain more influence on the magnetic behaviour of the trimer than frustration and the Kondo temperature starts to increase again.

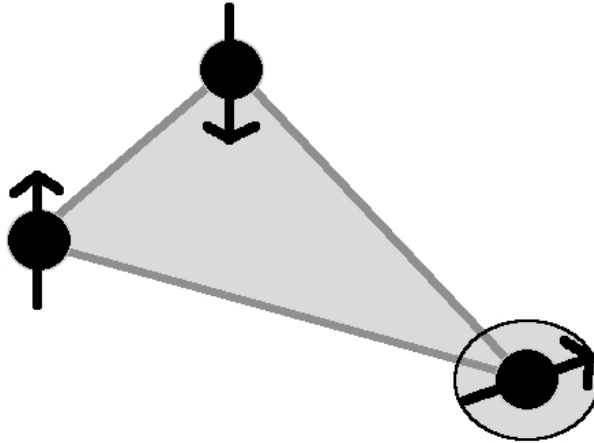


Figure 5.12: Alignment of the spins in a trimer with mixed type interactions for small ferromagnetic couplings between the apex and the basis. The basis impurities form an antiferromagnetic dimer while it is favourable for the apex spin to avoid having a non-vanishing projection on the basis spin axes. Therefore the spin is confined and the loss of freedom leads to a lower Kondo temperature compared to that of a single magnetic impurity. On the other hand, the basis spins also are confined, and the Kondo temperature at the basis sites is also reduced.

5.6 Summary

In this chapter we investigated the influence of geometric effects on the Kondo temperature in an isosceles trimer. As a preparatory work for further considerations we computed the local density of states formally at the position of the apex atom (5.1.29) and the position of the other atoms (5.1.30). This can be used as a starting point for investigations of arbitrary trimer configurations. However, we concentrated on cases where the couplings g_1 and g_2 were either real-valued, corresponding to ferromagnetic atomic interactions, or purely imaginary, which describes antiferromagnetic interactions. We considered the limiting case of a dimer isolated from the remaining atom. It is the most simple case, where one would expect the geometry (here only the dimer length) to have an influence on the system. As expected, the LDOS at the isolated atom in this case is the same as for a single magnetic impurity. We computed the LDOS at the dimer atoms for ferromagnetic and antiferromagnetic coupling. In the domain of the Kondo effect, the width of the local density of states is proportional to the Kondo temperature. We determined the normalised width, which is the fraction of the given dimer width and the one of a single magnetic impurity. Figure 5.13 indicates that this normalised width, and thus the Kondo temperature, gets larger for increasing ferromagnetic coupling and diminishes in the antiferromagnetic case. This is due to the system tending to maximise (ferromagnetic case) or minimise (antiferromagnetic case) its total magnetic moment. In both cases, the dependence of the Kondo temperature on the couplings is approximately quadratic. This seems plausible, since the couplings quadratically enter the RKKY interaction which is expected to be responsible for the geometric influence.

5 Isosceles Trimer

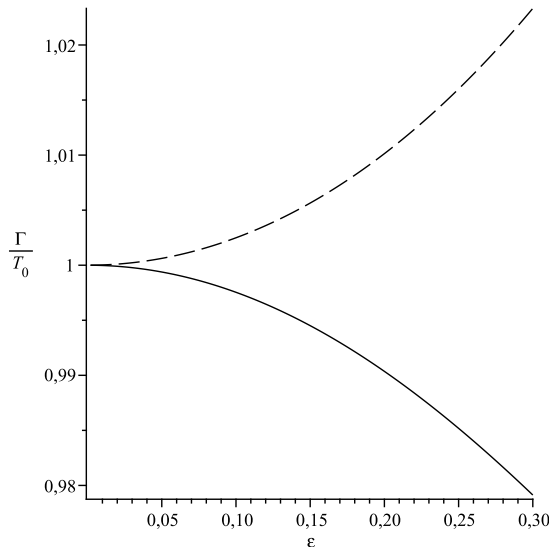


Figure 5.13: Dependence of the normalised Kondo temperature on ferromagnetic coupling (dashed line) and on antiferromagnetic coupling (solid line) in a magnetic dimer. ε is g_2^R/g_0 in the first case and g_2^I/g_0 in the latter. Ferromagnetic dimer interactions lead to an enhancement of the Kondo temperature while antiferromagnetic interactions suppress the Kondo effect.

As another limiting case we considered the trimer atoms to form an equilateral triangle. This is also quite a simple system in which the geometry is only depending on the distance of the atoms. The LDOS coincides at all trimer sites, and we computed it for ferromagnetic and antiferromagnetic inter atomic interactions. Staying in the domain of the Kondo effect, we determined the normalised width of the LDOS which is proportional to the Kondo temperature of the system. According to figure 5.14, the normalised Kondo temperature increases with the coupling strength in the ferromagnetic case and decreases for antiferromagnetic couplings. For ferromagnetic interactions this can be explained by the tendency of the system to maximise its total spin, while in the antiferromagnetic case the occurring influences on the geometrical behaviour are due to minimisation of the total spin. Frustration effects do not seem to play an important role in this case. The normalised Kondo temperature depends approximately quadratic on couplings ε less than 0.3 and it is

$$\frac{\Gamma}{T_0} \approx 1 \pm \frac{1}{2} \cdot \varepsilon^2,$$

where ”+” means the ferromagnetic and ”-” the antiferromagnetic case.

As the last limiting case of a degenerate isosceles trimer we considered a linear magnetic chain, where we restricted ourselves to next neighbour interactions. We solved the mean field equations numerically and computed the LDOS at the centre and the boundary of the chain as well as the normalised Kondo temperatures. Figure 5.15 shows the dependence of the normalised Kondo temperature on the couplings. In the ferromagnetic case, the Kondo effect is increased while it is suppressed for antiferromagnetic couplings. In general, the geometrical influence is larger on the centre of the chain than on the boundary impurities. For ferromagnetic couplings, the boundaries can be seen as being part of a dimer, while the central atom is the link between two dimers,

5 Isosceles Trimer

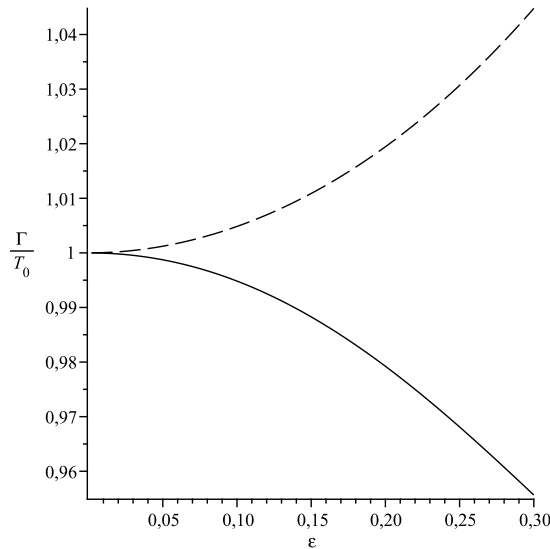


Figure 5.14: Dependence of the normalised Kondo temperature on ferromagnetic coupling (dashed line) and on antiferromagnetic coupling (solid line) in a equilateral magnetic trimer. ϵ is $g_{1/2}^R/g_0$ in the first case and $g_{1/2}^I/g_0$ in the latter. Ferromagnetic interactions lead to an enhancement of the Kondo temperature while antiferromagnetic interactions suppress the Kondo effect.

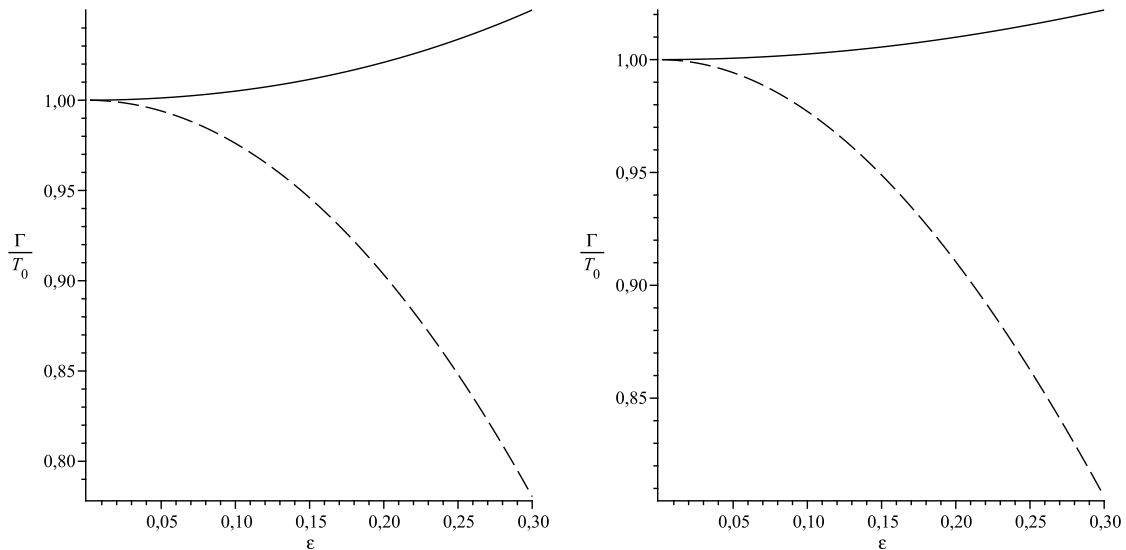


Figure 5.15: Normalised Kondo temperature at chain centre (lhs) and boundary (rhs) for ferromagnetic (solid) and antiferromagnetic (dashed) coupling.

both influencing the geometric behaviour of the Kondo temperature. For antiferromagnetic interactions, things are quite different. The suppression of the Kondo effect due to the coupling is much stronger than in the ferromagnetic case. The antiferromagnetically geometric behaviour cannot be described by a dimer decomposition of the chain.

5 Isosceles Trimer

We also considered an actual non-degenerate isosceles trimer with varying geometry, in which the trimer impurities were either coupled ferromagnetically or antiferromagnetically. We modelled this system by fixing the coupling strength ε^2 between the impurity spins opposite the apex and varying ε^1 , the one between the apex atom and the remaining two. For ferromagnetic couplings, an increase of the normalised Kondo temperature was observed, while the influence of antiferromagnetic interactions leads to decreasing Kondo temperature. In both, the ferromagnetic and the antiferromagnetic case, we approximated the system by splitting up the trimer into distinct dimers. Each of the trimer impurities was then part of two dimers which had a cumulative influence on the normalised temperature at that impurity. The results of the numerically computed geometric dependencies of the Kondo temperatures and the approximated ones were given in figure 5.8 (ferromagnetic case) and figure 5.9 (antiferromagnetic case). The approximation was better in the ferromagnetic case than in the antiferromagnetic one, since for antiferromagnetic interactions, chain-like system cannot be thought of as decomposing into distinct dimers. However, in both cases, the approximation was the better, the smaller the quotient $\varepsilon^1/\varepsilon^2$ was, meaning that the system comes closer to the limiting case of a dimer.

As the last example, we considered an isosceles trimer with mixed interactions. The apex atom was coupled ferromagnetically to the remaining two which among themselves interacted antiferromagnetically. The behaviour of the normalised Kondo temperature was quite different from any of the former cases. Neither could the geometric dependence be approximated by splitting up the trimer into distinct dimers nor could it be fitted to a quadratic function. Moreover, the normalised Kondo temperature at the apex and the basis impurities decreased with increasing ferromagnetic coupling down to a minimal value and then increased again, if the coupling strength became even larger. The decrease of the Kondo temperature for small ferromagnetic couplings could be explained with frustration of the trimer spins. In that case, the spin orientation axes of the apex spin and the basis spins tend to align perpendicular to each other in order to avoid frustration. This results in a reduction of the degrees of freedom of the spin axis and therefore in a lower normalised Kondo temperature. If the ferromagnetic interaction gets large enough, its tendency to align the spins parallelly gets stronger and the normalised Kondo temperature is increased.

6 Conclusion

We computed the local density of states of a system composed of N magnetic impurities on a metallic surface. To describe the system, we employed an Anderson model in the regime of small tunnelling (Schrieffer-Wolff-transformation). We assumed that there were exactly N electrons in the magnetic cluster which they were distributed upon uniformly. To model this fact, we assumed the Hubbard interaction to be very large compared to all other occurring energies ($U \rightarrow \infty$). We chose a mean field approach, where the "mean field" refers to the mean interaction of the itinerant degrees of freedom with the localised ones. To fulfill the constraint of each impurity being only singly occupied, we used the Popov-Fedotov method of imaginary chemical potentials when we computed the partition function of the system.

In mean field theory, the geometry of the magnetic cluster is encoded by a matrix product $\underline{b} \underline{g} \underline{b}$, which is determined by the mean field equations. The matrix \underline{b} is real-valued and diagonal, its entries being the mean hybridisations of the impurity degrees of freedom with the surrounding substrate electrons. The matrix \underline{g} is complex-valued and symmetric. Its real-valued diagonal is given by $\rho_0/N \mathbb{1}$, describing the effect of the unperturbed substrate on a single impurity, while its off-diagonal elements correspond to the effective couplings between different cluster sites. The elements $\underline{b} \underline{g} \underline{b}$ enter quadratically in the RKKY interaction, which has the most important influence on the geometrical behaviour of the system. The RKKY interaction between the i -th and the j -th impurity is given as

$$H_{RKKY}^{ij} = -\pi^2 (b_i g_{ij} b_j)^2. \quad (6.0.1)$$

Therefore, real-valued entries of the matrix \underline{g} correspond to ferromagnetic RKKY interactions between the impurities, while antiferromagnetic interactions are given for imaginary matrix elements.

Using this model, we saw that the local density of states taken at any impurity site develops a dip around the Fermi energy. The conclusion was that the model is only valid in the regime of the Kondo effect, where such behaviour is expected. The results of our computations lose validity, if the inter atomic distance becomes smaller than the Fermi wavelength. Above it, the Kondo effect dominates, while below it, the cluster cannot be thought of as being composed of distinct atoms anymore.

In the Kondo regime, the only important quantity describing the whole system is the Kondo temperature. If the external temperature is below the Kondo temperature, the Kondo effect occurs; the formation of the Kondo cloud takes place. At low temperatures, the Kondo temperature is proportional to the width of the local density of states. We can compute the width of the LDOS at different cluster sites, giving rise to different Kondo temperatures for every site. We can thus say, that if we cool down the system to a certain external temperature, the Kondo effect will occur at some site, while it will not occur at another. Therefore, the most important quantity to determine is the width of the LDOS at any site in the cluster.

As a concrete example of such a magnetic cluster, we considered an isosceles trimer. There are two quantities which fix its geometry: the distance between the apex atom and the other two

6 Conclusion

and the distance between the atoms opposite the apex. These distances determine the couplings between the atoms, given as entries of the matrix

$$\underline{g} = \begin{pmatrix} g_0 & g_1 & g_2 \\ g_1 & g_0 & g_1 \\ g_2 & g_1 & g_0 \end{pmatrix}.$$

g_0 is the on-site interaction for each atom, being related to the unperturbed density of states of the substrate electrons by $g_0 = \rho_0/3$, g_1 is the coupling between the apex and the basis of the triangle and g_2 is the one between the basis atoms. In two dimensions, the trimer being placed on the surface of a metallic substrate, these couplings decrease with increasing inter atomic distance as $1/\sqrt{R}$. We took g_1 and g_2 as varying parameters of our model and computed the local density of states at each atom to determine its width at low temperatures and thus the local Kondo temperature. The width $\pi\Gamma$ was compared to that of the LDOS of a single magnetic impurity given by πT_0 . The quotient Γ/T_0 could then be interpreted as the normalised Kondo temperature at a given site. If the apex atom is infinitely far away (and therefore $g_1 = 0$) the basis atoms form a dimer. The dependence of the normalised Kondo temperature at a dimer site on the coupling g_2 is approximately given as

$$\frac{\Gamma}{T_0} = 1 \pm \frac{1}{4} \left(\frac{|g_2|}{g_0} \right)^2$$

where ”+” refers to ferromagnetic dimer coupling (real-valued g_2) and ”-” to antiferromagnetic coupling (imaginary g_2). This approximation is the better, the smaller the coupling is, however, it is quite good as long as the dimer length is well above the Fermi wavelength. The geometric influence on the Kondo temperature in a dimer is thus

$$\Delta \frac{\Gamma}{T_0} = \pm \frac{1}{4} \left(\frac{|g_2|}{g_0} \right)^2. \quad (6.0.2)$$

Ferromagnetic inter atomic couplings give rise to higher Kondo temperatures, thus enhancing the Kondo effect, while antiferromagnetic ones suppress the formation of the Kondo cloud. The influence of the couplings on the normalised Kondo temperature is quadratic as it is (in lowest order) for the RKKY interaction (6.0.1). The enhancement (suppression) of the Kondo effect is due to the dimer maximising (minimising) its total spin.

For arbitrary isosceles trimers, we have to distinguish between two different cases of geometrical configurations. Either the distance of the apex to the basis atoms is larger than the distance between themselves, or it is smaller. The asymptotic limit of the first case is the dimer system (the apex being infinitely far away) while the limit of the second case is the linear chain (where we assumed only next neighbour interactions). We call configurations of the first kind ”dimer like“ and those of the second kind ”chain like“. Dimer like configurations are characterised by $|g_1| < |g_2|$ while for chain like it is $|g_2| < |g_1|$.

For dimer like isosceles trimers which are completely ferromagnetically or antiferromagnetically coupled, the geometric influence on the normalised Kondo temperature at a certain impurity is quite accurately approximated by superposition of the influences (6.0.2) of each dimer the impurity is connected to. The normalised Kondo temperature at the apex is given as

$$\left(\frac{\Gamma}{T_0} \right)_{Apex} = 1 \pm \frac{1}{2} \left(\frac{|g_1|}{g_0} \right)^2 \quad (6.0.3)$$

6 Conclusion

while for the basis atoms it is

$$\left(\frac{\Gamma}{T_0}\right)_{Basis} = 1 \pm \frac{1}{4} \left(\frac{|g_1|}{g_0}\right)^2 \pm \frac{1}{4} \left(\frac{|g_2|}{g_0}\right)^2. \quad (6.0.4)$$

Again ”+” corresponds to the ferromagnetic case while ”-” describes the behaviour for antiferromagnetic couplings. In this approximation, the influence of the dimer interaction between the remaining two atoms on the impurity under consideration is neglected.

For chain like isosceles trimers, the approximations (6.0.3) and (6.0.4) are not as good anymore. However, in the ferromagnetic case, the errors are still tolerable, even for a linear chain where $g_2 = 0$. For a ferromagnetic chain, the geometric influence at the apex is given by

$$\Delta \frac{\Gamma}{T_0} = 0.549 \cdot \left(\frac{|g_1|}{g_0}\right)^2,$$

if one quadratically fits the widths for couplings up to $|g_1|/g_0 = 0.3$, which compared to (6.0.3) means an error of 9.8 per cent, while at the basis atoms it is

$$\Delta \frac{\Gamma}{T_0} = 0.246 \cdot \left(\frac{|g_1|}{g_0}\right)^2$$

meaning an error of 1.6 per cent. These errors become the smaller the less chain like the system is.

For antiferromagnetic couplings, chain like systems strongly deviate from (6.0.3) and (6.0.4). For an antiferromagnetic chain and a coupling strength of $|g_1|/g_0 = 0.3$ the error at the apex using those formulas is about 490 per cent, while it is even about 870 per cent at the basis atoms. The geometric influence on the normalised Kondo temperature at a given atom cannot be modelled anymore as cumulative dimer influences for chain like antiferromagnetic systems, the antiferromagnetic interactions tend to prevent the system from dimerisation. This behaviour is not totally unexpected. To explain the differences between the dimer like and the chain like case qualitatively, we use the following (a little too simple) classical picture. The influence on a given spin by another can either be direct (meaning that it is mediated by the substrate electrons on a direct way, it is still an indirect coupling) or via the remaining spin. The latter is the result of combined scattering, while the first only involves one scattering process, so in general the effect of the indirect influence will be less than that of the direct one. For dimer like systems, the indirect influence will almost be negligible compared to the direct one, since it is quite unlikely for a substrate electron to travel from one impurity to another by passing the remaining one. For chain like systems, the probability of a spin being influenced by a combined scattering process gets larger (compared to the one in a dimer like system of the same scale), so the indirect influence becomes more important. Hence, in dimer like systems the influence on a given spin by the other two is mostly due to direct scattering, which leads to a dimerisation of the system. In chain like systems, dimerisation will only occur, if the growing influence of the indirect scattering processes does not change the nature of the interactions between a given spin and another. This is the case for ferromagnetic couplings, and dimerisation can still be observed, though it is not as pronounced as for dimer like systems. For antiferromagnetic interactions, this is not the case anymore, dimerisation is strongly suppressed.

For completely antiferromagnetically coupled trimers, we expected frustration of spins to have an influence on the geometric behaviour of the Kondo temperature. It is quite remarkable, that frustration does not seem to be of great importance in that case. The geometric configuration

6 Conclusion

in which frustration of spins should have the largest effect, is the most symmetric, namely the equilateral trimer. For the antiferromagnetic equilateral trimer, the ground state should be the most degenerate compared to all other cases. However, the geometrical behaviour of the Kondo temperature is still very well described by (6.0.3) and (6.0.4). Moreover, as figure 5.9 shows, there is no dramatic change in the behaviour of the normalised Kondo temperature, when the symmetry point $g_2 = g_1$ is crossed. It seems that the tendency of the system to dimerise is stronger than any frustration effects.

In chain like antiferromagnetic systems, where dimerisation is not so likely to occur, frustration is also not as strong as in the most symmetric case. In an antiferromagnetic chain, there is no frustration at all and still the deviation from the dimerisation approximations (6.0.3) and (6.0.4) is largest compared to all other cases. Hence, frustration cannot have any influence on this behaviour in the chain case. It is rather explained by the indirect spin influences already described above. All in all, frustration effects seem to play a minor role for completely antiferromagnetically coupled trimers.

The only system of the ones we investigated here, where a hint of frustration influence arose, was the trimer with mixed type interactions. The basis atoms were coupled antiferromagnetically in that case while the apex spin was interacting ferromagnetically with the basis. None of the normalised Kondo temperatures could be described by dimerisation. For a fixed antiferromagnetic basis interaction, the normalised Kondo temperature as a function of the ferromagnetic apex-basis interaction develops a minimal value, the position of which depends on the given basis interaction. For small ferromagnetic couplings, the Kondo temperature at all three sites was lower than that of a single magnetic impurity, and in case of the basis, even lower than that of an antiferromagnetic dimer. At first sight, this seemed rather peculiar since ferromagnetic interactions tended to increase the Kondo temperature in all previous cases. However, this effect can be explained with frustration of the spins (at least in a classical picture). If the ferromagnetic coupling is small compared to the antiferromagnetic basis interaction, the basis impurities form an antiferromagnetic dimer. If the apex spin has a non-vanishing projection on the spin orientation axis of the dimer, it will be frustrated and so will be one of the dimer spins. Therefore, the dimer spin axis and the one of the apex tend to be perpendicular, so confining the spin directions and reducing the Kondo temperature due to the loss of degrees of freedom. This effect gets larger as the ferromagnetic coupling does, since frustration becomes stronger. However, above a certain ferromagnetic coupling strength (which depends on the basis interaction), the tendency of the trimer spins to align parallelly becomes more important and the Kondo temperatures begin to rise again. The combination of frustration of spins and, for stronger ferromagnetic couplings, the preference of the system to align its spins parallelly

It is remarkable that this sort of system behaves so different from an overall antiferromagnetically coupled trimer. In the case of mixed type interactions, the decrease of the Kondo temperature for small ferromagnetic couplings is much larger than the dimerisation approximations (6.0.3) and (6.0.4) suggest for small antiferromagnetic interactions (and as said already, these approximations are in very good accordance with the numerical results for an antiferromagnetic dimer like trimer). One would think that the above explanation of the influence of frustration on the Kondo temperature in the mixed type interaction case would still be valid if the apex was coupled antiferromagnetically to the basis. However, this is not the case. The tendency of an antiferromagnetic system to dimerise suppresses effects of frustration, while dimerisation does not take place in the mixed interaction case and frustration effects dominate. The explanation for that behaviour has to be the different nature of the couplings. In a dimer like geometrical configuration, it seems to be preferable for a spin to be part of two antiferromagnetic dimers,

6 Conclusion

but not of an antiferromagnetic one and a ferromagnetic one. The problem in explaining this effect using an easy picture is, that our model of three magnetic impurities in a bath of substrate electrons cannot be described entirely by the more simple model of three coupled spins, which we used here as a thought model in our explanations. In fact, a simple model of an isosceles trimer of coupled spins, where the spin-spin interaction is the only relevant part and where the basis spins are interacting antiferromagnetically, does not show any differences in the ground state energies for a ferromagnetically or an antiferromagnetically coupled apex spin.

The results in this work are different from the measured behaviour of the Kondo temperature in the experiments of Jamneala *et al.* (see [70]). They observed that the Kondo temperature of a (dimer like) isosceles trimer can be higher than both that of a single magnetic impurity and that of an equilateral trimer. Our results do not allow for such a conclusion. However, the starting point of the experiments in [70] was quite different from the one of our model. As outlined, mean field theory is only valid for systems of "loosely" arranged trimers, in which the inter impurity distances are sufficiently large. Such systems stay in the Kondo state and will only be slightly altered by the long-ranged RKKY interactions. In the very compact systems Jamneala *et al.* considered, additional effects like direct exchange couplings have to be taken into account, which may be responsible for the differences.

In summary, we have considered an Anderson model in the small tunnelling regime to describe an arbitrary number of magnetic impurities on a metallic substrate and formally computed the local density of states at low temperatures, using mean field theory. We showed that the mean field approach is only valid, if the inter atomic distances of the magnetic cluster are sufficiently large. As a concrete example for such a cluster, we considered an isosceles trimer. We determined the dependence of the Kondo temperature taken at each trimer site on the effective inter impurity couplings. The result was that the Kondo effect is enhanced in completely ferromagnetically coupled trimers, compared to a single magnetic impurity, while it is weakened for completely antiferromagnetically coupled ones. In the case of mixed type interactions, frustration effects come into play, and the Kondo temperature can both increase or decrease, depending on the configuration of the trimer.

7 Outlook

In this section we want to discuss some ideas on how the present model could be generalised to more complicated systems. The key characteristics of the model should be untouched. That means, that the interacting part of the underlying effective Hamiltonian should still be Kondo like, that one stays in the regime $U \rightarrow \infty$ and that everything is computed in mean field.

The first thing to do would be to consider concrete examples of a cluster different from an isosceles trimer. First of all, one could skip the restriction that the trimer is isosceles. For an arbitrary triangle, the matrix \underline{g} would be less symmetric which means that the eigenvalues of the matrix $\underline{b}\underline{g}\underline{b}$ are not determined as easily. In principle, it is of course possible to compute the eigenvalues of an arbitrary 3×3 matrix analytically, but the results will in general be quite complicated. This means, that the mean field equations will be rather cumbersome and therefore should be solved numerically, which is not really a strong restriction, since for most cases we already had to rely on numerical methods to solve the mean field equations in our more symmetric model. However, it is quite unlikely that an arbitrary trimer will give rise to completely different results. Most of the geometric influences on the Kondo temperature should already be observed in the system we presented here. It might be possible though, to investigate the influence of frustration on the Kondo temperature a bit more. Starting with an antiferromagnetically coupled equilateral triangle, in which the spins are maximally frustrated, one could shift one of the trimer atoms parallel to the other two, so breaking the symmetry entirely and thus cancelling frustration. This might allow to quantify the (as we observed rather weak) effect of frustration.

The next thing one could do, is to consider more than three magnetic impurities. 4×4 matrices can still be diagonalised analytically and therefore, computations could be extended to magnetic clusters of four atoms without immoderate effort. It would be interesting to see under which conditions the system still develops a dimerisation behaviour, if at all. One would expect such a system to dimerise for completely ferromagnetic couplings, but it is not at all obvious how dimerisation in the ferromagnetic case would translate from a trimer to a cluster of four impurities.

For clusters of more than four atoms, additional problems in solving the mean field equations arise. Since $N \times N$ matrices cannot be diagonalised analytically in general, their eigenvalues cannot be formally derived. Since these enter the mean field equations, those could not be formally written down. Hence, the mean field equations have to be solved under the condition, that their solutions give rise to eigenvalues of the matrix $\underline{b}\underline{g}\underline{b}$, which enter the mean field equations. Such a self-consistent approach would rather be tackled with entirely numerical techniques. Assuming that those problems could be solved, it would again be of interest if dimerisation occurs in such "large" clusters, or under which condition they separate into smaller clusters.

Up to now, we only discussed how one could treat more complicated clusters with the model presented here. Another idea would be to slightly change the model by skipping the restriction that the total occupation in a given cluster coincides with the number of the cluster atoms. In that case, the Hamiltonian is still Kondo like, but can not be seen as a spin- $\frac{1}{2}$ Hamiltonian anymore. This should lead to quite different results from what we observed here, since the

7 Outlook

system then cannot be thought of as coupled spins anymore. Technically, the only difference to the present model is that the assumption of each impurity to be singly occupied is changed to the assumption that the total occupation of the cluster is fixed and that its total spin is maximal. The latter could be described by reintroducing the Hubbard term and transforming it into the form of a spin-spin interaction term for the cluster. Using a Hubbard-Stratonovich transform on this term will give rise to another auxiliary field which enters the mean field equations. However, this field plays a minor role in the limit $U \rightarrow \infty$ (which has to be performed in the mean field equations).

In order to incorporate the boundary condition of the cluster having a fixed occupation number, one would use the generalised method of imaginary chemical potentials as presented by Kiselev et al. in [85]. In this framework, the Hamiltonian would not be seen as a $SU(2)$ Hamiltonian composed of N different $SU(2)$ spins with spin- $\frac{1}{2}$. Instead the whole cluster would represent a single $SU(2 \times N)$ pseudo spin, and the total occupation of the cluster would determine which irreducible representation of the $SU(2 \times N)$ group would be used (quite analogous to the ordinary spin). The approach via imaginary chemical potentials to such a system is quite analogous to the one presented here, but instead of one imaginary chemical potential there occur several ones and the partition function cannot be computed as a single path integral anymore but as a weighted sum of path integrals. Still, each of these path integrals can be calculated the same way we did here.

Such a system with fixed cluster occupation that does not coincide with the size of the cluster is expected to develop effects due to hopping of the cluster electrons from site to site, which cannot play any role in the present model.

Appendices

A Preliminary Considerations

A.1 Mathematical definitions and useful relations

In this section we are going to state some general mathematical definitions and give some useful relations, which we use throughout this appendix. We start with the Fourier transformation from the imaginary time space to frequency space. The Fourier transform of a function f in the space of imaginary time is given as

$$\hat{f}_{i\omega_n} = \int_0^\beta d\tau f(\tau) e^{i\omega_n \tau}$$

and the inverse transformation is

$$f(\tau) = \sum_{i\omega_n} \hat{f}_{i\omega_n} e^{-i\omega_n \tau}$$

where the summation is performed over the Matsubara frequencies. Using this definition, one arrives at the relations

$$\delta_{\omega_n \omega'_n} = \int_0^\beta d\tau e^{i(\omega_n - \omega'_n) \tau}$$

and

$$\delta_{\tau \tau'} = \sum_{i\omega_n} e^{i\omega_n (\tau - \tau')}.$$

Hence, for any two functions f and g it is

$$\int_0^\beta d\tau f(\tau) \partial_\tau g(\tau) = \sum_{i\omega_n} \hat{f}_{i\omega_n} (-i\omega_n) \hat{g}_{i\omega_n}$$

and

$$\int_0^\beta d\tau f(\tau) A g(\tau) = \sum_{i\omega_n} \hat{f}_{i\omega_n} A \hat{g}_{i\omega_n}.$$

We state some more relations which will be used later. The trace of the tensor product of two operators A and B is the product of their traces:

$$\text{Tr}(A \otimes B) = \text{Tr} A \cdot \text{Tr} B. \quad (\text{A.1.1})$$

This simply follows from the definition of the tensor product. It is

$$\begin{aligned} \text{Tr}(A \otimes B) &= \sum_{i\sigma} A_{ij} \delta_{ij} B_{\sigma\rho} \delta_{\sigma\rho} \\ &= \sum_i A_{ii} \sum_\sigma B_{\sigma\sigma} \\ &= \text{Tr} A \cdot \text{Tr} B. \end{aligned}$$

A Preliminary Considerations

The determinant of an operator A is defined as

$$\det A = \exp \operatorname{Tr} \log A. \quad (\text{A.1.2})$$

For finite dimensional operators A and B (which therefore can be written as matrices) it holds

$$\det(A \otimes B) = (\det A)^{\dim B} \cdot (\det B)^{\dim A}. \quad (\text{A.1.3})$$

For any operator A and $N \in \mathbb{N}$ it is

$$\det(A \otimes \mathbb{1}_N) = (\det A)^N = \exp N \operatorname{Tr} \log A.$$

In the following we give a very useful formula for block triangular operators, say operators whose representation matrix has the form

$$A = \begin{pmatrix} A_1 & 0 \\ B & A_2 \end{pmatrix}$$

with any operators A_1 , A_2 and B . For those triangular operators, it is

$$\operatorname{Tr} \log \begin{pmatrix} A_1 & 0 \\ B & A_2 \end{pmatrix} = \operatorname{Tr} \log A_1 + \operatorname{Tr} \log A_2. \quad (\text{A.1.4})$$

Using the definition of the determinant (A.1.2), this apparently means

$$\det \begin{pmatrix} A_1 & 0 \\ B & A_2 \end{pmatrix} = \det A_1 \cdot \det A_2.$$

Equation (A.1.4) can be shown easily if one is not too rigid on convergence conditions for the Taylor series of the logarithm. Since we have to deal with a power series of matrices A as defined above, we first determine the form of the monomials A^n . It is

$$\begin{pmatrix} A_1 & 0 \\ B & A_2 \end{pmatrix}^n = \begin{pmatrix} A_1^n & 0 \\ B' & A_2^n \end{pmatrix}$$

for some matrix B' . This can be easily shown for A^2 and then follows for A^n by induction. Using this formula and the power series of the logarithm, we write

$$\begin{aligned} \operatorname{Tr} \log \begin{pmatrix} A_1 & 0 \\ B & A_2 \end{pmatrix} &= \operatorname{Tr} \sum_{n=1}^{\infty} \frac{1}{n} \left[\begin{pmatrix} A_1 & 0 \\ B & A_2 \end{pmatrix} - \mathbb{1} \right]^n \\ &= \operatorname{Tr} \sum_{n=1}^{\infty} \frac{1}{n} \sum_{k=0}^n \binom{n}{k} (-1)^{n+k} \begin{pmatrix} A_1 & 0 \\ B & A_2 \end{pmatrix}^k \\ &= \operatorname{Tr} \sum_{n=1}^{\infty} \frac{1}{n} \sum_{k=0}^n \binom{n}{k} (-1)^{n+k} \begin{pmatrix} A_1^k & 0 \\ B_k & A_2^k \end{pmatrix} \\ &= \sum_{n=1}^{\infty} \frac{1}{n} \sum_{k=0}^n \binom{n}{k} (-1)^{n+k} [\operatorname{Tr} A_1^k + \operatorname{Tr} A_2^k] \\ &= \operatorname{Tr} \sum_{n=1}^{\infty} \frac{1}{n} [A_1 - \mathbb{1}]^n + \operatorname{Tr} \sum_{n=1}^{\infty} \frac{1}{n} [A_2 - \mathbb{1}]^n \\ &= \operatorname{Tr} \log A_1 + \operatorname{Tr} \log A_2. \end{aligned}$$

This proves (A.1.4).

A.2 $SU(N)$ -generators

In this chapter, we are going to show some general properties of the $SU(N)$ generators. In what follows, we always assume the generators to be represented by $N^2 - 1$ linearly independent $N \times N$ matrices. Those are hermitian and traceless. Moreover, the generators of the $SU(N)$ algebra satisfy the product rule

$$G^\nu G^\mu = \frac{1}{N} \delta_{\nu\mu} \mathbb{1}_N + \frac{1}{\sqrt{2}} \sum_{a=1}^{N^2-1} (if_{\nu\mu a} + d_{\nu\mu a}) G^a \quad (\text{A.2.1})$$

for $\nu, \mu = 1 \dots N^2 - 1$. The product here is the matrix product. $f_{\nu\mu a}$ and $d_{\nu\mu a}$ are the so called structure constants. $f_{\nu\mu a}$ is completely antisymmetric under exchange of any two indices, while $d_{\nu\mu a}$ is completely symmetric. Moreover they fulfill the following contraction rules:

$$\sum_{\mu, \nu=1}^{N^2-1} f_{a\mu\nu} f_{b\mu\nu} = N \delta_{ab} \quad (\text{A.2.2})$$

$$\sum_{\mu, \nu=1}^{N^2-1} d_{a\mu\nu} d_{b\mu\nu} = \frac{N^2 - 4}{N} \delta_{ab} \quad (\text{A.2.3})$$

$$\sum_{\mu, \nu=1}^{N^2-1} f_{a\mu\nu} d_{b\mu\nu} = 0 \quad (\text{A.2.4})$$

$$\sum_{\mu=1}^{N^2-1} d_{a\mu\mu} = 0. \quad (\text{A.2.5})$$

We define

$$G^0 = \frac{1}{\sqrt{N}} \mathbb{1}_N.$$

The matrices $G^0, G^1, \dots, G^{N^2-1}$ span the space \mathcal{H}_N of the hermitian $N \times N$ matrices, its field being \mathbb{R} . Because of the tracelessness of $G^1 \dots G^{N^2-1}$ and due to (A.2.1) it holds

$$\text{Tr } G^\nu G^\mu = \frac{1}{N} \delta_{\nu\mu} \text{Tr } \mathbb{1}_N = \delta_{\nu\mu} \quad (\text{A.2.6})$$

for all $\nu, \mu = 0 \dots N^2 - 1$. Let A and B any hermitian $N \times N$ matrices. They can be represented as

$$A = \sum_{\nu} a_{\nu} G^{\nu} \quad \text{and} \quad B = \sum_{\mu} b_{\mu} G^{\mu}$$

with real valued coefficients. The mapping

$$\langle \cdot, \cdot \rangle : \mathcal{H}_N \times \mathcal{H}_N \rightarrow \mathbb{R} \quad (\text{A.2.7})$$

defined by

$$\langle A, B \rangle = \text{Tr } AB = \sum_{\nu\mu} a_{\nu} b_{\mu} \text{Tr } G^{\nu} G^{\mu} = \sum_{\mu} a_{\mu} b_{\mu}$$

is bilinear and symmetric because of linearity and cyclicity of the trace. Moreover

$$\langle A, A \rangle = \text{Tr } A^2 = \sum_{\mu} (a_{\mu})^2 \geq 0$$

A Preliminary Considerations

for all A , and $\langle A, A \rangle = 0$ if and only if $A = 0$. Thus, the mapping (A.2.7) is a real symmetric scalar product. It implies a norm on \mathcal{H}_N , and being finite dimensional, \mathcal{H}_N is complete with respect to this norm. Thus, \mathcal{H}_N is a Hilbert space w.r.t. the scalar product (A.2.7).

In the following, we show a projection theorem which will be used when performing the Hubbard-Stratonovich transformation of the action. Let $\nu = 0$. Then

$$\begin{aligned}
\sum_{\mu=0}^{N^2-1} G^\mu G^\nu G^\mu &= \frac{1}{\sqrt{N}} \sum_{\mu=0}^{N^2-1} G^\mu G^\mu \\
&= \frac{1}{N} \cdot \frac{1}{\sqrt{N}} \mathbb{1}_N + \frac{1}{\sqrt{N}} \sum_{\mu=1}^{N^2-1} G^\mu G^\mu \\
&= \frac{1}{N} G^0 + \frac{1}{N} \sum_{\mu=1}^{N^2-1} \frac{1}{\sqrt{N}} \mathbb{1}_N + \frac{1}{\sqrt{2N}} \sum_{a=1}^{N^2-1} (if_{\mu\mu a} + d_{\mu\mu a}) G^a \\
&= \frac{1}{N} G^0 + (N^2 - 1) \frac{1}{N} G^0 \\
&= N \cdot G^0,
\end{aligned}$$

where we made use of (A.2.1), (A.2.5) and the antisymmetry of f . Now let $\nu \neq 0$. Then

$$\begin{aligned}
\sum_{\mu=0}^{N^2-1} G^\mu G^\nu G^\mu &= \frac{1}{N} G^\nu + \sum_{\mu=1}^{N^2-1} G^\mu G^\nu G^\mu \\
&= \frac{1}{N} G^\nu + \sum_{\mu=1}^{N^2-1} G^\mu \left(\frac{1}{N} \delta_{\nu\mu} \mathbb{1}_N + \frac{1}{\sqrt{2}} \sum_{a=1}^{N^2-1} (if_{\nu\mu a} + d_{\nu\mu a}) G^a \right) \\
&= \frac{2}{N} G^0 + \frac{1}{\sqrt{2}} \sum_{\mu, a=1}^{N^2-1} (if_{\nu\mu a} + d_{\nu\mu a}) \left(\frac{1}{N} \delta_{\mu a} \mathbb{1}_N + \frac{1}{\sqrt{2}} \sum_{b=1}^{N^2-1} (if_{\mu a b} + d_{\mu a b}) G^b \right) \\
&= \frac{2}{N} G^\nu + \frac{1}{\sqrt{2N}} \sum_{\mu=1}^{N^2-1} (if_{\nu\mu\mu} + d_{\nu\mu\mu}) \mathbb{1}_N + \frac{1}{2} \sum_{\mu, a, b=1}^{N^2-1} (if_{\nu\mu a} + d_{\nu\mu a}) (if_{b\mu a} + d_{b\mu a}) G^b \\
&= \frac{2}{N} G^\nu + \frac{1}{2} \sum_{\mu, a, b=1}^{N^2-1} (-f_{\nu\mu a} f_{b\mu a} + if_{\nu\mu a} d_{b\mu a} + if_{b\mu a} d_{\nu\mu a} + d_{\nu\mu a} d_{b\mu a}) G^b \\
&= \frac{2}{N} G^\nu + \frac{1}{2} \sum_{b=1}^{N^2-1} \left(-N \delta_{\nu b} + \frac{N^2 - 4}{N} \delta_{\nu b} \right) G^b \\
&= \left(\frac{2}{N} + \frac{N^2 - 4}{2N} - \frac{N}{2} \right) G^\nu \\
&= 0,
\end{aligned}$$

where we used (anti-)symmetry of f and d and the contraction rules (A.2.2)-(A.2.5). Hence, we have proven the relation

$$\sum_{\mu=0}^{N^2-1} G^\mu G^\nu G^\mu = N \cdot \delta_{\nu 0} G^0 \tag{A.2.8}$$

for every $\nu = 0 \dots N^2 - 1$.

The $SU(2)$ generators can be represented as the famous Pauli matrices

$$\sigma^0 = \frac{1}{\sqrt{2}} \begin{pmatrix} 1 & 0 \\ 0 & 1 \end{pmatrix}, \quad \sigma^1 = \frac{1}{\sqrt{2}} \begin{pmatrix} 0 & 1 \\ 1 & 0 \end{pmatrix}, \quad \sigma^2 = \frac{1}{\sqrt{2}} \begin{pmatrix} 0 & -i \\ i & 0 \end{pmatrix}$$

and

$$\sigma^3 = \frac{1}{\sqrt{2}} \begin{pmatrix} 1 & 0 \\ 0 & -1 \end{pmatrix}.$$

We are going to use them to describe spin degrees of freedom.

A.3 Conductance at low temperatures

We outline the connection between the local density of states and the differential conductance dI/dV for low temperatures. The outcome is that the latter is just proportional to the first. In order to derive this result, we first show the following δ identity: the functional sequence

$$\delta_{\beta,y} : \quad \delta_{\beta,y}(f) = \frac{\beta}{2} \int_{-\infty}^{\infty} dx \frac{1}{1 + \cosh(\beta(x-y))} f(x)$$

is converging pointwisely towards the δ functional for all continuous polynomially bound functions f . The latter assumption on f just ensures the integral to exist. We show this claim by direct computation. It is

$$\frac{\beta}{2} \int_{-\infty}^{\infty} dx \frac{1}{1 + \cosh(\beta(x-y))} = \frac{\beta}{2} \frac{1}{\beta} \tanh \left(\frac{\beta}{2} [x-y] \right) \Bigg|_{-\infty}^{\infty} = \frac{1}{2} (1 - [-1]) = 1$$

for all $\beta > 0$. Hence

$$\lim_{\beta \rightarrow \infty} \frac{\beta}{2} \int_{-\infty}^{\infty} dx \frac{1}{1 + \cosh(\beta(x-y))} f(x) = \frac{1}{2} \int_{-\infty}^{\infty} d\bar{x} \frac{1}{1 + \cosh(\bar{x})} \lim_{\beta \rightarrow \infty} f \left(\frac{\bar{x}}{\beta} + y \right) = f(y),$$

where we used continuity of f and the dominated convergence theorem, which is valid for β large enough (finitely large being sufficient).

Assuming a broad and flat conduction band, the current in an STM experiment is approximately given as

$$I(V, \mathbf{r}) = \frac{e}{\hbar} \rho_0 |t_{tip}|^2 \int_{-\infty}^{\infty} d\varepsilon \rho_\varepsilon(\mathbf{r}) [f(\varepsilon) - f(\varepsilon + eV)],$$

where e is the elementary charge, ρ_0 the local density of states in the metal at the Fermi level, t_{tip} the tunnelling strength in the tip, ρ_ε the normalised local density of states and f the Fermi distribution

$$f(\varepsilon) = \frac{1}{e^{\beta\varepsilon} + 1}.$$

A Preliminary Considerations

The differential conductance is thus given as

$$\begin{aligned}
\sigma(V, \mathbf{r}) &= \frac{dI}{dV}(V, \mathbf{r}) \\
&= \frac{e}{\hbar} \rho_0 |t_{tip}|^2 \int_{-\infty}^{\infty} d\varepsilon \rho_{\varepsilon}(\mathbf{r}) \frac{\beta e^{\beta(\varepsilon+eV)}}{(1 + e^{\beta(\varepsilon+eV)})^2} \\
&= \frac{e^2}{\hbar} \rho_0 |t_{tip}|^2 \beta \int_{-\infty}^{\infty} d\varepsilon \rho_{\varepsilon}(\mathbf{r}) \frac{1}{(1 + e^{\beta(\varepsilon+eV)}) (1 + e^{-\beta(\varepsilon+eV)})} \\
&= \frac{e^2}{\hbar} \rho_0 |t_{tip}|^2 \beta \int_{-\infty}^{\infty} d\varepsilon \rho_{\varepsilon}(\mathbf{r}) \frac{1}{2 + 2 \cosh(\beta[\varepsilon + eV])} \\
&= \frac{e^2}{\hbar} \rho_0 |t_{tip}|^2 \int_{-\infty}^{\infty} d\bar{\varepsilon} \rho_{\frac{\bar{\varepsilon}}{\beta} - eV}(\mathbf{r}) \frac{1}{2} \frac{1}{1 + 1 \cosh(\bar{\varepsilon})}.
\end{aligned}$$

Hence, for $\beta \rightarrow \infty$ we get

$$\lim_{\beta \rightarrow \infty} \sigma(V, \mathbf{r}) = \frac{e^2}{\hbar} \rho_0 |t_{tip}|^2 \rho_{-eV}(\mathbf{r}).$$

For very low temperatures, the conductance at a given point is proportional to the local density of states.

A.4 Schrieffer-Wolff transformation

In this section, we are going to map the original Hamiltonian of the microscopic Anderson model to the low energy sector, thus achieving an effective Kondo like Hamiltonian. The transformation applied here is the well known Schrieffer-Wolff transformation [8]. It is based on the idea of applying a unitary transformation which maps the Anderson Hamiltonian to the one of the Kondo model if the tunnelling amplitude is sufficiently small. After this transformation any terms linear in the tunnelling amplitude will not contribute to the effective Hamiltonian anymore. We start with proving a short lemma. Let $\hat{H} = H_0 + H_1$ and S an operator with $[H_0, S] = H_1$. Then

$$H = e^S \hat{H} e^{-S} = H_0 + \sum_{n=1}^{\infty} \frac{n}{(n+1)!} [S, H_1]_n, \tag{A.4.1}$$

where $[S, A]_n = [S, [S, A]_{n-1}]$ and $[S, A]_0 = A$.

By induction, we prove $[S, \hat{H}]_n = -[S, H_1]_{n-1} + [S, H_1]_n$ for $n \geq 1$. For $n = 1$ it is $[S, \hat{H}]_1 = -H_1 + [S, H_1]$ due to the form of the commutator of S and H_0 . Assume the lemma to be correct for some n . Then for $n + 1$

$$[S, \hat{H}]_{n+1} = [S, [S, \hat{H}]_n] = [S, -[S, H_1]_{n-1} + [S, H_1]_n] = -[S, H_1]_n + [S, H_1]_{n+1},$$

A Preliminary Considerations

and we have proven the claim. Due to the Baker-Campbell-Hausdorff theorem it is

$$\begin{aligned}
H &= e^S \hat{H} e^{-S} \\
&= \sum_{n=0}^{\infty} \frac{1}{n!} [S, \hat{H}]_n \\
&= \hat{H} + \sum_{n=1}^{\infty} \frac{1}{n!} (-[S, H_1]_{n-1} + [S, H_1]_n) \\
&= \hat{H} - H_1 + \sum_{n=1}^{\infty} \left(\frac{1}{n!} - \frac{1}{(n+1)!} \right) [S, H_1]_n \\
&= H_0 + \sum_{n=1}^{\infty} \frac{n}{(n+1)!} [S, H_1]_n.
\end{aligned}$$

We remark that for an anti-hermitian operator S , the transformation is unitary.

We will now turn to the Hamiltonian of interest. The Anderson Hamiltonian in our case is given by

$$\hat{H} = \sum_{\mathbf{k}\sigma} \varepsilon_{\mathbf{k}} N_{\mathbf{k}\sigma} + \sum_{i\sigma} \varepsilon_d n_{i\sigma} + \sum_i U n_{i\uparrow} n_{i\downarrow} + \sum_i \sum_{\mathbf{k}\sigma} \left(T_{i\mathbf{k}} c_{i\sigma}^\dagger a_{\mathbf{k}\sigma} + \text{h.c.} \right), \quad (\text{A.4.2})$$

where $N_{\mathbf{k}\sigma} = a_{\mathbf{k}\sigma}^\dagger a_{\mathbf{k}\sigma}$ with a the construction operators of the substrate electrons, $n_{i\sigma} = c_{i\sigma}^\dagger c_{i\sigma}$ with c_i the construction operators of the electrons in the i -th atom of the cluster. U is the Hubbard-interaction energy and $T_{i\mathbf{k}}$ is proportional to the tunnelling amplitude $|T(\mathbf{k})|$. We denote the first three terms of the Hamiltonian by H_0 and the interaction term by H_1 . We now seek an anti-hermitian operator S which fulfills $[H_0, S] = H_1$, so that we can use (A.4.1). The aim is to get rid of all terms which are linear in the tunnelling amplitude, so that the first nontrivial term in the expansion (A.4.1) is of quadratic order in $|T(\mathbf{k})|$. We use the following ansatz for S :

$$S = s - s^\dagger$$

with

$$s = \sum_i \sum_{\mathbf{k}\sigma} T_{i\mathbf{k}} (A_{i\mathbf{k}} n_{i,-\sigma} + B_{i\mathbf{k}}) c_{i\sigma}^\dagger a_{\mathbf{k}\sigma},$$

where all A, B are real valued coefficients. It is

$$[H_0, S] = [H_0, s] - [H_0, s^\dagger] = [H_0, s] + [H_0, s]^\dagger.$$

We compute

$$\begin{aligned}
[H_0, s] &= \left[\sum_{\mathbf{k}\sigma} \varepsilon_{\mathbf{k}} N_{\mathbf{k}\sigma} + \sum_{i\sigma} \varepsilon_d n_{i\sigma} + \sum_i U n_{i\uparrow} n_{i\downarrow}, \sum_j \sum_{\mathbf{k}'\sigma'} T_{j\mathbf{k}'} (A_{j\mathbf{k}'} n_{j,-\sigma'} + B_{j\mathbf{k}'}) c_{i\sigma}^\dagger a_{\mathbf{k}\sigma} \right] \\
&= - \sum_{i\mathbf{k}\sigma} \varepsilon_{\mathbf{k}} T_{i\mathbf{k}} (A_{i\mathbf{k}} n_{i,-\sigma} + B_{i\mathbf{k}}) c_{i\sigma}^\dagger a_{\mathbf{k}\sigma} + \sum_{i\mathbf{k}\sigma} \varepsilon_d T_{i\mathbf{k}} (A_{i\mathbf{k}} n_{i,-\sigma} + B_{i\mathbf{k}}) c_{i\sigma}^\dagger a_{\mathbf{k}\sigma} \\
&\quad + \sum_{i\mathbf{k}\sigma} U T_{i\mathbf{k}} (A_{i\mathbf{k}} + B_{i\mathbf{k}}) n_{i,-\sigma} c_{i\sigma}^\dagger a_{\mathbf{k}\sigma} \\
&= \sum_{i\mathbf{k}\sigma} T_{i\mathbf{k}} [A_{i\mathbf{k}} (U + \varepsilon_d - \varepsilon_{\mathbf{k}}) n_{i,-\sigma} + B_{i\mathbf{k}} (U n_{i,-\sigma} + \varepsilon_d - \varepsilon_{\mathbf{k}})] c_{i\sigma}^\dagger a_{\mathbf{k}\sigma}
\end{aligned}$$

A Preliminary Considerations

Here, we used

$$\begin{aligned} [A, BC] &= B[A, C] + [A, B]C, \\ [n_\alpha, n_\beta] &= 0, \\ [N_{\mathbf{k}\sigma}, c_{j\sigma'}^\dagger a_{\mathbf{k}'\sigma'}] &= -\delta_{\mathbf{k}\mathbf{k}'} \delta_{\sigma\sigma'} c_{j\sigma'}^\dagger a_{\mathbf{k}\sigma}, \\ [n_{i\sigma}, c_{j\sigma'}^\dagger a_{\mathbf{k}'\sigma'}] &= \delta_{ij} \delta_{\sigma\sigma'} c_{j\sigma'}^\dagger a_{\mathbf{k}'\sigma'} \end{aligned}$$

and $n_\mu^2 = n_\mu$. The requirement $[H_0, S] = H_1$ reads

$$[H_0, s] = \sum_{\mathbf{ik}} T_{\mathbf{ik}} c_{i\sigma}^\dagger a_{\mathbf{k}\sigma} =: h_1$$

which is fulfilled for

$$A_{\mathbf{ik}} = \frac{1}{U + \varepsilon_d - \varepsilon_{\mathbf{k}}} - \frac{1}{\varepsilon_d - \varepsilon_{\mathbf{k}}}$$

and

$$B_{\mathbf{ik}} = \frac{1}{\varepsilon_d - \varepsilon_{\mathbf{k}}}.$$

So $S = s - s^\dagger$ with

$$s = \sum_i \sum_{k\sigma} T_{\mathbf{ik}} \left(\frac{1}{U + \varepsilon_d - \varepsilon_{\mathbf{k}}} n_{i,-\sigma} + \frac{1}{\varepsilon_d - \varepsilon_{\mathbf{k}}} [1 - n_{i,-\sigma}] \right) c_{i\sigma}^\dagger a_{\mathbf{k}\sigma} \quad (\text{A.4.3})$$

fulfills (A.4.1). Since S is already proportional to $T_{\mathbf{ik}}$, all terms in (A.4.1) apart from H_0 will be at least quadratic in the tunnelling amplitude. For (in some sense) small tunnelling amplitudes this justifies to approximate

$$H = H_0 + \frac{1}{2} [S, H_1].$$

It is $H_1 = h_1 + h_1^\dagger$ and so

$$[S, H_1] = [s - s^\dagger, h_1 + h_1^\dagger] = [s, h_1] + [s, h_1]^\dagger + [s, h_1^\dagger] + [s, h_1^\dagger]^\dagger.$$

So, we have to know $[s, h_1]$ and $[s, h_1^\dagger]$. Before we compute the commutators in question, we make some further assumptions to simplify the problem. First, we assume $\varepsilon_{\mathbf{k}} \ll \varepsilon_d$. This is justified, if mostly conduction electrons near the Fermi energy are expected to play an important role for the physics of the system. With this assumption it is

$$A_{\mathbf{ik}} \approx \frac{1}{U + \varepsilon_d} - \frac{1}{\varepsilon_d} = A$$

and

$$B_{\mathbf{ik}} \approx \frac{1}{\varepsilon_d} = B.$$

Moreover, we assume the absolute value of the tunnelling amplitude to be the same for all sites, giving $T_{\mathbf{ik}}$ the form

$$T_{\mathbf{ik}} = \frac{1}{\sqrt{N}} T_F e^{-i\mathbf{R}_i \mathbf{k}} = T_F t_{\mathbf{ik}},$$

where $t_{\mathbf{ik}}$ has been defined. Using this assumptions, we get

$$[s, h_1] = T_F^2 \sum_{\substack{ij \\ \sigma\sigma'}} \sum_{\mathbf{k}\mathbf{k}'} t_{\mathbf{ik}} t_{j\mathbf{k}'} [(A n_{i,-\sigma} + B) c_{i\sigma'}^\dagger a_{\mathbf{k}'\sigma'} + c_{j\sigma}^\dagger a_{\mathbf{k}\sigma}].$$

A Preliminary Considerations

It is

$$[c_{i\sigma'}^\dagger a_{\mathbf{k}'\sigma'}, c_{j\sigma}^\dagger a_{\mathbf{k}\sigma}] = 0,$$

so

$$\begin{aligned} [s, h_1] &= T_F^2 \sum_{\substack{ij \\ \sigma\sigma'}} \sum_{\mathbf{k}\mathbf{k}'} t_{i\mathbf{k}} t_{j\mathbf{k}'} A [n_{i,-\sigma}, c_{j\sigma}^\dagger a_{\mathbf{k}\sigma}] c_{i\sigma'}^\dagger a_{\mathbf{k}'\sigma'} \\ &= T_F^2 \sum_{\substack{ij \\ \sigma\sigma'}} \sum_{\mathbf{k}\mathbf{k}'} t_{i\mathbf{k}} t_{j\mathbf{k}'} A \delta_{ij} \delta_{\sigma', -\sigma} c_{j\sigma}^\dagger a_{\mathbf{k}\sigma} c_{i\sigma'}^\dagger a_{\mathbf{k}'\sigma'} \\ &= T_F^2 \sum_{\substack{i\sigma \\ \mathbf{k}\mathbf{k}'}} t_{i\mathbf{k}} t_{i\mathbf{k}'} A c_{i\sigma}^\dagger a_{\mathbf{k}\sigma} c_{i-\sigma}^\dagger a_{\mathbf{k}'-\sigma}. \end{aligned} \tag{A.4.4}$$

Equation (A.4.4) contains two creators for the localised electrons. $[s, h_1]$ and $[s, h_1]^\dagger$ correspond to creating and annihilating two site electrons respectively. These terms do not conserve the particle number within the cluster; they will lead to energetically excited states. Since we are only interested in the low energy behaviour, we will skip these terms altogether.

Let us turn to the computation of $[s, h_1^\dagger]$. It is

$$[s, h_1^\dagger] = T_F^2 \sum_{\substack{ij \\ \sigma\sigma'}} \sum_{\mathbf{k}\mathbf{k}'} t_{i\mathbf{k}'} \bar{t}_{j\mathbf{k}} [(A n_{i,-\sigma'} + B) c_{i\sigma'}^\dagger a_{\mathbf{k}'\sigma'}, a_{\mathbf{k}\sigma}^\dagger c_{j\sigma}].$$

We use

$$[n_{i,-\sigma'}, a_{\mathbf{k}\sigma}^\dagger c_{j\sigma}] = a_{\mathbf{k}\sigma}^\dagger [n_{i,-\sigma'}, c_{j\sigma}] = -\delta_{ij} \delta_{-\sigma'\sigma} a_{\mathbf{k}\sigma}^\dagger c_{i-\sigma'}$$

and

$$[c_{i\sigma'}^\dagger a_{\mathbf{k}'\sigma'}, a_{\mathbf{k}\sigma}^\dagger c_{j\sigma}] = \delta_{\mathbf{k}\mathbf{k}'} \delta_{\sigma\sigma'} c_{i\sigma'}^\dagger c_{j\sigma} - \delta_{ij} \delta_{\sigma\sigma'} a_{\mathbf{k}\sigma}^\dagger a_{\mathbf{k}'\sigma'}.$$

Hence we get

$$\begin{aligned} [s, h_1^\dagger] &= T_F^2 \sum_{\substack{ij \\ \sigma\sigma'}} \sum_{\mathbf{k}\mathbf{k}'} t_{i\mathbf{k}'} \bar{t}_{j\mathbf{k}} \left(A n_{i,-\sigma'} [c_{i\sigma'}^\dagger a_{\mathbf{k}'\sigma'}, a_{\mathbf{k}\sigma}^\dagger c_{j\sigma}] + A [n_{i,-\sigma}, a_{\mathbf{k}\sigma}^\dagger c_{j\sigma}] c_{i\sigma'}^\dagger a_{\mathbf{k}'\sigma'} \right. \\ &\quad \left. + B [c_{i\sigma'}^\dagger a_{\mathbf{k}'\sigma'}, a_{\mathbf{k}\sigma}^\dagger c_{j\sigma}] \right) \\ &= T_F^2 \sum_{\substack{ij \\ \sigma\sigma'}} \sum_{\mathbf{k}\mathbf{k}'} t_{i\mathbf{k}'} \bar{t}_{j\mathbf{k}} \left(A n_{i,-\sigma'} c_{i\sigma'}^\dagger c_{j\sigma} \delta_{\mathbf{k}\mathbf{k}'} \delta_{\sigma\sigma'} - A n_{i,-\sigma'} a_{\mathbf{k}\sigma}^\dagger a_{\mathbf{k}'\sigma'} \delta_{ij} \delta_{\sigma\sigma'} \right. \\ &\quad \left. - A a_{\mathbf{k}\sigma}^\dagger c_{i-\sigma'} c_{i\sigma'}^\dagger a_{\mathbf{k}'\sigma'} \delta_{ij} \delta_{-\sigma'\sigma} + B c_{i\sigma'}^\dagger c_{j\sigma} \delta_{\mathbf{k}\mathbf{k}'} \delta_{\sigma\sigma'} - B a_{\mathbf{k}\sigma}^\dagger a_{\mathbf{k}'\sigma'} \delta_{ij} \delta_{\sigma\sigma'} \right) \\ &= T_F^2 \sum_{\substack{ij \\ \sigma\mathbf{k}}} t_{i\mathbf{k}} \bar{t}_{j\mathbf{k}} A n_{i,-\sigma} c_{i\sigma}^\dagger c_{j\sigma} - T_0^2 \sum_{\substack{\mathbf{k}\mathbf{k}' \\ \sigma i}} t_{i\mathbf{k}'} \bar{t}_{i\mathbf{k}} A n_{i,-\sigma} a_{\mathbf{k}\sigma}^\dagger a_{\mathbf{k}'\sigma} \\ &\quad - T_F^2 \sum_{\substack{\mathbf{k}\mathbf{k}' \\ \sigma i}} t_{i\mathbf{k}'} \bar{t}_{i\mathbf{k}} A a_{\mathbf{k}\sigma}^\dagger c_{i\sigma} c_{i-\sigma}^\dagger a_{\mathbf{k}'-\sigma} + T_0^2 \sum_{\substack{ij \\ \sigma\mathbf{k}}} t_{i\mathbf{k}} \bar{t}_{j\mathbf{k}} B c_{i\sigma}^\dagger c_{j\sigma} - T_0^2 \sum_{\substack{\mathbf{k}\mathbf{k}' \\ \sigma i}} t_{i\mathbf{k}'} \bar{t}_{i\mathbf{k}} B a_{\mathbf{k}\sigma}^\dagger a_{\mathbf{k}'\sigma}. \end{aligned}$$

The term $[s, h_1^\dagger](3)$ is not normally ordered yet. It is

$$-T_F^2 \sum_{\substack{\mathbf{k}\mathbf{k}' \\ \sigma i}} t_{i\mathbf{k}'} \bar{t}_{i\mathbf{k}} A a_{\mathbf{k}\sigma}^\dagger c_{i\sigma} c_{i-\sigma}^\dagger a_{\mathbf{k}'-\sigma} = T_F^2 \sum_{\substack{\mathbf{k}\mathbf{k}' \\ \sigma i}} t_{i\mathbf{k}'} \bar{t}_{i\mathbf{k}} A c_{i-\sigma}^\dagger c_{i\sigma} a_{\mathbf{k}\sigma}^\dagger a_{\mathbf{k}'-\sigma}.$$

A Preliminary Considerations

Moreover, it is

$$t_{i\mathbf{k}}\overline{t_{j\mathbf{k}}} = \frac{1}{N} e^{-i(\mathbf{R}_i - \mathbf{R}_j)\mathbf{k}}.$$

Hence

$$\sum_{\mathbf{k}} t_{i\mathbf{k}}\overline{t_{j\mathbf{k}}} = \frac{1}{N} \delta_{ij}.$$

So

$$[s, h_1^\dagger](1) + [s, h_1^\dagger](4) = T_F^2 \sum_{i\sigma} (An_{i,-\sigma} + B)n_{i,\sigma} = T_F^2 A \sum_{i\sigma} n_{i,-\sigma}n_{i,\sigma} + T_F^2 B \sum_{i\sigma} n_{i,\sigma}.$$

These terms have the same form as the Hubbard part and the cluster electron part of the Anderson Hamiltonian. They only redefine U and ε_d a bit. Since T_F^2 is assumed to be small compared to the other occurring energies, those changes are negligible. As we can see by direct computation for all its parts, $[s, h_1^\dagger]$ is hermitian.

The terms $[s, h_1^\dagger](2)$ and $[s, h_1^\dagger](3)$ contain the Kondo term. To see this, we compute

$$\begin{aligned} \vec{S}_i \cdot \vec{s}_{\mathbf{k}\mathbf{k}'} &= \sum_{\nu=1}^3 \sum_{\substack{\sigma\sigma' \\ \rho\rho'}} c_{i\sigma}^\dagger \sigma_{\sigma\sigma'}^\nu c_{i\sigma'} a_{\mathbf{k}\rho}^\dagger \sigma_{\rho\rho'}^\nu a_{\mathbf{k}'\rho'} \\ &= \sum_{\substack{\sigma\sigma' \\ \rho\rho'}} c_{i\sigma}^\dagger c_{i\sigma'} a_{\mathbf{k}\rho}^\dagger a_{\mathbf{k}'\rho'} \left(\sum_{\nu=1}^3 \sigma_{\sigma\sigma'}^\nu \sigma_{\rho\rho'}^\nu \right) \\ &= \sum_{\substack{\sigma\sigma' \\ \rho\rho'}} \frac{1}{2} (2\delta_{\sigma\rho'} \delta_{\sigma'\rho} - \delta_{\sigma\sigma'} \delta_{\rho\rho'}) c_{i\sigma}^\dagger c_{i\sigma'} a_{\mathbf{k}\rho}^\dagger a_{\mathbf{k}'\rho'} \\ &= \sum_{\sigma\rho} c_{i\sigma}^\dagger c_{i\rho} a_{\mathbf{k}\rho}^\dagger a_{\mathbf{k}'\sigma} - \frac{1}{2} \sum_{\sigma\rho} c_{i\sigma}^\dagger c_{i\sigma} a_{\mathbf{k}\rho}^\dagger a_{\mathbf{k}'\rho} \\ &= \frac{1}{2} \sum_{\sigma} n_{i\sigma} a_{\mathbf{k}\sigma}^\dagger a_{\mathbf{k}'\sigma} + \frac{1}{2} \sum_{\sigma} n_{i,-\sigma} a_{\mathbf{k}\sigma}^\dagger a_{\mathbf{k}'\sigma} + \sum_{\sigma} c_{i-\sigma}^\dagger c_{i\sigma} a_{\mathbf{k}\sigma}^\dagger a_{\mathbf{k}'-\sigma} - \sum_{\sigma} c_{i-\sigma}^\dagger c_{i-\sigma} a_{\mathbf{k}\sigma}^\dagger a_{\mathbf{k}'\sigma}. \end{aligned}$$

It is

$$[s, h_1^\dagger](2) + [s, h_1^\dagger](3) = T_F^2 A \sum_{\substack{\mathbf{k}\mathbf{k}' \\ i}} t_{i\mathbf{k}'} \overline{t_{i\mathbf{k}}} \sum_{\sigma} \left(c_{i-\sigma}^\dagger c_{i\sigma} a_{\mathbf{k}\sigma}^\dagger a_{\mathbf{k}'-\sigma} - c_{i-\sigma}^\dagger c_{i-\sigma} a_{\mathbf{k}\sigma}^\dagger a_{\mathbf{k}'\sigma} \right),$$

so

$$[s, h_1^\dagger](2) + [s, h_1^\dagger](3) = T_F^2 A \sum_{\substack{\mathbf{k}\mathbf{k}' \\ i}} t_{i\mathbf{k}'} \overline{t_{i\mathbf{k}}} \sum_{(i)} \vec{S}_i \cdot \vec{s}_{\mathbf{k}\mathbf{k}'} - \frac{1}{2} T_F^2 A \sum_{\substack{\mathbf{k}\mathbf{k}' \\ i\sigma}} t_{i\mathbf{k}'} \overline{t_{i\mathbf{k}}} (n_{i,\sigma} + n_{i,-\sigma}) a_{\mathbf{k}\sigma}^\dagger a_{\mathbf{k}'\sigma}. \quad (\text{A.4.5})$$

Expression (i) is the Kondo term. It can be useful to ascribe the $t_{i\mathbf{k}}$ to the construction operators of the conduction electrons. Since

$$t_{i\mathbf{k}} = \frac{1}{\sqrt{N}} e^{-i\mathbf{R}_i\mathbf{k}},$$

the Kondo term (i) can be written as

$$T_F^2 A \sum_{\substack{\mathbf{k}\mathbf{k}' \\ i}} t_{i\mathbf{k}'} \overline{t_{i\mathbf{k}}} \vec{S}_i \cdot \vec{s}_{\mathbf{k}\mathbf{k}'} = \frac{1}{N} T_F^2 A \sum_i \vec{S}_i \cdot \vec{s}(\mathbf{R}_i),$$

A Preliminary Considerations

where we performed the wave vector summations. We define

$$N \cdot J = T_F^2 A = T_F^2 \left(\frac{1}{U + \varepsilon_d} - \frac{1}{\varepsilon_d} \right), \quad (\text{A.4.6})$$

where the factor N is for normalisation. It arises due to the fact that the tunnelling amplitudes are assumed to be normalised. In the proper Kondo regime, where $\varepsilon_d < 0 < U + \varepsilon_d$, the interaction constant J is positive.

The part (ii) of equation (A.4.5) can be combined with $[s, h_1^\dagger](5)$. It is

$$\begin{aligned} [s, h_1^\dagger](5) - \frac{1}{2} T_F^2 A \sum_{\substack{\mathbf{k}\mathbf{k}' \\ i\sigma}} t_{i\mathbf{k}'} \bar{t}_{i\mathbf{k}} (n_{i,\sigma} + n_{i,-\sigma}) a_{\mathbf{k}\sigma}^\dagger a_{\mathbf{k}'\sigma} \\ = -T_F^2 \sum_{\substack{\mathbf{k}\mathbf{k}' \\ i\sigma}} t_{i\mathbf{k}'} \bar{t}_{i\mathbf{k}} \left[\frac{1}{2} A (n_{i,\sigma} + n_{i,-\sigma}) + B \right] a_{\mathbf{k}\sigma}^\dagger a_{\mathbf{k}'\sigma}, \end{aligned}$$

which in the half filled case (where either $n_{i,\sigma} = 1$ and $n_{i,-\sigma} = 0$ or the other way round) becomes

$$= -T_F^2 \frac{1}{2} \frac{U + 2\varepsilon_d}{(U + \varepsilon_d)\varepsilon_d} \sum_{\substack{\mathbf{k}\mathbf{k}' \\ i\sigma}} t_{i\mathbf{k}'} \bar{t}_{i\mathbf{k}} a_{\mathbf{k}\sigma}^\dagger a_{\mathbf{k}'\sigma}.$$

This redefines the conduction electron term in the original Hamiltonian. As with the redefining terms before, the deviations from the original term is rather small.

Let ε'_k , ε'_d and U' be the redefined energies for the conduction term, the site term and the Hubbard interaction term. Let

$$H'_0 = \sum_{\mathbf{k}\sigma} \varepsilon'_k N_{\mathbf{k}\sigma} + \sum_{i\sigma} \varepsilon'_d n_{i\sigma} + \sum_i U' n_{i\uparrow} n_{i\downarrow}.$$

Then

$$\begin{aligned} H &\approx H_0 + \frac{1}{2} [S, H_1] \\ &\approx H_0 + \frac{1}{2} [s, h_1^\dagger] + \frac{1}{2} [s, h_1^\dagger]^\dagger \\ &= H_0 + [s, h_1^\dagger] \\ &= H'_0 + J \sum_i \vec{S}_i \cdot \vec{s}(\mathbf{R}_i). \end{aligned} \quad (\text{A.4.7})$$

The mapping of the Anderson Hamiltonian to the low energy sector yields an effective Hamiltonian of Kondo form. This Hamiltonian is the starting point of all further investigation made in this work. Although the form (A.4.7) is very instructive, we use the alternative form

$$H = H'_0 + N J \sum_i \sum_{\nu=1}^3 \sum_{\substack{\sigma\sigma' \\ \rho\rho'}} \left[c_{i\sigma}^\dagger \sigma_{\sigma\sigma'}^\nu c_{i\sigma'} \right] \left[\psi_{i\rho}^\dagger(\mathbf{k}) \sigma_{\rho\rho'}^\nu \psi_{i\rho'}(\mathbf{k}') \right], \quad (\text{A.4.8})$$

where

$$\psi_{i\sigma}(\mathbf{k}) = t_{i\mathbf{k}} a_{\mathbf{k}\sigma}.$$

A.5 Spin Hamiltonians and the Popov-Fedotov method

In the system under consideration, we deal with a magnetic cluster on a metallic substrate. A crucial boundary condition is, that the total occupation number within of the cluster is fixed to its size (there are always N electrons in a cluster of N atoms). The boundary conditions, we assume here, are even more restrictive, only allowing each cluster atom to be exactly singly occupied. In general, such conditions cannot be implemented easily into the model. The model Hamiltonian is given as

$$H = \sum_{\mathbf{k}\sigma} \varepsilon_{\mathbf{k}} N_{\mathbf{k}\sigma} + N \cdot J \sum_{\mathbf{k}\mathbf{k}'} \sum_{i=1}^N \sum_{\nu=1}^3 \left[\Phi_i^\dagger \sigma^\nu \Phi_i \right] \cdot \left[\Psi_i^\dagger(\mathbf{k}) \sigma^\nu \Psi_i(\mathbf{k}') \right], \quad (\text{A.5.1})$$

with the two-dimensional vectors

$$\Phi_i = (c_{i\uparrow}, c_{i\downarrow})^\text{T}$$

and

$$\Psi_i(\mathbf{k}) = (\psi_{i\uparrow}(\mathbf{k}), \psi_{i\downarrow}(\mathbf{k}))^\text{T}.$$

If one simply computed the partition function

$$Z = \text{Tr} e^{-\beta H},$$

by means of a fermionic path integral, the trace would involve states which correspond to doubly occupied or empty sites, which does not comply to the condition of each impurity being exactly singly occupied. The contributions of those states to the partition function therefore have to be cancelled. In 1988 Popov and Fedotov proposed a method to cancel out the contribution of these states (see [82]) which we will make use of here.

The original goal of Popov and Fedotov was to describe Spin-Hamiltonians in a way such that one could make use of the usual path integral method when computing the partition function, and such that the diagrammatical techniques well known for fermionic systems could be applied. Let us consider a Hamiltonian being composed of localised spins with $S = \frac{1}{2}$ (have in mind a Heisenberg model for example). For spin Hamiltonians, there is no way to represent the partition function of the model as a fermionic or bosonic path integral, since spins are neither bosons nor fermions but angular momenta. However, it would be very convenient to be able to resort on such a representation as a path integral, for the diagrammatic techniques related to it are rather easy. Moreover, it is well known how to compute those integrals, if they are of Gaussian type. Therefore, it would be desirable to find a fermionic or bosonic representation of the spin operators. In the spin- $\frac{1}{2}$ case, the spins are described by Pauli matrices, which in fact can be represented as combinations of fermionic operators at each site j :

$$\sigma_j^z \rightarrow a_j^\dagger a_j - b_j^\dagger b_j, \quad (\text{A.5.2})$$

$$\sigma_j^+ \rightarrow a_j^\dagger b_j, \quad (\text{A.5.3})$$

$$\sigma_j^- \rightarrow b_j^\dagger a_j, \quad (\text{A.5.4})$$

or in short

$$\mathbf{S}_j \rightarrow (a_j^\dagger, b_j^\dagger) \cdot \vec{\sigma}_j \cdot \begin{pmatrix} a_j \\ b_j \end{pmatrix},$$

A Preliminary Considerations

where $\vec{\sigma}_j = (\sigma_j^x, \sigma_j^y, \sigma_j^z)^T$ is the vector composed of the Pauli matrices. a_j and b_j are fermionic operators, therefore fulfilling

$$\{a_j^\dagger, a_j\} = \{b_j^\dagger, b_j\} = 1.$$

All other possible anti-commutators vanish, including those taken on different sites. Let H_σ denote the original spin Hamiltonian. The above mappings then transform this Hamiltonian into a Hamiltonian H_F which is composed of fermionic operators. One can easily show by direct computation that the definitions (A.5.2) - (A.5.3) fulfill the commutation relations of the spin operators

$$[\sigma^+, \sigma^-] = \sigma^z, [\sigma^z, \sigma^+] = 2\sigma^+ \quad \text{and} \quad [\sigma^z, \sigma^-] = -2\sigma^-,$$

and one can show that these definitions also are in accordance to the requirement that spin operators at different sites commute. Therefore, the mappings (A.5.2) - (A.5.3) in fact give rise to a representation of the spin operators, up to their domain of definition. And this is, where a crucial problem arises: the dimensionality of the Pauli spin matrices is 2 while the fermionic space corresponding to the j -th site is four-dimensional, being generated by the vectors

$$a_j^\dagger \Phi_0 = |1, 0\rangle, \quad b_j^\dagger \Phi_0 = |0, 1\rangle, \quad \Phi_0 = |0, 0\rangle \quad \text{and} \quad a_j^\dagger b_j^\dagger \Phi_0 = |1, 1\rangle,$$

where Φ_0 is the vacuum. We call the subspace spanned by $|1, 0\rangle$ and $|0, 1\rangle$ the *space of physical states*. This is reasonable since

$$(a_j^\dagger a_j - b_j^\dagger b_j)|1, 0\rangle = |1, 0\rangle \quad \text{and} \quad (a_j^\dagger a_j - b_j^\dagger b_j)|0, 1\rangle = -|0, 1\rangle$$

as well as

$$a_j^\dagger b_j|0, 1\rangle = |1, 0\rangle \quad \text{and} \quad b_j^\dagger a_j|1, 0\rangle = |0, 1\rangle,$$

so the relations

$$\sigma^z \psi_+ = \psi_+, \quad \sigma^z \psi_- = -\psi_-, \quad \sigma^+ \psi_- = \psi_+, \quad \sigma^- \psi_+ = \psi_-$$

are reproduced. Because of the relations

$$(a_j^\dagger a_j - b_j^\dagger b_j)|1, 1\rangle = |1, 1\rangle - |1, 1\rangle = 0, \quad (a_j^\dagger a_j - b_j^\dagger b_j)|0, 0\rangle = 0$$

and

$$a_j^\dagger b_j|1, 1\rangle = 0, \quad a_j^\dagger b_j|0, 0\rangle = 0, \quad b_j^\dagger a_j|1, 1\rangle = 0, \quad b_j^\dagger a_j|0, 0\rangle = 0,$$

the spin operators vanish on the unphysical subspace. The physical subspace is given by all states Φ which fulfill $N_j \Phi = \Phi$, where $N_j = a_j^\dagger a_j + b_j^\dagger b_j$ is the fermionic number operator on the j -th site. For the physical states, each site is only singly occupied, therefore giving rise to a non-vanishing spin- $\frac{1}{2}$. Obviously, H_F is not the same as H_σ , since its domain is larger than that of the original spin Hamiltonian, additionally containing the unphysical states. Instead, it is the restriction of H_F to the direct product of the physical subspaces at all different sites which coincides with H_σ .

The quantity of interest, if one wants to characterise a system in statistical physics, is the partition function. For the original problem, it is given as

$$Z_\sigma = \text{Tr} e^{-\beta H_\sigma}. \tag{A.5.5}$$

However, if we simply computed the partition function as

$$Z = \text{Tr} e^{-\beta H_F},$$

A Preliminary Considerations

it would not coincide with (A.5.5) because taking the trace would involve summing over the unphysical states as well as the physical ones. One would take into account states, which the system simply cannot be in. Popov and Fedotov proposed a solution to this problem which still allows to use the fermionic version of the Hamiltonian for computing the partition function. They stated that in case of spin- $\frac{1}{2}$ Hamiltonians, it holds

$$Z_\sigma = \text{Tr} \exp(-\beta H_\sigma) = i^M \text{Tr} \exp\left(-\beta \left[H_F + \frac{i\pi}{2\beta} N_F \right]\right). \quad (\text{A.5.6})$$

Here M is the number of sites and

$$N_F = \sum_{j=1}^M N_j = \sum_{j=1}^M (a_j^\dagger a_j + b_j^\dagger b_j)$$

is the total occupation number. The term involving the purely imaginary chemical potential

$$\mu = -\frac{i\pi}{2\beta}$$

is introduced to cancel the contributions of the unphysical states to the trace. We will give a short justification of (A.5.6) in the following. To this end we decompose $H_F = (H_F)_j + (H_F)'_j$ and $N_F = N_j + (N_F)'_j$ where $(H_F)_j$ and N_j are the Hamiltonian and the number operator for the j -th site and the primed operators are those for all other sites. For the unphysical states at the j -th site it is

$$\text{Tr}_{j, \text{unphys.}} \exp\left(-\beta \left[H_F + \frac{i\pi}{2\beta} N_F \right]\right) = \exp(O'_j) \text{Tr}_{j, \text{unphys.}} \exp\left(-\beta \left[(H_F)_j + \frac{i\pi}{2\beta} N_j \right]\right),$$

with

$$O'_j = -\beta \left[(H_F)'_j + \frac{i\pi}{2\beta} (N_F)'_j \right].$$

Since H_σ is composed only of σ^z, σ^+ and σ^- , $(H_F)_j$ vanishes on the unphysical states (see calculations above). It is $N_j|0, 0\rangle = 0$ and $N_j|1, 1\rangle = 2|1, 1\rangle$. Hence

$$\text{Tr}_{j, \text{unphys.}} \exp\left(-\beta \left[H_F + \frac{i\pi}{2\beta} N_F \right]\right) = \exp(O'_j) (e^0 + e^{-i\pi}) = 0.$$

The contributions of the unphysical states to the trace vanish. On the physical states, H_F and H_σ coincide and $N_F \Phi_j = M \Phi_j$, since $N_j \Phi_j = \Phi_j$. Hence, we get

$$\begin{aligned} \text{Tr} \exp\left(-\beta \left[H_F + \frac{i\pi}{2\beta} N_F \right]\right) &= e^{-\frac{i\pi}{2} M} \text{Tr}_{\text{phys.}} \exp(-\beta H_F) \\ &= (-i)^M \text{Tr}_{\text{phys.}} \exp(-\beta H_F) \\ &= (-i)^M \text{Tr} \exp(-\beta H_\sigma). \end{aligned}$$

This proves (A.5.6). The usefulness of this equation is, that its left hand side can be computed like a usual fermionic path integral.

How can we make use of this method in the present system of a magnetic cluster on a metallic surface? We did not start with a pure spin Hamiltonian in the first place, but nevertheless, the

A Preliminary Considerations

technique presented here is applicable to our problem. As we have outlined, equation (A.5.6) gives a possibility to incorporate the boundary condition of each impurity site being singly occupied into the computation of the partition function as long as the Hamiltonian vanishes on the unphysical states (which correspond to doubly occupied or empty cluster sites). This is the case for our model Hamiltonian (A.5.1). Or we could look at the Hamiltonian in another way. As we have shown in appendix A.4, the Anderson Hamiltonian after the Schrieffer-Wolff transformation (when neglecting the free term for the cluster sites and for large Hubbard interaction) becomes

$$H_\sigma = \sum_{\mathbf{k}\sigma} \varepsilon_{\mathbf{k}} N_{\mathbf{k}\sigma} + N \cdot J \sum_{\substack{\mathbf{k}\mathbf{k}' \\ \sigma\sigma'}}^N \sum_{i=1}^3 \sum_{\nu=1}^3 \mathbf{S}_i^\nu \cdot \left[\overline{t_{i\mathbf{k}}} a_{\mathbf{k}\sigma}^\dagger \sigma_{\sigma\sigma'}^\nu t_{i\mathbf{k}'} a_{\mathbf{k}'\sigma'} \right].$$

Here, we already included the condition of each impurity being singly occupied which leads to non-vanishing spin- $\frac{1}{2}$ at each site. Concerning the localised degrees of freedom, this Hamiltonian is in fact a spin Hamiltonian and equation (A.5.6) can be applied to compute the partial trace on the localised states. Instead of computing

$$\text{Tr} e^{-\beta H_\sigma},$$

the partition function of the system is given as

$$Z = i^N \cdot \text{Tr} \exp \left(-\beta \left[H - \mu \sum_{j\sigma} n_{j\sigma} \right] \right) \quad (\text{A.5.7})$$

with H given as in (A.5.1) and with the purely imaginary chemical potential

$$\mu = -\frac{i\pi}{2\beta}.$$

Equation (A.5.7) is the proper partition function of the system, since it already complies to the boundary conditions, but it still can be calculated in terms of a fermionic path integral.

The method of Popov and Fedotov can be generalised to spin Hamiltonians for arbitrary spins (which was done by Veits et al. in 1993, see [84]) and even to general $SU(N)$ Hamiltonians with arbitrary occupation numbers (see [85]). The latter generalisation would be made use of if one considered a cluster of N impurities with a total occupation other than N . For example, one could alter the present system of a magnetic trimer of three spin- $\frac{1}{2}$ to one with two or less electrons in the cluster. The formula for computing the partition function of the system then gets more complicated but it still can be computed as a fermionic path integral.

B General calculations for a cluster of N atoms

B.1 Hubbard-Stratonovich transformation

We perform the calculations for section (4.1) in more detail. After the Schrieffer-Wolff transformation, the interaction of the cluster electrons with the substrate is given as

$$H_I = N J' \sum_{i=1}^N \sum_{\nu=1}^3 \left(\Phi_i^\dagger \sigma^\nu \Phi_i \right) \left(\hat{\Psi}_i^\dagger(0) \sigma^\nu \hat{\Psi}_i(0) \right).$$

Here, $\phi_{i\alpha} = c_{i\alpha}$ are the construction operators of the cluster fermions and $\psi_{i\alpha}(\mathbf{k}) = t_{i\mathbf{k}} a_{\mathbf{k}\alpha}$ are combinations of construction operators for the itinerant electrons and the tunnelling amplitude. It is

$$\sum_{\mathbf{k}} \psi_{i\alpha}(\mathbf{k}) = \hat{\psi}_{i\alpha}(0)$$

and the capital Greek Φ_i and Ψ_i are vectors composed of the $\phi_{i\alpha}$ and $\psi_{i\alpha}$. H_I is part of the action and for each imaginary time τ gives rise to a term

$$e^{-H_I^\tau(\bar{\Phi}^\tau, \Phi^\tau, \bar{\Psi}^\tau, \Psi^\tau)}$$

where all fermionic operators are replaced by their respective Grassman numbers. For the sake of simplicity, we omit the τ -dependence in the following but keep it in mind. Moreover, we omit the coordinate dependence for the $\hat{\Psi}_i$ simply writing $\hat{\psi}_{i\alpha}(0) \equiv \hat{\psi}_{i\alpha}$.

The Hubbard-Stratonovich transformation essentially is a completion of the square (see [87]). We define the matrix A by

$$A_{\alpha\beta', \alpha'\beta} = \sum_{\nu=1}^3 \sigma_{\alpha\alpha'}^\nu \sigma_{\beta\beta'}^\nu$$

(one can think of the combinations $\alpha\beta'$ and $\alpha'\beta$ as single indices) and write down the product of Gaussian integrals

$$(C'')^{-1} = \prod_{i=1}^N \int d\chi^i \exp \left\{ - \sum_{\alpha\beta', \alpha'\beta} \chi_{\alpha\beta'}^i A_{\alpha\beta', \alpha'\beta} \chi_{\alpha'\beta}^i \right\}$$

with complex valued χ^i and some constant C'' (essentially the N th power of the determinant of A). For each i we perform a transformation of the integration variable defining

$$\chi_{\alpha'\beta}^i = \frac{1}{\sqrt{NJ'}} Q_{\alpha'\beta}^i + \sqrt{NJ'} \bar{\psi}_{i\beta} \phi_{i\alpha'}. \quad (\text{B.1.1})$$

Here, Q is the new variable on integration and ψ and ϕ are Grassman numbers, their product being complex valued. Overlining denotes the adjoint Grassman number, not complex conjugation. The complex conjugate of χ^i is given as

$$\chi_{\alpha\beta'}^{i*} = \frac{1}{\sqrt{NJ'}} Q_{\alpha\beta'}^{i*} + \sqrt{NJ'} \bar{\phi}_{i\alpha} \hat{\psi}_{i\beta'},$$

B General calculations for a cluster of N atoms

since the usual definition of the complex conjugate of a product of Grassman number is

$$(\bar{a}b)^* = \bar{b}a.$$

The $Q_{\alpha'\beta}^i$ define (hermitian) 2×2 -matrices \underline{Q}^i . Using the transformation (B.1.1) we get

$$\begin{aligned} (C')^{-1} &= \prod_{i=1}^N \int d\underline{Q}^i \exp \left\{ - \sum_{\alpha'\beta\alpha'\beta'} \left[\frac{1}{\sqrt{NJ'}} Q_{\alpha'\beta}^{i*} + \sqrt{NJ'} \bar{\phi}_{i\alpha} \hat{\psi}_{i\beta'} \right] A_{\alpha'\beta, \alpha'\beta} \left[\frac{1}{\sqrt{NJ'}} Q_{\alpha'\beta}^i + \sqrt{NJ'} \bar{\psi}_{i\beta} \phi_{i\alpha'} \right] \right\} \\ &= e^{-NJ' \sum_{i=1}^N \sum_{\alpha'\beta\beta'} \bar{\phi}_{i\alpha} \hat{\psi}_{i\beta'} A_{\alpha'\beta, \alpha'\beta} \bar{\psi}_{i\beta} \phi_{i\alpha'}} \prod_{i=1}^N \int d\underline{Q}^i \exp \left\{ - \frac{1}{NJ'} \sum_{\alpha'\beta\beta'} Q_{\alpha'\beta}^{i*} A_{\alpha'\beta, \alpha'\beta} Q_{\alpha'\beta}^i \right. \\ &\quad \left. - \sum_{\alpha'\beta\beta'} Q_{\alpha'\beta}^{i*} A_{\alpha'\beta, \alpha'\beta} \bar{\psi}_{i\beta} \phi_{i\alpha'} - \sum_{\alpha'\beta\beta'} \bar{\phi}_{i\alpha} \hat{\psi}_{i\beta'} A_{\alpha'\beta, \alpha'\beta} Q_{\alpha'\beta}^i \right\}. \end{aligned}$$

Using the definition of A , it is

$$\begin{aligned} -NJ' \sum_{i=1}^N \sum_{\alpha'\beta\beta'} \bar{\phi}_{i\alpha} \hat{\psi}_{i\beta'} A_{\alpha'\beta, \alpha'\beta} \bar{\psi}_{i\beta} \phi_{i\alpha'} &= NJ' \sum_{i=1}^N \sum_{\nu=1}^3 \sum_{\alpha'\beta\beta'} \bar{\phi}_{i\alpha} \sigma_{\alpha\alpha'}^\nu \phi_{i\alpha'} \bar{\psi}_{i\beta} \sigma_{\beta\beta'}^\nu \hat{\psi}_{i\beta'} \\ &= NJ' \sum_{i=1}^N \sum_{\nu=1}^3 (\bar{\Phi}_i \sigma^\nu \Phi_i) \left(\bar{\Psi}_i(0) \sigma^\nu \hat{\Psi}_i(0) \right) \\ &= H_I(\bar{\Phi}, \Phi, \bar{\Psi}, \hat{\Psi}). \end{aligned}$$

The change of sign is due to Grassman multiplication. Hence, we can write

$$\begin{aligned} e^{-H_I(\bar{\Phi}, \Phi, \bar{\Psi}, \hat{\Psi})} &= C' \prod_{i=1}^N \int d\underline{Q}^i \exp \left\{ - \frac{1}{NJ'} \sum_{\nu=1}^3 \sum_{\substack{\alpha\alpha' \\ \beta\beta'}} Q_{\alpha\beta}^{i*} \sigma_{\alpha\alpha'}^\nu \sigma_{\beta\beta'}^\nu Q_{\alpha'\beta}^i \right. \\ &\quad \left. - \sum_{\nu=1}^3 \sum_{\substack{\alpha\alpha' \\ \beta\beta'}} Q_{\alpha\beta}^{i*} \sigma_{\alpha\alpha'}^\nu \sigma_{\beta\beta'}^\nu \bar{\psi}_{i\beta} \phi_{i\alpha'} - \sum_{\nu=1}^3 \sum_{\substack{\alpha\alpha' \\ \beta\beta'}} \bar{\phi}_{i\alpha} \hat{\psi}_{i\beta'} \sigma_{\alpha\alpha'}^\nu \sigma_{\beta\beta'}^\nu Q_{\alpha'\beta}^i \right\}. \quad (\text{B.1.2}) \end{aligned}$$

Being a hermitian 2×2 -matrix, \underline{Q}^i can be represented as

$$\underline{Q}^i = \sum_{\mu} q_{\mu}^i \sigma^{\mu} \quad (\text{B.1.3})$$

with real-valued q_{μ}^i and $\mu = 0 \dots 3$. For the remainder of the section, we stick to the following notation: if no lower and upper summation limits are given, the sum is performed over full range

B General calculations for a cluster of N atoms

(i.e. $\mu = 0 \dots 3$ rather than $\mu = 1 \dots 3$). Using (B.1.3) we compute

$$\begin{aligned}
(i) &= -\frac{1}{NJ'} \sum_{\substack{\alpha\alpha' \\ \beta\beta'}} \sum_{\mu\mu'} \sum_{\nu=1}^3 q_\mu^i (\sigma^\mu)_{\alpha\beta'}^* \sigma_{\alpha\alpha'}^\nu \sigma_{\beta\beta'}^\nu q_{\mu'}^i \sigma_{\alpha'\beta}^{\mu'} \\
&= -\frac{1}{NJ'} \sum_{\substack{\alpha\alpha' \\ \beta\beta'}} \sum_{\mu\mu'} \sum_{\nu=1}^3 q_\mu^i q_{\mu'}^i \sigma_{\beta'\alpha}^\mu \sigma_{\alpha\alpha'}^\nu \sigma_{\alpha'\beta}^{\mu'} \sigma_{\beta\beta'}^\nu \\
&= -\frac{1}{NJ'} \sum_{\mu\mu'} \sum_{\nu=1}^3 q_\mu^i q_{\mu'}^i \text{Tr} \sigma^\mu \sigma^\nu \sigma^{\mu'} \sigma^\nu \\
&= -\frac{1}{NJ'} \sum_{\mu\mu'} q_\mu^i q_{\mu'}^i \text{Tr} \sigma^\mu \sigma^\nu \sigma^{\mu'} \sigma^\nu + \frac{1}{2} \frac{1}{NJ'} \sum_{\mu\mu'} q_\mu^i q_{\mu'}^i \text{Tr} \sigma^\mu \sigma^{\mu'},
\end{aligned}$$

using $\sigma^0 = 1/\sqrt{2}\mathbb{1}_2$,

$$= -\frac{1}{NJ'} \sum_{\mu\mu'} q_\mu^i q_{\mu'}^i 2 \cdot \delta_{0\mu'} \text{Tr} \sigma^\mu \sigma^0 + \frac{1}{2} \frac{1}{NJ'} \sum_{\mu} (q_\mu^i)^2,$$

where we used the $SU(N)$ properties (A.2.6) and (A.2.8),

$$= \frac{1}{2} \frac{1}{NJ'} \sum_{\mu} (q_\mu^i)^2 - \frac{2}{NJ'} (q_0^i)^2.$$

(B.1.4)

Quite analogously and using the same theorems for $SU(N)$ generators, we compute

$$\begin{aligned}
(ii) &= -\sum_{\mu} \sum_{\nu=1}^3 q_\mu^i \bar{\psi}_{i\beta} (\sigma^\nu \sigma^\mu \sigma^\nu)_{\beta\alpha'} \phi_{i\alpha'} \\
&= -\sum_{\mu\nu} q_\mu^i \bar{\psi}_{i\beta} (\sigma^\nu \sigma^\mu \sigma^\nu)_{\beta\alpha'} \phi_{i\alpha'} + \frac{1}{2} \sum_{\mu} q_\mu^i \bar{\psi}_{i\beta} \sigma_{\beta\alpha'}^\mu \phi_{i\alpha'} \\
&= \bar{\Psi}_i(0) \left[\frac{1}{2} \underline{\mathbf{Q}}^i - 2q_0^i \sigma^0 \right] \Phi_i \\
&= \sum_{\mathbf{k}} \bar{\Psi}_i(\mathbf{k}) \left[\frac{1}{2} \underline{\mathbf{Q}}^i - 2q_0^i \sigma^0 \right] \Phi_i
\end{aligned}$$

(B.1.5)

(where we used $\sum_{\mathbf{k}} \psi_{i\sigma}(\mathbf{k}) = \hat{\psi}_{i\sigma}(0)$) and

$$(iii) = \sum_{\mathbf{k}} \bar{\Phi}_i \left[\frac{1}{2} \underline{\mathbf{Q}}^i - 2q_0^i \sigma^0 \right] \Psi_i(\mathbf{k}).$$

(B.1.6)

In the static mean field approximation, the $\underline{\mathbf{Q}}^i$ are all fixed to certain time independent values and so are not integrated over anymore in equation (B.1.2). Moreover, we assume that the spin does not prefer any specific direction. Hence, we adopt the form

$$\underline{\mathbf{Q}}^i = b_i \mathbb{1}_2 = q_0^i \sigma^0,$$

B General calculations for a cluster of N atoms

where b_i is real valued. Putting this in (B.1.4) - (B.1.6), we get

$$(i) = -\frac{3}{NJ'} b_i^2, \quad (ii) = -\frac{3}{2} b_i \sum_{\mathbf{k}} \bar{\Psi}_i(\mathbf{k}) \cdot \Phi_i \quad \text{and} \quad (iii) = -\frac{3}{2} b_i \sum_{\mathbf{k}} \bar{\Phi}_i \cdot \Psi_i(\mathbf{k}).$$

We absorb the factor $3/2$ into the b_i and redefine

$$J = \frac{3}{4} J'.$$

Then

$$(i) = -\frac{1}{NJ} b_i^2, \quad (ii) = -b_i \sum_{\mathbf{k}} \bar{\Psi}_i(\mathbf{k}) \cdot \Phi_i \quad \text{and} \quad (iii) = -b_i \sum_{\mathbf{k}} \bar{\Phi}_i \cdot \Psi_i(\mathbf{k}).$$

To simplify the notation a bit and to get rid of the orbital index i , we define the $N \times N$ - matrix

$$\underline{b} = \text{diag}(b_i | i = 1 \dots N)$$

and the vectors

$$\Psi(\mathbf{k}) = (\Psi_i(\mathbf{k}) | i = 1 \dots N)^T \quad \text{and} \quad \Phi = (\Phi_i | i = 1 \dots N)^T.$$

Using this definitions equation, (B.1.2) in the static mean field approach becomes

$$e^{-H_I(\bar{\Phi}^\tau, \Phi^\tau, \bar{\Psi}^\tau, \Psi^\tau)} = C' \exp \left\{ -\frac{1}{NJ} \text{Tr} \underline{b}^2 - \sum_{\mathbf{k}} \bar{\Psi}^\tau(\mathbf{k}) [\underline{b} \otimes \mathbb{1}_2] \Phi^\tau - \bar{\Phi}^\tau [\underline{b} \otimes \mathbb{1}_2] \Psi^\tau(\mathbf{k}) \right\}.$$

B.2 Partition function in mean field theory

In this section we are going to perform the calculations which yield the partition function in detail. We compute the partition function by means of a fermionic path integral. For the theory of path integrals see [90].

The partition function in mean field is given as

$$Z_{MF} = \int [D\bar{a}^\tau][Da^\tau][D\bar{\Phi}^\tau][D\Phi^\tau] \exp(-S(\bar{a}^\tau, a^\tau, \bar{\Phi}^\tau, \Phi^\tau))$$

with S being the action of the model. In the system under consideration we use the Popov-Fedotov method of imaginary chemical potentials to deal with the unphysical states arising from treating the localised spin degrees of freedom as ordinary fermions. For singly occupied cluster sites, this means we have to introduce an additional term in the action which has the form

$$\frac{i\pi}{2\beta} \bar{\Phi}^\tau \cdot \Phi^\tau.$$

The action is thus given as

$$S = \int_0^\beta d\tau \left\{ \sum_{\mathbf{k}} \bar{a}_{\mathbf{k}}^\tau \partial_\tau \mathbb{1}_2 a_{\mathbf{k}}^\tau + \bar{\Phi}^\tau \left(\partial_\tau + \frac{i\pi}{2\beta} \right) \mathbb{1}_{2N} \Phi^\tau + H_0^\tau + H_I^\tau \right\}$$

As stated in the introduction, the only term left in H_0^τ is the term describing the free substrate electrons. $\exp(-H_I^\tau)$ was Hubbard-Stratonovich transformed with the auxiliary fields being

B General calculations for a cluster of N atoms

fixed in the static mean field approach. For actual calculations, it is more convenient to use the Fourier transformed form of the action, depending on the Matsubara frequencies ω_n instead of imaginary time. In order to keep notation simple, we define the free electronic Green's function $G_{i\omega_n}(\mathbf{k})$ by

$$G_{i\omega_n}^{-1}(\mathbf{k}) = i\omega_n - \varepsilon_{\mathbf{k}} \quad (\text{B.2.1})$$

and its cluster pendant $D_{i\omega_n}$ by

$$D_{i\omega_n}^{-1} = i\omega_n - \frac{i\pi}{2\beta}. \quad (\text{B.2.2})$$

Then finally, the Fourier transformed action is given as

$$S = \frac{\beta}{NJ} \sum_i b_i^2 - \sum_{i\omega_n} \left\{ \sum_{\mathbf{k}} \bar{a}_{\mathbf{k}}^{i\omega_n} G_{i\omega_n}^{-1}(\mathbf{k}) \mathbb{1}_2 a_{\mathbf{k}}^{i\omega_n} + \bar{\Phi}^{i\omega_n} D_{i\omega_n}^{-1} \mathbb{1}_{2N} \Phi^{i\omega_n} - \sum_{\mathbf{k}} (t_{\mathbf{k}}^\dagger \otimes \bar{a}_{\mathbf{k}}^{i\omega_n})(\underline{\mathbf{b}} \otimes \mathbb{1}_2) \Phi^{i\omega_n} - \sum_{\mathbf{k}} \bar{\Phi}^{i\omega_n} (\underline{\mathbf{b}} \otimes \mathbb{1}_2) (t_{\mathbf{k}} \otimes a_{\mathbf{k}}^{i\omega_n}) \right\}. \quad (\text{B.2.3})$$

The frequency depending part of the action can be rewritten in a more convenient form. To this end, we combine the vectors $\Phi^{i\omega_n}$ and $a_{\mathbf{k}}^{i\omega_n}$ for all \mathbf{k} into a single vector $\chi^{i\omega_n}$ defined by

$$\chi^{i\omega_n} = \left(\phi_{1\uparrow}^{i\omega_n}, \phi_{1\downarrow}^{i\omega_n}, \dots, \phi_{N\uparrow}^{i\omega_n}, \phi_{N\downarrow}^{i\omega_n}, \{a_{\mathbf{k}\uparrow}^{i\omega_n}, a_{\mathbf{k}\downarrow}^{i\omega_n} | \mathbf{k}\} \right)^T. \quad (\text{B.2.4})$$

The action then reads

$$S = \frac{\beta}{NJ} \sum_i b_i^2 - \sum_{i\omega_n} \bar{\chi}^{i\omega_n} \cdot (\underline{\mathbf{M}}_{i\omega_n} \otimes \mathbb{1}_2) \cdot \chi^{i\omega_n} \quad (\text{B.2.5})$$

with an operator $\underline{\mathbf{M}}_{i\omega_n}$ defined by the matrix product. $\underline{\mathbf{M}}_{i\omega_n}$ can be written as a matrix if we assume the wave vectors to be discrete. Of course, a continuous limit is meant, but we can perform all computation using the discrete form of $\underline{\mathbf{M}}_{i\omega_n}$ and perform the continuum limit for the wave vectors afterwards. In the discrete form, the matrix looks like

$$\underline{\mathbf{M}}_{i\omega_n} = \left(\begin{array}{ccc|ccc} & & & -(bt_{\mathbf{k}_1})_1 & \cdots & -(bt_{\mathbf{k}_1})_N \\ & & & -(bt_{\mathbf{k}_2})_1 & \cdots & -(bt_{\mathbf{k}_2})_N \\ & & & \vdots & \vdots & \vdots \\ \hline & & D_{i\omega_n}^{-1} \mathbb{1}_N & & & \\ \hline -(t_{\mathbf{k}_1}^\dagger \underline{\mathbf{b}})_1 & -(t_{\mathbf{k}_2}^\dagger \underline{\mathbf{b}})_1 & \cdots & & & \\ \vdots & \vdots & \vdots & & & \\ -(t_{\mathbf{k}_1}^\dagger \underline{\mathbf{b}})_N & -(t_{\mathbf{k}_2}^\dagger \underline{\mathbf{b}})_N & \cdots & & & \text{diag}(G_{i\omega_n}^{-1}(\mathbf{k}) | \mathbf{k}) \end{array} \right). \quad (\text{B.2.6})$$

As already stated, a continuous limit for the wave vectors is meant. Using this definitions the partition function in mean field is given as

$$\begin{aligned} Z_{MF} &= C e^{-\frac{\beta}{NJ} \sum_i b_i^2} \int [D\bar{\chi}] [D\chi] \exp \left[- \sum_{i\omega_n} \bar{\chi}^{i\omega_n} \cdot (-\underline{\mathbf{M}}_{i\omega_n} \otimes \mathbb{1}_2) \cdot \chi^{i\omega_n} \right] \\ &= C e^{-\frac{\beta}{NJ} \sum_i b_i^2} \prod_{i\omega_n} (\det \underline{\mathbf{M}}_{i\omega_n})^2, \end{aligned} \quad (\text{B.2.7})$$

B General calculations for a cluster of N atoms

where we used

$$\det(A \otimes B) = (\det A)^{\dim B} \cdot (\det B)^{\dim A}.$$

In order to compute the partition function, we have to calculate the determinant of $\underline{M}_{i\omega_n}$. Keeping in mind that $\underline{M}_{i\omega_n}$ is rather an operator than a matrix, its determinant is defined as

$$\det \underline{M}_{i\omega_n} = \exp \text{Tr} \log \underline{M}_{i\omega_n}.$$

As stated in section A.1 in equation (A.1.4), this expression becomes easier for block trigonal matrices. Since the determinant is invariant with respect to unitary transformations, so is the above formula. We therefore define an operator $\tilde{\underline{M}}_{i\omega_n}$ which is a unitary transform of $\underline{M}_{i\omega_n}$ and fulfills

$$\det \underline{M}_{i\omega_n} = \det \tilde{\underline{M}}_{i\omega_n} = \exp \text{Tr} \log \tilde{\underline{M}}_{i\omega_n}.$$

The goal of the unitary transformation is to get rid of the upper right block matrix in (B.2.6). To this end, one adds to the n -th row of the matrix (where $n = 1 \dots N$)

$$(\underline{b} t_{\mathbf{k}_m})_n \cdot G_{i\omega_n}(\mathbf{k}_m) \quad \times \quad \text{the } k_m\text{-th row}$$

for all possible \mathbf{k}_m (here, we assumed discrete wave vectors, still a continuous limit is meant). If one does so for the first N rows, the resulting transformed matrix is given as

$$\tilde{\underline{M}}_{i\omega_n} = \left(\begin{array}{c|c} \hat{\underline{X}}_{i\omega_n} & 0 \\ \hline \underline{A}^\dagger & \text{diag}(G_{i\omega_n}^{-1}(\mathbf{k})|\mathbf{k}) \end{array} \right), \quad (\text{B.2.8})$$

where \underline{A}^\dagger is the lower left block matrix in (B.2.6) and where $\hat{\underline{X}}_{i\omega_n}$ is defined by

$$\left(\hat{\underline{X}}_{i\omega_n} \right)_{ij} = D_{i\omega_n}^{-1} \delta_{ij} - \sum_{\mathbf{k}_m} \left(t_{\mathbf{k}_m}^\dagger \underline{b} \right)_i (\underline{b} t_{\mathbf{k}_m})_j G_{i\omega_n}(\mathbf{k}_m). \quad (\text{B.2.9})$$

We perform the continuum limit for the wave vectors in (B.2.9) by replacing the summation over all \mathbf{k}_m by a summation over all wave vectors. Using (A.1.4) the determinant of $\underline{M}_{i\omega_n}$ is thus given as

$$\det \underline{M}_{i\omega_n} = \exp \text{Tr} \log \tilde{\underline{M}}_{i\omega_n} = \exp \left[\text{Tr} \log \text{diag}(G_{i\omega_n}^{-1}(\mathbf{k})|\mathbf{k}) + \text{Tr} \log \hat{\underline{X}}_{i\omega_n} \right].$$

We write down a more explicit form for the matrix $\hat{\underline{X}}_{i\omega_n}$. To this end, we recall the form of $t_{\mathbf{k}}$

$$(t_{\mathbf{k}})_i = t_{i\mathbf{k}} = \frac{1}{\sqrt{N}} e^{-i\mathbf{R}_i \cdot \mathbf{k}}$$

and

$$(\underline{b})_{ij} = b_i \delta_{ij}.$$

Thus,

$$\left(\hat{\underline{X}}_{i\omega_n} \right)_{ij} = D_{i\omega_n}^{-1} \delta_{ij} - b_i \left(\frac{1}{N} \sum_{\mathbf{k}} \frac{e^{i(\mathbf{R}_i - \mathbf{R}_j) \cdot \mathbf{k}}}{i\omega_n - \varepsilon_{\mathbf{k}}} \right) b_j. \quad (\text{B.2.10})$$

B General calculations for a cluster of N atoms

The term in brackets on the right hand side of (B.2.10) defines the entries of a matrix $\tilde{\mathbf{g}}(i\omega_n)$. Using some approximations, we will now compute those entries formally for a two-dimensional substrate to derive a general form of $\tilde{\mathbf{g}}(i\omega_n)$, starting with the diagonal elements. For $i = j$ it is

$$\begin{aligned} [\tilde{\mathbf{g}}(i\omega_n)]_{ii} &= \frac{1}{N} \sum_{\mathbf{k}} \frac{1}{i\omega_n - \varepsilon_{\mathbf{k}}} \\ &= -\frac{1}{N} \frac{1}{2\pi} \int d^2k \frac{1}{\varepsilon_{\mathbf{k}} - i\omega_n} \\ &= -\frac{1}{N} \frac{1}{2\pi} \int_0^{2\pi} d\varphi \int_{-\frac{\Delta}{2}}^{\frac{\Delta}{2}} d\varepsilon \rho(\varepsilon) \frac{1}{\varepsilon - i\omega_n}. \end{aligned}$$

Here, Δ is the bandwidth and $\rho(\varepsilon)$ is the energy density in the unperturbed substrate. We assume a flat and broad band, so that we can approximate $\rho(\varepsilon) = \rho_0$ with the Fermi density ρ_0 and $\Delta \rightarrow \infty$. So

$$\begin{aligned} [\tilde{\mathbf{g}}(i\omega_n)]_{ii} &= -\frac{\rho_0}{N} \int d\varepsilon \frac{1}{\varepsilon - i\omega_n} \\ &= -\frac{\rho_0}{N} \left(\int d\varepsilon \frac{\varepsilon}{\varepsilon^2 + \omega_n^2} + \int d\varepsilon \frac{i\omega_n}{\varepsilon^2 + \omega_n^2} \right) \\ &= -\frac{\rho_0}{N} i\omega_n \int d\varepsilon \frac{1}{(\varepsilon - i\omega_n)(\varepsilon + i\omega_n)}, \end{aligned}$$

where we used that $\varepsilon/(\varepsilon^2 + \omega_n^2)$ is antisymmetric,

$$\begin{aligned} &= -\frac{\rho_0}{N} i\omega_n 2\pi i \operatorname{sgn}(\omega_n) \frac{1}{2i\omega_n} \\ &= -i\pi \operatorname{sgn}(\omega_n) \frac{\rho_0}{N} \\ &= -i\pi \operatorname{sgn}(\omega_n) g_0, \end{aligned}$$

where we used the residue theorem and where we defined $g_0 = \rho_0/N$. We will come now to the off-diagonal elements. It is

$$\begin{aligned} [\tilde{\mathbf{g}}(i\omega_n)]_{ij} &= \frac{1}{N} \sum_{\mathbf{k}} \frac{e^{i(\mathbf{R}_i - \mathbf{R}_j)\mathbf{k}}}{i\omega_n - \varepsilon_{\mathbf{k}}} \\ &= -\frac{1}{N} \frac{1}{2\pi} \int d^2k \frac{e^{i(\mathbf{R}_i - \mathbf{R}_j)\mathbf{k}}}{\varepsilon_{\mathbf{k}} - i\omega_n} \\ &= -\frac{1}{N} \frac{1}{2\pi} \int_0^{2\pi} d\varphi \int_{-\frac{\Delta}{2}}^{\frac{\Delta}{2}} d\varepsilon \rho(\varepsilon) \frac{e^{i|\mathbf{R}_i - \mathbf{R}_j|k_\varepsilon \cos(\varphi)}}{\varepsilon - i\omega_n} \\ &= -\frac{1}{N} \int_{-\frac{\Delta}{2}}^{\frac{\Delta}{2}} d\varepsilon \rho(\varepsilon) \frac{J_0(k_\varepsilon |\mathbf{R}_i - \mathbf{R}_j|)}{\varepsilon - i\omega_n}, \end{aligned}$$

where k_ε is the absolute value of the wave vector at energy ε , ϕ is the angle between the wave vector and $\mathbf{R}_i - \mathbf{R}_j$ and J_0 is the Bessel function defined by

$$J_0(z) = \frac{1}{2\pi} \int_0^{2\pi} d\varphi e^{iz \cos(\varphi)}.$$

B General calculations for a cluster of N atoms

In order to proceed, we make some very rough assumptions. $J_0(k_\varepsilon|\mathbf{R}_i - \mathbf{R}_j|)$ is assumed to be analytic in ε and very weakly depending on it, being approximately given everywhere by its value at the Fermi level. Since it is analytic, we can expand the function in the vicinity of the Fermi level as

$$J_0(k_\varepsilon|\mathbf{R}_i - \mathbf{R}_j|) = \sum_m a_m(\varepsilon_F) \varepsilon^m.$$

Moreover, we again assume $\rho(\varepsilon) \approx \rho_0$ and $\Delta \rightarrow \infty$. Then

$$\begin{aligned} [\tilde{\mathbf{g}}(i\omega_n)]_{ij} &= -\frac{\rho_0}{N} \sum_m a_m(\varepsilon_F) \int d\varepsilon \frac{\varepsilon^m}{\varepsilon - i\omega_n} \\ &= -\frac{\rho_0}{N} \sum_m a_m(\varepsilon_F) \left(\int d\varepsilon \frac{\varepsilon^{m+1}}{\varepsilon^2 + \omega_n^2} + i\omega_n \int d\varepsilon \frac{\varepsilon^m}{\varepsilon^2 + \omega_n^2} \right) \\ &= -\frac{\rho_0}{N} \sum_m a_m(\varepsilon_F) (I_m + J_m), \end{aligned}$$

where we defined the integrals I_m and J_m in the order of their appearance. We compute those integrals formally using the residue theorem. If m is even, the integrand of I_m is antisymmetric and therefore $I_m = 0$. If m is odd, one formally gets

$$\begin{aligned} I_m &= \int d\varepsilon \frac{\varepsilon^{m+1}}{(\varepsilon - i\omega_n)(\varepsilon + i\omega_n)} \\ &= 2\pi i \operatorname{sgn}(\omega_n) \frac{\operatorname{sgn}(\omega_n)^{m+1} (i\omega_n)^{m+1}}{2i\omega_n} \\ &= i\pi (i|\omega_n|)^m. \end{aligned}$$

We remark, that I_m is real-valued since m is odd. For odd m , the integrand of J_m is antisymmetric and the integral vanishes. For even m , it is

$$\begin{aligned} J_m &= i\omega_n \int d\varepsilon \frac{\varepsilon^m}{(\varepsilon_{i\omega_n})(\varepsilon + i\omega_n)} \\ &= i\omega_n 2\pi i \operatorname{sgn}(\omega_n) \frac{\operatorname{sgn}(\omega_n)^m i\omega_n^m}{2i\omega_n} \\ &= i\pi \operatorname{sgn}(\omega_n) (i|\omega_n|)^m. \end{aligned}$$

This is imaginary, since m is even. So formally

$$[\tilde{\mathbf{g}}(i\omega_n)]_{ij} = -i\pi \operatorname{sgn}(\omega_n) \frac{\rho_0}{N} \sum_m a_{2m}(\varepsilon_F) (i|\omega_n|)^{2m} - \pi \frac{\rho_0}{N} i \sum_m a_{2m+1}(\varepsilon_F) (i|\omega_n|)^{2m+1}.$$

$\sum_m a_{2m}(\varepsilon_F) (i|\omega_n|)^{2m}$ is the symmetric part of $J(k_\varepsilon|\mathbf{R}_i - \mathbf{R}_j|)$ which should only depend weakly on $i|\omega_n|$ so we write

$$\frac{\rho_0}{N} \sum_m a_{2m}(\varepsilon_F) (i|\omega_n|)^{2m} \approx g_{ij}^R$$

where g_{ij}^R is independent of ω_n . Analogously, we define

$$-i \frac{\rho_0}{N} \sum_m a_{2m+1}(\varepsilon_F) (i|\omega_n|)^{2m+1} \approx g_{ij}^I.$$

B General calculations for a cluster of N atoms

g_{ij}^R and g_{ij}^I are both real-valued and define the real symmetric matrices \mathbf{g}^R and \mathbf{g}^I . Using $[-i\text{sgn}(\omega_n)][i\text{sgn}(\omega_n)] = 1$, we get

$$\begin{aligned}\tilde{\mathbf{g}}(i\omega_n) &= -i\pi \text{sgn}(\omega_n) (\mathbf{g}^R + i \text{sgn}(\omega_n) \mathbf{g}^I) \\ &= -i\pi \text{sgn}(\omega_n) \mathbf{g}(i\omega_n),\end{aligned}\tag{B.2.11}$$

where we defined the matrix $\mathbf{g}(i\omega_n)$. We remark that the derivation of (B.2.11) given here is only formally correct, a "best of all worlds" approximation with many harsh assumptions involved. However, if one computes the occurring integrals numerically for a given band structure (for example truncated parabolic), the approximation of \mathbf{g}^R and \mathbf{g}^I to be independent of ω_n is very well fulfilled over several magnitudes of ω_n , and $\tilde{\mathbf{g}}(i\omega_n)$ has the structure given in (B.2.11). The approximations become the better, the higher the Fermi energy, the broader the band and the lower the temperature.

We show another property of the entries of $\mathbf{g}(i\omega_n)$. In a very rough approximation, it is $J_0(k_\varepsilon|\mathbf{R}_i - \mathbf{R}_j|) = J_0(k_F|\mathbf{R}_i - \mathbf{R}_j|)$. Then

$$\begin{aligned}\left| \int d\varepsilon \frac{J_0(k_\varepsilon|\mathbf{R}_i - \mathbf{R}_j|)}{\varepsilon - i\omega_n} \right| &= \left| \int d\varepsilon \frac{J_0(k_F|\mathbf{R}_i - \mathbf{R}_j|)}{\varepsilon - i\omega_n} \right| \\ &= |i\pi \text{sgn}(\omega_n) J_0(k_\varepsilon|\mathbf{R}_i - \mathbf{R}_j)| \\ &\leq \pi,\end{aligned}$$

since $|J_0(z)| \leq 1$ for real-valued z . Hence, it is

$$|g_{ij}^R| \leq g_0 \quad \text{and} \quad |g_{ij}^I| \leq g_0$$

for all i, j , and as mentioned earlier, $g_{ii}^R = g_0$ and $g_{ii}^I = 0$ for the diagonals. One final remark about the coordinate dependence of $\mathbf{g}(i\omega_n)$. In two dimensions, the most important contributions to the off-diagonal elements depend on the product $k_F|\mathbf{R}_i - \mathbf{R}_j|$ like Bessel functions. Since k_F is the inverse of the Fermi wavelength, this gives a natural length scale for the system. The distance of the impurities is measured as multiples of the Fermi wavelength. For large arguments z , Bessel functions decay like $\sqrt{2/\pi z} \cdot \cos(z - \pi/4)$ and so do the off-diagonal terms of $\mathbf{g}(i\omega_n)$.

Having computed $\tilde{\mathbf{g}}(i\omega_n)$, the matrix $\hat{\mathbf{X}}_{i\omega_n}$ takes the form

$$\hat{\mathbf{X}}_{i\omega_n} = D_{i\omega_n}^{-1} \mathbb{1}_n + i\pi \text{sgn}(\omega_n) \underline{\mathbf{b}} \mathbf{g}(i\omega_n) \underline{\mathbf{b}}.\tag{B.2.12}$$

With this form of the matrix $\hat{\mathbf{X}}_{i\omega_n}$ we can write the partition function (B.2.7) as

$$Z_{MF} = C e^{-\frac{\beta}{N} \sum_i b_i^2} \exp 2 \sum_{i\omega_n} \text{Tr} \log [D_{i\omega_n}^{-1} \mathbb{1}_n + i\pi \text{sgn}(\omega_n) \underline{\mathbf{b}} \mathbf{g}(i\omega_n) \underline{\mathbf{b}}],\tag{B.2.13}$$

where we absorbed the factor

$$e^{2 \sum_{i\omega_n} \sum_{\mathbf{k}} G_{i\omega_n}^{-1}(\mathbf{k})}$$

into the prefactor C . We can do so, because this term does not depend on b_i , and all quantities of interest will be derivatives of the logarithm of the partition function with respect to the mean field parameters. To determine (B.2.13) one has to compute the eigenvalues of $\hat{\mathbf{X}}_{i\omega_n}$ which means

that one has to compute the eigenvalues of $\underline{\mathbf{b}}\underline{\mathbf{g}}(i\omega_n)\underline{\mathbf{b}}$. Those can be complex valued and are determined by the roots of the characteristic polynomial

$$\det\left(\underline{\mathbf{b}}\underline{\mathbf{g}}(i\omega_n)\underline{\mathbf{b}} - \hat{T}(i\omega_n)\mathbb{1}_N\right) = 0.$$

The structure of the eigenvalues $\hat{T}_j(i\omega_n)$ is the same as the one of the matrix $\underline{\mathbf{g}}(i\omega_n)$:

$$\hat{T}_j(i\omega_n) = T_j^R + i\text{sgn}(\omega_n)T_j^I, \quad (\text{B.2.14})$$

where $j = 1 \dots N$ and where $T_j^{R/I}$ are real-valued. This is due to the fact, that for each complex number $x + i\text{sgn}(\omega_n)y$ with real-valued x and y the real parts of $[x + i\text{sgn}(\omega_n)y]^n$ and $[x + i\text{sgn}(\omega_n)y]^{1/n}$ do not depend on $\text{sgn}(\omega_n)$ while the respective imaginary parts are proportional to $\text{sgn}(\omega_n)$ (which can easily be proved by direct computation using the polar coordinate representation of complex numbers). The actual form of the eigenvalues strongly depends on the geometry of the cluster, which determines the matrices $\underline{\mathbf{g}}(i\omega_n)$ and $\underline{\mathbf{b}}$. However, for the rest of the chapter, we assume the eigenvalues have been found. Using the eigenvalues of $\underline{\mathbf{b}}\underline{\mathbf{g}}(i\omega_n)\underline{\mathbf{b}}$ the partition function (B.2.13) can be written as

$$Z_{MF} = C e^{-\frac{\beta}{NJ} \sum_i b_i^2} \exp 2 \sum_{i\omega_n} \sum_{j=1}^N \log \left[i\omega_n - \frac{i\pi}{2\beta} + i\pi\text{sgn}(\omega_n)T_j^R - \pi T_j^I \right]. \quad (\text{B.2.15})$$

Knowing the partition function, one can state the mean field equations determining the parameters b_j , which we are going to continue with in the following section.

B.3 Mean field equations

In this section we mostly are going to perform the frequency summations appearing in section 4.3 in detail. The mean field parameters b_i are the solutions of the system of equations given by

$$\frac{\partial \log Z_{MF}}{\partial b_i} = 0$$

for each b_i . Using the partition function (B.2.15) these equations write

$$0 = -\frac{2\beta}{NJ} b_i + 2 \sum_{j=1}^N \left[\frac{\partial T_j^R}{\partial b_i} \sum_{i\omega_n} \frac{i\pi\text{sgn}(\omega_n)}{i\omega_n - \frac{i\pi}{2\beta} + i\pi\text{sgn}(\omega_n)T_j^R - \pi T_j^I} - \frac{\partial T_j^I}{\partial b_i} \sum_{i\omega_n} \frac{\pi}{i\omega_n - \frac{i\pi}{2\beta} + i\pi\text{sgn}(\omega_n)T_j^R - \pi T_j^I} \right]. \quad (\text{B.3.1})$$

We perform the frequency summations in (B.3.1). The summations are over fermionic Matsubara frequencies

$$i\omega_n = \frac{i\pi}{\beta}(2n+1)$$

for $n = -\infty \dots \infty$. To perform the summations, we use the Digamma function Ψ which is defined by

$$\sum_{n=0}^{N-1} \frac{1}{n+z} = \Psi(N+z) - \Psi(z) \quad (\text{B.3.2})$$

B General calculations for a cluster of N atoms

for each complex number $z \neq 0$. We will see that the first frequency sum in (B.3.1) can only be performed using an energy cut-off while the second does not depend on this cut-off. We start writing down

$$\begin{aligned}
& \sum_{i\omega_n} \frac{i\pi \operatorname{sgn}(\omega_n)}{i\omega_n - \frac{i\pi}{2\beta} + i\pi \operatorname{sgn}(\omega_n) T_j^R - \pi T_j^I} \\
&= \lim_{N \rightarrow \infty} \left(\sum_{n=0}^{N-1} \frac{i\pi}{\frac{i\pi}{\beta}(2n+1) - \frac{i\pi}{2\beta} + i\pi T_j^R - \pi T_j^I} + \sum_{n=1}^{N-1} \frac{-i\pi}{\frac{i\pi}{\beta}(-2n+1) - \frac{i\pi}{2\beta} - i\pi T_j^R - \pi T_j^I} \right) \\
&= \lim_{N \rightarrow \infty} \left(\frac{\beta}{2} \sum_{n=0}^{N-1} \frac{1}{n + \frac{1}{4} + \frac{\beta}{2} T_j^R + i\frac{\beta}{2} T_j^I} + \frac{\beta}{2} \sum_{n=0}^{N-1} \frac{1}{n + \frac{3}{4} + \frac{\beta}{2} T_j^R - i\frac{\beta}{2} T_j^I} \right) \\
&= \frac{\beta}{2} \lim_{n \rightarrow \infty} \left[\Psi \left(N + \frac{1}{4} + \frac{\beta}{2} T_j^R + i\frac{\beta}{2} T_j^I \right) - \Psi \left(\frac{1}{4} + \frac{\beta}{2} T_j^R + i\frac{\beta}{2} T_j^I \right) \right. \\
&\quad \left. + \Psi \left(N + \frac{3}{4} + \frac{\beta}{2} T_j^R - i\frac{\beta}{2} T_j^I \right) - \Psi \left(\frac{3}{4} + \frac{\beta}{2} T_j^R - i\frac{\beta}{2} T_j^I \right) \right],
\end{aligned}$$

where we used (B.3.2). Having a closer look at (B.3.2), we see that the Digamma function logarithmically diverges with N , since so does

$$\sum_{n=0}^N \frac{1}{n+z}.$$

Thus, the above expression does not converge. We have to use a cut-off for N in order to have a finite expression. Having in mind the meaning of the Matsubara frequencies, this cut-off can be translated to a cut-off in frequency space which corresponds to the highest achievable energy for the conduction electrons. Hence, it is determined by the width Δ of the conduction band. Due to symmetry considerations for negative and positive frequencies, we therefore set the cut-off to

$$N = \frac{\beta}{2} \Delta.$$

Then

$$\begin{aligned}
& \sum_{i\omega_n} \frac{i\pi \operatorname{sgn}(\omega_n)}{i\omega_n - \frac{i\pi}{2\beta} + i\pi \operatorname{sgn}(\omega_n) T_j^R - \pi T_j^I} \\
&= \frac{\beta}{2} \left[\Psi \left(\frac{\beta}{2} \Delta + \frac{1}{4} + \frac{\beta}{2} T_j^R + i\frac{\beta}{2} T_j^I \right) - \Psi \left(\frac{1}{4} + \frac{\beta}{2} T_j^R + i\frac{\beta}{2} T_j^I \right) \right. \\
&\quad \left. + \Psi \left(\frac{\beta}{2} \Delta + \frac{3}{4} + \frac{\beta}{2} T_j^R - i\frac{\beta}{2} T_j^I \right) - \Psi \left(\frac{3}{4} + \frac{\beta}{2} T_j^R - i\frac{\beta}{2} T_j^I \right) \right] \\
&= \frac{\beta}{2} \left[\Psi \left(\frac{\beta}{2} \Delta + \frac{1}{4} + \frac{\beta}{2} T_j^* \right) - \Psi \left(\frac{1}{4} + \frac{\beta}{2} T_j^* \right) + \Psi \left(\frac{\beta}{2} \Delta + \frac{3}{4} + \frac{\beta}{2} T_j \right) - \Psi \left(\frac{3}{4} + \frac{\beta}{2} T_j \right) \right],
\end{aligned} \tag{B.3.3}$$

where we defined

$$T_j = T_j^R - iT_j^I \tag{B.3.4}$$

and its complex conjugate T_j^* . Using this expression, one could start analysing the mean field equations for arbitrary inverse temperatures β . However, this task is analytically not so easily manageable and one would rather make use of numerical techniques. In this work, we want to investigate cases which can be treated analytically, so we stick to the limiting case of very low temperature. Then, $\beta \rightarrow \infty$ and (B.3.3) becomes much simpler. As already mentioned, the Digamma function behaves like a logarithm for large arguments (see [88]):

$$\Psi(z) \rightarrow \log(z) \quad \text{if} \quad |z| \gg 1, \quad \text{Re}z \neq 0.$$

So we get

$$\begin{aligned} & \sum_{i\omega_n} \frac{i\pi \text{sgn}(\omega_n)}{i\omega_n - \frac{i\pi}{2\beta} + i\pi \text{sgn}(\omega_n) T_j^R - \pi T_j^I} \\ &= \frac{\beta}{2} \left[\log \left(\frac{\beta}{2} \Delta + \frac{\beta}{2} T_j \right) - \log \left(\frac{\beta}{2} T_j \right) + \log \left(\frac{\beta}{2} \Delta + \frac{\beta}{2} T_j^* \right) - \log \left(\frac{\beta}{2} T_j^* \right) \right] \\ &= -\frac{\beta}{2} \left[\log \frac{T_j}{\Delta + T_j} + \log \frac{T_j^*}{\Delta + T_j^*} \right] \\ &= -\beta \text{Re} \left(\log \frac{T_j}{\Delta + T_j} \right). \end{aligned} \tag{B.3.5}$$

Quite analogously to the latter considerations, we can compute the second frequency summation in (B.3.1). It is

$$\begin{aligned} & \sum_{i\omega_n} \frac{-\pi}{i\omega_n - \frac{i\pi}{2\beta} + i\pi \text{sgn}(\omega_n) T_j^R - \pi T_j^I} \\ &= \lim_{N \rightarrow \infty} \left(i \frac{\beta}{2} \sum_{n=0}^{N-1} \frac{1}{n + \frac{1}{4} + \frac{\beta}{2} T_j^*} - i \frac{\beta}{2} \sum_{n=0}^{N-1} \frac{1}{n + \frac{3}{4} + \frac{\beta}{2} T_j} \right) \\ &= i \frac{\beta}{2} \lim_{N \rightarrow \infty} \left[\Psi \left(N + \frac{1}{4} + \frac{\beta}{2} T_j^* \right) - \Psi \left(\frac{1}{4} + \frac{\beta}{2} T_j^* \right) - \Psi \left(N + \frac{3}{4} + \frac{\beta}{2} T_j \right) + \Psi \left(\frac{3}{4} + \frac{\beta}{2} T_j \right) \right] \\ &= -i \frac{\beta}{2} \left[\Psi \left(\frac{\beta}{2} T_j^* + \frac{1}{4} \right) - \Psi \left(\frac{\beta}{2} T_j + \frac{3}{4} \right) \right]. \end{aligned} \tag{B.3.6}$$

Here, no cut-off is needed. The expression

$$\Psi \left(N + \frac{1}{4} + \frac{\beta}{2} T_j^* \right) - \Psi \left(N + \frac{3}{4} + \frac{\beta}{2} T_j \right)$$

vanishes in the limit of large N . This is due to the analyticity of the Digamma function everywhere in the complex plane except for the negative real axis. As for (B.3.5), we investigate (B.3.6) in the low temperature limit using the logarithmic behavior of the Digamma function for large arguments, which yields

$$\sum_{i\omega_n} \frac{-\pi}{i\omega_n - \frac{i\pi}{2\beta} + i\pi \text{sgn}(\omega_n) T_j^R - \pi T_j^I} = -i \frac{\beta}{2} \log \frac{T_j^*}{T_j}. \tag{B.3.7}$$

B General calculations for a cluster of N atoms

We remark that this is a real-valued expression, which vanishes if $T_j^I = 0$. With the two quantities (B.3.5) and (B.3.7) the mean field equations (B.3.1) in the low temperature limit are given as

$$\sum_{j=1}^N \left[\frac{\partial T_j^R}{\partial b_i} 2 \operatorname{Re} \left(\log \frac{T_j}{\Delta + T_j} \right) + i \frac{\partial T_j^I}{\partial b_i} \log \frac{T_j^*}{T_j} \right] = -\frac{2}{NJ} b_i. \quad (\text{B.3.8})$$

This can be even more simplified if one assumes $|T_j|/\Delta \ll 1$ for all $j = 1 \dots N$. We will see that this assumption is justified since it corresponds to the condition $J\rho_0 \ll 1$ which is initially assumed to treat the model in the low energy regime. Then, the mean field equations become

$$\sum_{j=1}^N \left[\frac{\partial T_j^R}{\partial b_i} 2 \operatorname{Re} \left(\log \frac{T_j}{\Delta} \right) + i \frac{\partial T_j^I}{\partial b_i} \log \frac{T_j^*}{T_j} \right] = -\frac{2}{NJ} b_i. \quad (\text{B.3.9})$$

We remark that one could rewrite these equations using

$$2 \operatorname{Re} \log \frac{T_j}{\Delta} = \log \frac{T_j}{\Delta} + \log \frac{T_j^*}{\Delta} = \log \frac{|T_j|^2}{\Delta^2} = 2 \log \frac{|T_j|}{\Delta}$$

and

$$i \log \frac{T_j^*}{T_j} = i \log \frac{|T_j| e^{i \arctan \frac{T_j^I}{T_j^R}}}{|T_j| e^{-i \arctan \frac{T_j^I}{T_j^R}}} = -2 \arctan \frac{T_j^I}{T_j^R}.$$

B.4 Green's function and local density of states in mean field theory

In the following we are going to perform the computations that lead to the results in section 4.4. The quantity describing the whole system is its Matsubara Green's function. To get it, we introduce a source term in the action (B.2.5):

$$\begin{aligned} S_{Source} &= \sum_{i\omega_n} \sum_{\mathbf{k}} \left(\bar{\eta}_{i\omega_n}^{\mathbf{k}} a_{\mathbf{k}}^{i\omega_n} + \bar{a}_{\mathbf{k}}^{i\omega_n} \eta_{i\omega_n}^{\mathbf{k}} \right) \\ &= \sum_{i\omega_n} \left(\bar{\Theta}_{i\omega_n} \cdot \chi^{i\omega_n} + \bar{\chi}^{i\omega_n} \cdot \Theta_{i\omega_n} \right), \end{aligned}$$

where we defined

$$\Theta_{i\omega_n} = \left(\underbrace{0, 0, \dots, 0}_{N\text{-times}}, \left\{ \eta_{i\omega_n}^{\mathbf{k}} | \mathbf{k} \right\} \right)^T$$

and made use of the vector (B.2.4). Adding the source term to the action (B.2.5) yields a partition function \hat{Z}_{MF} different from the original Z_{MF} . The Matsubara Green's function is given as

$$\hat{G}(i\omega_n; \mathbf{k}, \mathbf{k}') = \frac{\partial^2 \log \hat{Z}_{MF}}{\partial \bar{\eta}_{i\omega_n}^{\mathbf{k}} \partial \eta_{i\omega_n}^{\mathbf{k}'}} \Bigg|_{\bar{\eta}=\eta=0}. \quad (\text{B.4.1})$$

Any fermionic Gaussian integral computes to (see [90])

$$\int [D\xi] \exp \left[- \sum_{\alpha\beta} \bar{\xi}_\alpha H_{\alpha\beta} \xi_\beta + \sum_\alpha (\bar{\eta}_\alpha \xi_\alpha + \bar{\xi}_\alpha \eta_\alpha) \right] = \det(H) \cdot \exp \left(\sum_{\alpha\beta} \bar{\eta}_\alpha H_{\alpha\beta}^{-1} \eta_\beta \right).$$

B General calculations for a cluster of N atoms

So, the altered partition function \hat{Z}_{MF} can be computed as

$$\hat{Z}_{MF} = Z_{MF} \exp \left(\sum_{i\omega_n} \bar{\Theta}_{i\omega_n} [\underline{\mathbf{M}}_{i\omega_n}^{-1} \otimes \mathbb{1}_2] \Theta_{i\omega_n} \right)$$

with $\underline{\mathbf{M}}_{i\omega_n}^{-1}$ being the inverse of (B.2.6). The matrix $\underline{\mathbf{M}}_{i\omega_n}$ has the structure

$$\underline{\mathbf{M}}_{i\omega_n} = \left(\begin{array}{c|c} D_{i\omega_n}^{-1} \mathbb{1}_N & \underline{\mathbf{A}} \\ \hline \underline{\mathbf{A}}^\dagger & \text{diag} (G_{i\omega_n}^{-1}(\mathbf{k}) | \mathbf{k}) \end{array} \right),$$

and we assume a similar one for $\underline{\mathbf{M}}_{i\omega_n}^{-1}$:

$$\underline{\mathbf{M}}_{i\omega_n}^{-1} = \left(\begin{array}{c|c} \underline{\mathbf{Y}} & \underline{\mathbf{B}} \\ \hline \underline{\mathbf{B}}^\dagger & \underline{\mathbf{X}} \end{array} \right) \quad (\text{B.4.2})$$

with all blocks having the same dimension as their counterparts in $\underline{\mathbf{M}}_{i\omega_n}$. We suppressed all $i\omega_n$ - and \mathbf{k} -dependencies for the sake of a simple notation. Keeping in mind that we are only interested in the electronic Green's function given by (B.4.1) and what $\underline{\mathbf{M}}_{i\omega_n}^{-1}$ looks like, we only need to know the matrix $\underline{\mathbf{X}}$, and it is

$$\underline{\mathbf{X}}_{\mathbf{k}\mathbf{k}'} = \hat{G}(i\omega_n; \mathbf{k}, \mathbf{k}').$$

The matrices $\underline{\mathbf{X}}$, $\underline{\mathbf{Y}}$ and $\underline{\mathbf{B}}$ are determined by the condition $\underline{\mathbf{M}}_{i\omega_n} \cdot \underline{\mathbf{M}}_{i\omega_n}^{-1} = \mathbb{1}$, which yields

- 1) $D_{i\omega_n}^{-1} \underline{\mathbf{B}} + \underline{\mathbf{A}} \cdot \underline{\mathbf{X}} = 0,$
- 2) $\underline{\mathbf{A}}^\dagger \cdot \underline{\mathbf{B}} + \underline{\mathbf{G}}_{i\omega_n}^{-1} \cdot \underline{\mathbf{X}} = \mathbb{1},$
- 3) $D_{i\omega_n}^{-1} \underline{\mathbf{Y}} + \underline{\mathbf{A}} \cdot \underline{\mathbf{B}}^\dagger = \mathbb{1}_N,$
- 4) $\underline{\mathbf{A}}^\dagger \cdot \underline{\mathbf{Y}} + \underline{\mathbf{G}}_{i\omega_n}^{-1} \cdot \underline{\mathbf{B}}^\dagger = 0,$

with the abbreviation

$$\underline{\mathbf{G}}_{i\omega_n}^{-1} = \text{diag} (G_{i\omega_n}^{-1}(\mathbf{k}) | \mathbf{k}).$$

$\underline{\mathbf{X}}$ is computed using the first two of the four equations. Multiplying the first equation by $D_{i\omega_n} \underline{\mathbf{A}}^\dagger$ from the right, solving it for $\underline{\mathbf{A}}^\dagger \cdot \underline{\mathbf{B}}$ and putting this into the second equation, one arrives at

$$\left[-D_{i\omega_n} \underline{\mathbf{A}}^\dagger \cdot \underline{\mathbf{A}} + \underline{\mathbf{G}}_{i\omega_n}^{-1} \right] \cdot \underline{\mathbf{X}} = \mathbb{1}$$

which has the formal solution

$$\begin{aligned} \underline{\mathbf{X}} &= \left[\underline{\mathbf{G}}_{i\omega_n}^{-1} - D_{i\omega_n} \underline{\mathbf{A}}^\dagger \cdot \underline{\mathbf{A}} \right]^{-1} \\ &= \sum_{n=0}^{\infty} \left(D_{i\omega_n} \underline{\mathbf{G}}_{i\omega_n} \underline{\mathbf{A}}^\dagger \underline{\mathbf{A}} \right)^n \underline{\mathbf{G}}_{i\omega_n}, \end{aligned} \quad (\text{B.4.3})$$

B General calculations for a cluster of N atoms

with $\underline{\mathbf{G}}_{i\omega_n}$ being the inverse of $\underline{\mathbf{G}}_{i\omega_n}^{-1}$. The matrix $\underline{\mathbf{A}}^\dagger \cdot \underline{\mathbf{A}}$ has the same dimension as $\underline{\mathbf{G}}_{i\omega_n}$ and it is

$$\left(\underline{\mathbf{A}}^\dagger \cdot \underline{\mathbf{A}}\right)_{\mathbf{k}\mathbf{k}'} = \sum_{j=1}^N (t_{\mathbf{k}}^\dagger \underline{\mathbf{b}})_j (\underline{\mathbf{b}} t_{\mathbf{k}'})_j = t_{\mathbf{k}}^\dagger \underline{\mathbf{b}}^2 t_{\mathbf{k}'}$$

In order to compute the matrix elements of (B.4.3), we use the relation

$$\left[\left(\underline{\mathbf{G}}_{i\omega_n} \underline{\mathbf{A}}^\dagger \underline{\mathbf{A}}\right)^n \underline{\mathbf{G}}_{i\omega_n}\right]_{\mathbf{k}\mathbf{k}'} = G_{i\omega_n}(\mathbf{k}) t_{\mathbf{k}}^\dagger \underline{\mathbf{b}} \left[-i\pi \operatorname{sgn}(\omega_n) \underline{\mathbf{b}} \underline{\mathbf{g}}(i\omega_n) \underline{\mathbf{b}}\right]^{n-1} \underline{\mathbf{b}} t_{\mathbf{k}'} G_{i\omega_n}(\mathbf{k}') \quad (\text{B.4.4})$$

for $n \geq 1$. We prove (B.4.4) by induction. For $n = 1$ it is

$$\begin{aligned} \left[\underline{\mathbf{G}}_{i\omega_n} \underline{\mathbf{A}}^\dagger \underline{\mathbf{A}} \underline{\mathbf{G}}_{i\omega_n}\right]_{\mathbf{k}\mathbf{k}'} &= \sum_{\mathbf{l}\mathbf{l}'} G_{i\omega_n}(\mathbf{k}) \delta_{\mathbf{k}\mathbf{l}} t_{\mathbf{l}}^\dagger \underline{\mathbf{b}}^2 t_{\mathbf{l}'} G_{i\omega_n}(\mathbf{k}') \delta_{\mathbf{l}'\mathbf{k}'} \\ &= G_{i\omega_n}(\mathbf{k}) t_{\mathbf{k}}^\dagger \underline{\mathbf{b}}^2 t_{\mathbf{k}'} G_{i\omega_n}(\mathbf{k}'). \end{aligned}$$

Assume (B.4.4) is correct for some $n \geq 1$. Then it is

$$\begin{aligned} &\left[\left(\underline{\mathbf{G}}_{i\omega_n} \underline{\mathbf{A}}^\dagger \underline{\mathbf{A}}\right)^{n+1} \underline{\mathbf{G}}_{i\omega_n}\right]_{\mathbf{k}\mathbf{k}'} \\ &= \sum_{\mathbf{l}} \left(\underline{\mathbf{G}}_{i\omega_n} \underline{\mathbf{A}}^\dagger \underline{\mathbf{A}}\right)_{\mathbf{k}\mathbf{l}} \left[\left(\underline{\mathbf{G}}_{i\omega_n} \underline{\mathbf{A}}^\dagger \underline{\mathbf{A}}\right)^n \underline{\mathbf{G}}_{i\omega_n}\right]_{\mathbf{l}\mathbf{k}'} \\ &= \sum_{\mathbf{l}} G_{i\omega_n}(\mathbf{k}) t_{\mathbf{k}}^\dagger \underline{\mathbf{b}}^2 t_{\mathbf{l}} G_{i\omega_n}(\mathbf{l}) t_{\mathbf{l}}^\dagger \underline{\mathbf{b}} \left[-i\pi \operatorname{sgn}(\omega_n) \underline{\mathbf{b}} \underline{\mathbf{g}}(i\omega_n) \underline{\mathbf{b}}\right]^{n-1} \underline{\mathbf{b}} t_{\mathbf{k}'} G_{i\omega_n}(\mathbf{k}') \\ &= G_{i\omega_n}(\mathbf{k}) t_{\mathbf{k}}^\dagger \underline{\mathbf{b}} \left[-i\pi \operatorname{sgn}(\omega_n) \underline{\mathbf{b}} \underline{\mathbf{g}}(i\omega_n) \underline{\mathbf{b}}\right]^n \underline{\mathbf{b}} t_{\mathbf{k}'} G_{i\omega_n}(\mathbf{k}'), \end{aligned}$$

where we used the definition of the matrix $\underline{\mathbf{g}}(i\omega_n)$ as given in section B.2:

$$\left(\sum_{\mathbf{l}} t_{\mathbf{l}} G_{i\omega_n}(\mathbf{l}) t_{\mathbf{l}}^\dagger\right)_{ij} = \left(\frac{1}{N} \sum_{\mathbf{l}} \frac{e^{-i(\mathbf{R}_i - \mathbf{R}_j) \cdot \mathbf{l}}}{i\omega_n - \varepsilon_1}\right)_{ij} = -i\pi \operatorname{sgn}(\omega_n) [\underline{\mathbf{g}}(i\omega_n)]_{ij}.$$

So, we have proven (B.4.4). Using this relation, it is

$$\begin{aligned} \hat{G}(i\omega_n; \mathbf{k}, \mathbf{k}') &= G_{i\omega_n}(\mathbf{k}) \delta_{\mathbf{k}\mathbf{k}'} + G_{i\omega_n}(\mathbf{k}) t_{\mathbf{k}}^\dagger \underline{\mathbf{b}} \sum_{n=1}^{\infty} D_{i\omega_n}^n \left[-i\pi \operatorname{sgn}(\omega_n) \underline{\mathbf{b}} \underline{\mathbf{g}}(i\omega_n) \underline{\mathbf{b}}\right]^{n-1} \underline{\mathbf{b}} t_{\mathbf{k}'} G_{i\omega_n}(\mathbf{k}'). \\ &= G_{i\omega_n}(\mathbf{k}) \delta_{\mathbf{k}\mathbf{k}'} + G_{i\omega_n}(\mathbf{k}) D_{i\omega_n} t_{\mathbf{k}}^\dagger \underline{\mathbf{b}} \sum_{n=0}^{\infty} D_{i\omega_n}^n \left[-i\pi \operatorname{sgn}(\omega_n) \underline{\mathbf{b}} \underline{\mathbf{g}}(i\omega_n) \underline{\mathbf{b}}\right]^n \underline{\mathbf{b}} t_{\mathbf{k}'} G_{i\omega_n}(\mathbf{k}'). \end{aligned}$$

This can be more conveniently written by diagonalising the matrix $\underline{\mathbf{b}} \underline{\mathbf{g}}(i\omega_n) \underline{\mathbf{b}}$. Let $\hat{T}_j(i\omega_n)$ as defined in (B.2.14) be the eigenvalues of this matrix and

$$\hat{u}_j(i\omega_n) = u_j^R + i \operatorname{sgn}(\omega_n) u_j^I \quad (\text{B.4.5})$$

with real-valued $u_j^{R/I}$ the corresponding eigenvectors for $j = 1 \dots N$. The structure of the eigenvectors is due to that of $\underline{\mathbf{g}}(i\omega_n)$. Let the unitary matrix $\underline{\mathbf{U}}_{i\omega_n}$ be defined as

$$\underline{\mathbf{U}}_{i\omega_n} = \left(\hat{u}_1(i\omega_n)^* \mid \hat{u}_2(i\omega_n)^* \mid \dots \mid \hat{u}_N(i\omega_n)^*\right)^T,$$

B General calculations for a cluster of N atoms

so its rows are the complex conjugate of the eigenvectors. Let $\underline{U}_{i\omega_n}^\dagger$ denote the adjoint, its columns being the eigenvectors $\hat{u}_j(i\omega_n)$. Those matrices then diagonalise $\underline{b} \underline{g}(i\omega_n) \underline{b}$:

$$\hat{\underline{T}}_{i\omega_n} = \underline{U}_{i\omega_n} \underline{b} \underline{g}(i\omega_n) \underline{b} \underline{U}_{i\omega_n}^\dagger = \text{diag} \left(\hat{T}_j(i\omega_n) \mid j = 1 \dots N \right),$$

and it is

$$\left[\underline{b} \underline{g}(i\omega_n) \underline{b} \right]^n = \underline{U}_{i\omega_n}^\dagger \hat{\underline{T}}_{i\omega_n}^n \underline{U}_{i\omega_n}.$$

Hence,

$$\hat{G}(i\omega_n; \mathbf{k}, \mathbf{k}') = G_{i\omega_n}(\mathbf{k}) \delta_{\mathbf{k}\mathbf{k}'} + G_{i\omega_n}(\mathbf{k}) D_{i\omega_n} t_{\mathbf{k}}^\dagger \underline{b} \underline{U}_{i\omega_n}^\dagger \sum_{n=0}^{\infty} \left[-i\pi \text{sgn}(\omega_n) D_{i\omega_n} \right]^n \hat{\underline{T}}_{i\omega_n}^n \underline{U}_{i\omega_n} \underline{b} t_{\mathbf{k}'} G_{i\omega_n}(\mathbf{k}').$$

We compute the geometric series

$$\begin{aligned} D_{i\omega_n} \sum_{n=0}^{\infty} \left[-i\pi \text{sgn}(\omega_n) D_{i\omega_n} \hat{T}_j(i\omega_n) \right]^n &= D_{i\omega_n} \frac{1}{1 + i\pi \text{sgn}(\omega_n) D_{i\omega_n} \hat{T}_j(i\omega_n)} \\ &= \frac{1}{D_{i\omega_n}^{-1} + i\pi \text{sgn}(\omega_n) \hat{T}_j(i\omega_n)} \end{aligned}$$

and thus

$$\begin{aligned} &\left(\underline{U}_{i\omega_n}^\dagger D_{i\omega_n} \sum_{n=0}^{\infty} \left[-i\pi \text{sgn}(\omega_n) D_{i\omega_n} \right]^n \hat{\underline{T}}_{i\omega_n}^n \underline{U}_{i\omega_n} \right)_{ij} \\ &= \left(\underline{U}_{i\omega_n}^\dagger \text{diag} \left(\frac{1}{D_{i\omega_n}^{-1} + i\pi \text{sgn}(\omega_n) \hat{T}_l(i\omega_n)} \mid l = 1 \dots N \right) \underline{U}_{i\omega_n} \right)_{ij} \\ &= \sum_{l=1}^N \left(\underline{U}_{i\omega_n}^\dagger \right)_{il} \frac{1}{D_{i\omega_n}^{-1} + i\pi \text{sgn}(\omega_n) \hat{T}_l(i\omega_n)} \left(\underline{U}_{i\omega_n} \right)_{lj} \\ &= \sum_{l=1}^N \frac{(\hat{u}_l(i\omega_n))_i (\hat{u}_l(i\omega_n))_j^*}{D_{i\omega_n}^{-1} + i\pi \text{sgn}(\omega_n) \hat{T}_l(i\omega_n)}. \end{aligned}$$

Using this relations, we finally get the Matsubara Green's function

$$\hat{G}(i\omega_n; \mathbf{k}, \mathbf{k}') = G_{i\omega_n}(\mathbf{k}) \delta_{\mathbf{k}\mathbf{k}'} + \sum_{j=1}^N \frac{G_{i\omega_n}(\mathbf{k}) [t_{\mathbf{k}}^\dagger \underline{b} \hat{u}_j(i\omega_n)] \cdot [\hat{u}_j(i\omega_n)^\dagger \underline{b} t_{\mathbf{k}'}]}{D_{i\omega_n}^{-1} + i\pi \text{sgn}(\omega_n) \hat{T}_j(i\omega_n)}. \quad (\text{B.4.6})$$

Our overall goal is to get the coordinate resolved local density of states, so we have to compute the coordinate resolved Green's function. To this end, we perform a Fourier transformation of (B.4.6):

$$\tilde{G}(i\omega_n; \mathbf{r}) = \sum_{\mathbf{k}\mathbf{k}'} \hat{G}(i\omega_n; \mathbf{k}, \mathbf{k}') e^{-i\mathbf{r}(\mathbf{k}-\mathbf{k}')}$$

Bearing in mind the definition of the $t_{\mathbf{k}}$

$$(t_{\mathbf{k}})_i = \frac{1}{\sqrt{N}} e^{-i\mathbf{R}_i \mathbf{k}},$$

B General calculations for a cluster of N atoms

all occurring integrals are of the form

$$\sum_{\mathbf{k}} G_{i\omega_n}(\mathbf{k}) (t_{\mathbf{k}})_i e^{i\mathbf{r}\mathbf{k}} = \frac{1}{\sqrt{N}} \sum_{\mathbf{k}} \frac{e^{-i(\mathbf{R}_i - \mathbf{r})\mathbf{k}}}{i\omega_n - \varepsilon_{\mathbf{k}}}.$$

We already computed integrals of that kind when we defined the matrix $\mathbf{g}(i\omega_n)$ in section B.2. For certain assumptions as a wide and flat band, the general structure is

$$\sum_{\mathbf{k}} \frac{e^{-i(\mathbf{R}_i - \mathbf{r})\mathbf{k}}}{i\omega_n - \varepsilon_{\mathbf{k}}} = -i\pi \operatorname{sgn}(\omega_n) \rho_0 [f_{\mathbf{r}}^i + i \operatorname{sgn}(\omega_n) g_{\mathbf{r}}^i]$$

with real-valued $f_{\mathbf{r}}^i$ and $g_{\mathbf{r}}^i$ which do not depend on ω_n . Hence, we define the vector $\hat{v}_{\mathbf{r}}(i\omega_n)$ by

$$\sum_{\mathbf{k}'} G_{i\omega_n}(\mathbf{k}') t_{\mathbf{k}'} e^{i\mathbf{r}\mathbf{k}'} = -i\pi \operatorname{sgn}(\omega_n) \frac{\rho_0}{\sqrt{N}} \hat{v}_{\mathbf{r}}(i\omega_n) = -i\pi \operatorname{sgn}(\omega_n) \frac{\rho_0}{\sqrt{N}} [v_{\mathbf{r}}^R + i \operatorname{sgn}(\omega_n) v_{\mathbf{r}}^I], \quad (\text{B.4.7})$$

with real-valued vectors $v_{\mathbf{r}}^{R/I}$ independent of $i\omega_n$. It is quite important here, that

$$\sum_{\mathbf{k}} \frac{e^{-i(\mathbf{R}_i - \mathbf{r})\mathbf{k}}}{i\omega_n - \varepsilon_{\mathbf{k}}} = \sum_{\mathbf{k}} \frac{e^{i(\mathbf{R}_i - \mathbf{r})\mathbf{k}}}{i\omega_n - \varepsilon_{\mathbf{k}}},$$

because this means

$$\sum_{\mathbf{k}} G_{i\omega_n}(\mathbf{k}) t_{\mathbf{k}}^\dagger e^{-i\mathbf{r}\mathbf{k}} = -i\pi \operatorname{sgn}(\omega_n) \frac{\rho_0}{\sqrt{N}} \hat{v}_{\mathbf{r}}^\dagger(i\omega_n) = -i\pi \operatorname{sgn}(\omega_n) \frac{\rho_0}{\sqrt{N}} [(v_{\mathbf{r}}^R)^\dagger + i \operatorname{sgn}(\omega_n) (v_{\mathbf{r}}^I)^\dagger].$$

The Fourier transformations of $G_{i\omega_n}(\mathbf{k}) t_{\mathbf{k}}$ and $G_{i\omega_n}(\mathbf{k}) t_{\mathbf{k}}^\dagger$ give rise to the same vector $\hat{v}_{\mathbf{r}}(i\omega_n)$ (up to transposition). The $i\omega_n$ -dependence of both Fourier transformations is the same, no complex conjugation occurs. Performing these transformations in (B.4.6) and inserting the definition of $\hat{v}_{\mathbf{r}}(i\omega_n)$, one ends up with

$$\begin{aligned} \tilde{G}(i\omega_n; \mathbf{r}) &= -i\pi \operatorname{sgn}(\omega_n) \rho_0 - \pi^2 \rho_0 \frac{\rho_0}{N} \sum_{j=1}^N \frac{[\hat{v}_{\mathbf{r}}^\dagger(i\omega_n) \mathbf{h} \hat{u}_j(i\omega_n)] \cdot [\hat{u}_j(i\omega_n)^\dagger \mathbf{h} \hat{v}_{\mathbf{r}}(i\omega_n)]}{D_{i\omega_n}^{-1} + i\pi \operatorname{sgn}(\omega_n) \hat{T}_j(i\omega_n)} \\ &= \pi \rho_0 \left(-i \operatorname{sgn}(\omega_n) - \pi g_0 \sum_{j=1}^N \frac{[\hat{v}_{\mathbf{r}}^\dagger(i\omega_n) \mathbf{h} \hat{u}_j(i\omega_n)] \cdot [\hat{u}_j(i\omega_n)^\dagger \mathbf{h} \hat{v}_{\mathbf{r}}(i\omega_n)]}{D_{i\omega_n}^{-1} + i\pi \operatorname{sgn}(\omega_n) \hat{T}_j(i\omega_n)} \right), \end{aligned} \quad (\text{B.4.8})$$

where we used $(-i \operatorname{sgn}(\omega_n))^2 = -1$ and $g_0 = \rho_0/N$. We remark that the $\hat{v}_{\mathbf{r}}$ are related to the entries of the matrix $\mathbf{g}(i\omega_n)$, if they are taken at the site \mathbf{R}_i of a cluster atom, since

$$\begin{aligned} \left[\sum_{\mathbf{k}} G_{i\omega_n}(\mathbf{k}) t_{\mathbf{k}} e^{i\mathbf{R}_i \mathbf{k}} \right]_j &= -i\pi \operatorname{sgn}(\omega_n) \sqrt{N} [\mathbf{g}(i\omega_n)]_{ij} \\ &= -i\pi \operatorname{sgn}(\omega_n) \frac{\rho_0}{\sqrt{N}} [\hat{v}_{\mathbf{R}_i}(i\omega_n)]_j, \end{aligned}$$

so

$$[\hat{v}_{\mathbf{R}_i}(i\omega_n)]_j = \frac{[\mathbf{g}(i\omega_n)]_{ij}}{g_0}.$$

B General calculations for a cluster of N atoms

The local density of states essentially is given as the imaginary part of the advanced Green's function (see [90]):

$$\rho(\omega, \mathbf{r}) = \frac{1}{\pi} \text{Im} G^{adv}(\omega, \mathbf{r}). \quad (\text{B.4.9})$$

The advanced Green's function is achieved from its Matsubara form by complex continuation into the lower half plane. Usually, this is done by replacing $i\omega_n \rightarrow \omega + i\delta$ where $\delta \rightarrow 0^+$. However, in this model it is a little different. Due to the Popov-Fedotov ansatz of dealing with superfluous states in the partition function by introducing an imaginary chemical potential, the Matsubara frequencies are not simply fermionic ones but they have slightly changed. We denoted with $i\omega_n$ the usual Matsubara fermionic frequencies but the frequencies occurring here are rather

$$i\omega'_n = i\omega_n - \frac{i\pi}{2\beta} = \frac{i\pi}{\beta} \left(2n + \frac{1}{2} \right) = D_{i\omega_n}^{-1}.$$

It is these Matsubara frequencies ω'_n the continuation has to be applied to. However, this does not cause major problems, since

$$\text{sgn}(\omega_n) = \text{sgn}(\omega'_n).$$

The continuation therefore reads

$$i\omega'_n = D_{i\omega_n}^{-1} \rightarrow \omega - i\delta \quad \text{and} \quad i\text{sgn}(\omega'_n) = i\text{sgn}(\omega_n) \rightarrow -i. \quad (\text{B.4.10})$$

The transformation of $i\text{sgn}(\omega'_n)$ is due to the fact, that only negative ω_n are taken into account for the continuation into the lower half plane. The eigenvalues and eigenvectors of $\underline{\mathbf{b}}\mathbf{g}(i\omega_n)\underline{\mathbf{b}}$ and the vectors $\hat{v}_{\mathbf{r}}(i\omega_n)$ transform like

$$\begin{aligned} \hat{T}_j(i\omega_n) &\rightarrow T_j = T_j^R - iT_j^I \\ \hat{u}_j(i\omega_n) &\rightarrow u_j = u_j^R - iu_j^I \\ \hat{v}_{\mathbf{r}}(i\omega_n) &\rightarrow v_{\mathbf{r}} = v_{\mathbf{r}}^R - iv_{\mathbf{r}}^I, \end{aligned} \quad (\text{B.4.11})$$

where we introduced T_j, u_j and $v_{\mathbf{r}}$ for the sake of brief notation. We remark, that T_j and u_j are the eigenvalues and eigenvectors of the matrix

$$\underline{\mathbf{b}}\mathbf{g}\underline{\mathbf{b}} = \underline{\mathbf{b}}(\mathbf{g}^R - i\mathbf{g}^I)\underline{\mathbf{b}}$$

and that

$$[v_{\mathbf{R}_i}]_j = \frac{\mathbf{g}_{ij}}{g_0}$$

at any cluster site \mathbf{R}_i . The advanced Green's function is obtained from (B.4.8) by the continuation (B.4.10) and is given as

$$G^{adv}(\omega, \mathbf{r}) = \pi \rho_0 \left(i - \pi g_0 \sum_{j=1}^N \frac{[v_{\mathbf{r}}^T \underline{\mathbf{b}} u_j] \cdot [u_j^\dagger \underline{\mathbf{b}} v_{\mathbf{r}}]}{\omega - i\pi T_j} \right), \quad (\text{B.4.12})$$

where we already performed the limit $\delta \rightarrow 0^+$. According to (B.4.9), the local density of states reads

$$\rho(\omega, \mathbf{r}) = \rho_0 \left(1 - \pi g_0 \text{Im} \left[\sum_{j=1}^N \frac{[v_{\mathbf{r}}^T \underline{\mathbf{b}} u_j] \cdot [u_j^\dagger \underline{\mathbf{b}} v_{\mathbf{r}}]}{\omega - i\pi T_j} \right] \right). \quad (\text{B.4.13})$$

B General calculations for a cluster of N atoms

For each j and \mathbf{r} we determine the imaginary part of the fraction in (B.4.13). We omit the j - and \mathbf{r} -dependence in the following. It is

$$\begin{aligned} \operatorname{Im} \frac{[v^{\text{T}} \underline{\mathbf{b}} u] \cdot [u^{\dagger} \underline{\mathbf{b}} v]}{\omega - i\pi T} &= \frac{\operatorname{Im}([v^{\text{T}} \underline{\mathbf{b}} u] \cdot [u^{\dagger} \underline{\mathbf{b}} v] \cdot [\omega - \pi T^I + i\pi T^R])}{(\omega - \pi T^I)^2 + (\pi T^R)^2} \\ &= \frac{(\omega - \pi T^I) \operatorname{Im}([v^{\text{T}} \underline{\mathbf{b}} u] \cdot [u^{\dagger} \underline{\mathbf{b}} v]) + \pi T^R \operatorname{Re}([v^{\text{T}} \underline{\mathbf{b}} u] \cdot [u^{\dagger} \underline{\mathbf{b}} v])}{(\omega - \pi T^I)^2 + (\pi T^R)^2} \end{aligned}$$

and

$$\begin{aligned} v^{\text{T}} \underline{\mathbf{b}} u &= (v^R - iv^I)^{\text{T}} \underline{\mathbf{b}} (u^R - iu^I) \\ &= (v^R)^{\text{T}} \underline{\mathbf{b}} u^R - (v^I)^{\text{T}} \underline{\mathbf{b}} u^I - i(v^I)^{\text{T}} \underline{\mathbf{b}} u^R - i(v^R)^{\text{T}} \underline{\mathbf{b}} u^I \end{aligned}$$

as well as

$$\begin{aligned} u^{\dagger} \underline{\mathbf{b}} v &= (u^R + iu^I)^{\text{T}} \underline{\mathbf{b}} (v^R - iv^I) \\ &= (u^R)^{\text{T}} \underline{\mathbf{b}} v^R + (u^I)^{\text{T}} \underline{\mathbf{b}} v^I + i(u^I)^{\text{T}} \underline{\mathbf{b}} v^R - i(u^R)^{\text{T}} \underline{\mathbf{b}} v^I. \end{aligned}$$

Because of the symmetry of a real scalar product, it is

$$x^{\text{T}} \underline{\mathbf{b}} y = y^{\text{T}} \underline{\mathbf{b}} x$$

for any real-valued vectors x and y and any real symmetric matrix $\underline{\mathbf{b}}$. Let $X, Y \in \{R, I\}$. We define for each j and \mathbf{r}

$$B_{XY}^{j\mathbf{r}} = (v_{\mathbf{r}}^X)^{\text{T}} \underline{\mathbf{b}} u_j^Y = (u_j^Y)^{\text{T}} \underline{\mathbf{b}} v_{\mathbf{r}}^X. \quad (\text{B.4.14})$$

Again, we omit the j - and \mathbf{r} -dependence in the following calculations. It is

$$\begin{aligned} [v^{\text{T}} \underline{\mathbf{b}} u] \cdot [u^{\dagger} \underline{\mathbf{b}} v] &= (B_{RR} - B_{II} - iB_{RI} - iB_{IR}) \cdot (B_{RR} + B_{II} - iB_{IR} + iB_{RI}) \\ &= B_{RR}^2 - B_{II}^2 - B_{IR}^2 + B_{RI}^2 - 2i[B_{RR} B_{IR} + B_{II} B_{RI}]. \end{aligned}$$

Hence,

$$\operatorname{Im} \frac{[v^{\text{T}} \underline{\mathbf{b}} u] \cdot [u^{\dagger} \underline{\mathbf{b}} v]}{\omega - i\pi T} = \frac{\pi T^R [B_{RR}^2 - B_{II}^2 - B_{IR}^2 + B_{RI}^2] - 2(\omega - \pi T^I) [B_{RR} B_{IR} + B_{II} B_{RI}]}{(\omega - \pi T^I)^2 + (\pi T^R)^2}.$$

Using this relation and restoring the j - and \mathbf{r} -dependencies, we arrive at

$$\rho(\omega, \mathbf{r}) = \rho_0 \left(1 - \pi g_0 \sum_{j=1}^N \frac{\pi T_j^R [(B_{RR}^{j\mathbf{r}})^2 - (B_{II}^{j\mathbf{r}})^2 - (B_{IR}^{j\mathbf{r}})^2 + (B_{RI}^{j\mathbf{r}})^2] - 2(\omega - \pi T_j^I) [B_{RR}^{j\mathbf{r}} B_{IR}^{j\mathbf{r}} + B_{II}^{j\mathbf{r}} B_{RI}^{j\mathbf{r}}]}{(\omega - \pi T_j^I)^2 + (\pi T_j^R)^2} \right). \quad (\text{B.4.15})$$

The main task to perform in order to get the local density of states is to diagonalise the matrix $\underline{\mathbf{b}} \underline{\mathbf{g}} \underline{\mathbf{b}}$ formally to get its eigenvalues and eigenvectors. Having those, the mean field equations (B.3.9) can be solved and the solutions can be plugged into (B.4.15).

References

- [1] W.J. de Haas, J.H. de Boer, G.J. van den Berg, *Physica* **1**, 1115 (1934)
- [2] M. Sarachik, E. Corenzwit, L.D. Longinotti, *Phys. Rev. A* **135**, 1041 (1964)
- [3] J. Kondo, *Progr. Theor. Phys.* **32**, 37 (1964)
- [4] Y. Nagaoka, *Phys. Rev.* **138**, A 1112 (1965)
- [5] H. Suhl, *Phys. Rev.* **138**, A 515 (1965)
- [6] A.A. Anrikosov, *Physics* **2**, 5 (1965)
- [7] P.W. Anderson, *Phys. Rev.* **124**, 41 (1961)
- [8] J.R. Schrieffer, P.A. Wolf, *Phys. Rev.* **149**, 491 (1966)
- [9] P.W. Anderson, *J. Phys. C* **3**, 2436 (1970)
- [10] P. Nozières, *J. of Low Temp. Phys.* **17**, 31 (1974)
- [11] K.G. Wilson, *Rev. Mod. Phys.* **47**, 773 (1975)
- [12] H.R. Krishna-Murthy, K.W. Wilkins, K.G. Wilson, *Phys. Rev. Lett.* **35**, 1101 (1975)
- [13] H.R. Krishna-Murthy, K.W. Wilkins, K.G. Wilson, *Phys. Rev. B* **21**, 1003 (1980)
- [14] H.R. Krishna-Murthy, K.W. Wilkins, K.G. Wilson, *Phys. Rev. B* **21**, 1044 (1980)
- [15] L.N. Oliveira and J.W. Wilkins, *Phys. Rev. Lett.* **47**, 1553 (1981)
- [16] N. Andrei, *Phys. Rev. Lett.* **45**, 379 (1980)
- [17] P.B. Wiegmann, *Soviet. Phys. JETP Lett.* **31**, 392 (1980)
- [18] P.B. Wiegmann, *Phys. Lett. A* **80**, 165 (1980)
- [19] A. M. Tsvetick and P. B. Wiegmann, *Advances in Physics* **32**, 453 (1983)
- [20] C. Jayaprakash, H. R. Krishna-murthy and J. W. Wilkins, *Phys. Rev. Lett.* **47**, 737 (1981)
- [21] M.A. Rudermann and C. Kittel, *Phys. Rev.* **96**, 99 (1954)
- [22] T. Kasuya, *Prog. Theor. Phys.* **16**, 45 (1956)
- [23] K. Yosida, *Phys. Rev.* **106**, 893 (1957)
- [24] J. H. Van Vleck. *Rev. Mod. Phys.* **34**, 681 (1962)
- [25] K. Yosida: *Theory of Magnetism*. ed. P. Fulde. Springer-Verlag (1996)

References

- [26] V. Madhavan, W. Chen, T. Jamneala, M.F. Crommie and N.S. Wingreen, *Science* **280**, 567 (1998).
- [27] V. Madhavan, W. Chen, T. Jamneala, M.F. Crommie and N.S. Wingreen, *Phys. Rev. B* **64**, 165412 (2001)
- [28] J. Li, W.-D. Schneider, R. Berndt and B. Delley, *Phys. Rev. Lett.* **80**, 2893 (1998).
- [29] U. Fano, *Phys Rev.* **124**, 1866 (1961)
- [30] A. Schiller, S. Hershfield, *Phys. Rev. B* **61**, 9036 (2000)
- [31] O. Újsághy *et al.*, *Phys. Rev. Lett.* **85**, 2558 (2000)
- [32] L. Szunyogh *et al.*, *Phys. Rev. B* **49**, 2721 (1994)
- [33] C.-Y. Lin, A.H. Castro Neto and B.A. Jones, *Phys. Rev. B* **71**, 035417 (2005)
- [34] H.C. Manoharan, C.P. Lutz, D.M. Eigler, *Nature* **403**, 512 (2000)
- [35] N. Nagaoka, T. Jamneala, M. Grobis and M.F. Crommie, *Phys. Rev. Lett.* **88**, 077205 (2002)
- [36] N. Knorr *et al.*, *Phys. Rev. Lett* **88**, 096804 (2002)
- [37] P. Wahl *et al.*, *Phys. Rev. Lett.* **93** 176603 (2004)
- [38] A.C. Hewson: *The Kondo Problem to Heavy Fermions*. Cambridge University Press (1993)
- [39] L. I. Glazman and M. E. Raïkh, *JETP Lett.* **47**, 452 (1988)
- [40] T. K. Ng and P. A. Lee, *Phys. Rev. Lett.* **61**, 1768 (1988)
- [41] Y. Meir, N.S. Wingreen, P.A. Lee, *Phys. Rev. Lett.* **70**, 2601 (1993)
- [42] N.S. Wingreen and Y. Meir, *Phys. Rev. B* **49**, 11040 (1994)
- [43] S. Hershfield, J.H. Davies, J.W. Wilkins, *Phys. Rev. Lett.* **67**, 3720 (1991)
- [44] J. König *et al.*, *Phys. Rev. B* **54**, 16820 (1996)
- [45] D. Goldhaber-Gordon *et al.*, *Nature* **391**, 156 (1998)
- [46] S.M. Cronenwett, T.H. Oosterkamp and L.P. Kouwenhoven, *Science* **281**, 540 (1998)
- [47] J. Schmid *et al.*, *Phys. Rev. Lett.* **84**, 5824 (2000)
- [48] F. Simmel *et al.*, *Phys. Rev. Lett.* **83**, 804 (1999)
- [49] W.G. van der Wiel *et al.*, *Science* **289**, 2105 (2000)
- [50] S. Sasaki *et al.*, *Nature (London)* **405**, 764 (2000)
- [51] T. Inoshita *et al.*, *Phys. Rev. B* **48**, R14725 (1993)
- [52] T. Pohjola *et al.*, *Europhys. Lett.* **40**, 189 (1997)

References

- [53] A. Levy Yeyati, F. Flores, A. Martin-Rodero, Phys. Rev. Lett. **83**, 600 (1999)
- [54] M. Eto and Y. V. Nazarov, Phys. Rev. B **64**, 085322 (2001)
- [55] A. Kumar *et al.*, Phys. Rev. B **56**, 3145 (1997)
- [56] W. Chen, T. Jamneala, V. Madhavan, M.F. Crommie, Phys. Rev. B **60**, R8529 (1999)
- [57] H. Jeong, A. M. Chang, M. R. Melloch, Science **293**, 2221 (2001)
- [58] R. Aguado, D. C. Langreth, Phys. Rev. Lett. **85**, 1946 (2000)
- [59] C. A. Büsser, *et al.*, Phys. Rev. B **62**, 9907 (2000)
- [60] T. Aono and M. Eto, Phys. Rev. B **63**, 125327 (2001).
- [61] T. H. Oosterkamp *et al.*, Nature **395**, 873 (1998).
- [62] N. J. Craig, J. M. Taylor, E. A. Lester, C.M. Marcus, M. P. Hanson, A. C. Gossard, Science **304**, 565 (2004)
- [63] P. Simon, R. Lopez, Y. Oreg, Phys. Rev. Lett. **94**, 086602 (2005)
- [64] M.G. Vavilov and L.I. Glazman, Phys. Rev. Lett. **94**,086805 (2005)
- [65] J. Simonin, Phys. Rev. B **73**, 155102 (2006)
- [66] A. Georges and Y. Meir, Phys. Rev. Lett. **82**, 3508 (1999)
- [67] R. Aguado and D.C. Langreth, Phys. Rev. B **67**, 245307 (2003)
- [68] S. Uzdin, V. Uzdin and C. Demangeat, Europhys. Lett. **47**, 556 (1999)
- [69] C. Kohl and G.F. Bartsch, Phys. Rev B **60**, 4205 (1999)
- [70] T. Jamneala, V. Madhavan, M.F. Crommie, Phys. Rev. Lett. **87** (2001)
- [71] Y. B. Kudasov and V.M. Uzdin, Phys. Rev. Lett. **89**, 276802 (2002)
- [72] B. Coqblin and J.R. Schrieffer, Phys. Rev. **185**, 847 (1969)
- [73] B. Lanzarovits *et al.*, Phys. Rev. Lett. **95**, 077202 (2005)
- [74] V.V. Savkin, A. N. Rubtsov, M. I. Katsnelson, and A. I.Lichtenstein, Phys. Rev. Lett. **94**, 026402 (2005)
- [75] A. N. Rubtsov and A. I. Lichtenstein, JETP Lett. **80**, 61(2004)
- [76] A. A. Aligia, Phys. Rev. Lett. **96**, 096804 (2006)
- [77] N. Read and S. Sachdev, Nuc. Phys. B **316**, 609 (1989)
- [78] S.V. Maleev, Sov. Phys. JETP **6**, 776 (1958)
- [79] V.G. Vaks, A.I. Larkin, S.A. Pikin, Sov. Phys. JETP **26**, 188 (1967)
- [80] V.G. Bar'yakhtar, V.N. Krivoruchko, D.A. Yablonskii, Sov. Phys. JETP **58**, 351 (1984)

References

- [81] V.I. Belinicher and V.S. L'vov, Sov. Phys. JETP **59**, 564 (1984)
- [82] V. N. Popov, Fedotov, S.A., Sov. Phys. JETP **67** (3), 535 (1988)
- [83] G.D. Mahan: *Many-Particle Physics - 2nd. edition.* Plenum Press (1990)
- [84] Veits, O., Oppermann, R., Binderberger, M., Stein, J., J. Phys I France **4**, 493 (1993)
- [85] Kiselev, M.N., Feldmann, H., Oppermann, R., Eur. Phys. J. **B 22**, 53 (2001)
- [86] M.N.Kiselev, Int. J. of Mod. Phys. B **20**, 381 (2006)
- [87] J. Zinn-Justin: *Quantum Field Theory and Critical Phenomena.* Oxford University Press (1989)
- [88] M. Abramowitz and I.A. Stegun: *Pocketbook of mathematical functions.* Verlag Harri Deutsch (1984)
- [89] J.F. Cornwell: *Group Theory in Physics Vol. 1.* Academic Press (1984)
- [90] J.W. Negele and H. Orland: *Quantum many-particle systems.* Westview Press (ABP) (1998)

Danksagung

Ich danke meinem Doktorvater Alexander Chudnovskiy für die wertvolle Unterstützung und die vielen fachlichen Anregungen, die sehr zum Gelingen dieser Arbeit beigetragen haben. Er war stets auch kurzfristig bereit, sich für meine Fragen und die kritische Reflexion meiner Arbeit Zeit zu nehmen.

Prof. Lichtenstein gilt mein Dank dafür, dass er die Begutachtung meiner Dissertation übernommen hat. Desweiteren möchte ich Prof. Potthoff dafür danken, dass er sich dazu bereit erklärt hat, als Gutachter meiner Disputation beizuwohnen. Mein Dank gilt Prof. Oepen für die Übernahme des Prüfungsausschussvorsitzes.

Prof. Daniela Pfannkuche danke ich dafür, dass sie immer ein offenes Ohr für die fachlichen und sonstigen Probleme ihrer "Mädchen und Jungs" hatte. Sie schuf die Voraussetzungen für die konstruktive und angenehme Zusammenarbeit innerhalb unserer Arbeitsgruppe.

Besonderer Dank gilt meinen Kollegen. Wir haben viele Gespräche fachlicher und anderer Natur geführt, die ich oft als sehr anregend empfand, und wir haben viel gelacht. Mit Jacek, Stellan und Peter über Physik, Fußball und Philosophie zu diskutieren, war meistens lehrreich, manchmal komisch aber immer interessant. Auch mit Dirk, Daniel, Benjamin und allen anderen Mitgliedern unserer Arbeitsgruppe verbinde ich Erinnerungen an viele unterhaltsame und lehrreiche Gespräche. Ich danke auch allen anderen Mitgliedern des Instituts, die durch ihre umgängliche und kollegiale Art für ein angenehmes Arbeitsklima gesorgt haben.

Den Mitgliedern und Organisatoren des SFB 668 möchte ich für die vielen Anregungen danken, die ich aus Kolloquien und von Doktorandentreffen mitgenommen habe. Die finanzielle Unterstützung der Deutschen Forschungsgemeinschaft über den SFB 668 machte diese Doktorarbeit erst möglich.

Zu guter Letzt möchte ich meiner Frau und meiner Familie für ihre liebevolle und unermüdliche Unterstützung danken.